Improved fault localization method for electrical power distribution networks

Raphaël Marguet

UNIVERSITÉ DE GRENOBLE

THÈSE

Pour obtenir le grade de

DOCTEUR DE L'UNIVERSITÉ DE GRENOBLE

Spécialité : **Génie Electrique**

Arrêté ministériel : 7 août 2006

Présentée par

Raphaël MARGUET

Thèse dirigée par **Bertrand RAISON**

préparée au sein du **Laboratoire de Génie Electrique de Grenoble** dans **l'École Doctorale Electronique, Electrotechnique, Automatique et Traitement du Signal**

Improved Fault Localization Method for Electrical Power Distribution Networks

Améliorations de Méthodes de Localisation de Défauts pour les Réseaux de Distribution Electrique

Thèse soutenue publiquement le **05 mars 2015**
devant le jury composé de :

M. Jean-Claude MAUN Professeur, Ecole Polytechnique de Bruxelles	Rapporteur
M. Jean-Claude VANNIER Professeur, SUPELEC	Rapporteur
M. Nouredine HADJ-SAID Professeur, Université Grenoble Alpes	Examinateur
M. Patrick SCHWEITZER Maître de Conférences, Université de Lorraine	Examinateur
M. Bertrand RAISON Professeur, Université Grenoble Alpes	Directeur

Remerciements

Mars 2010 - Mars 2015.
Voilà le temps que j'aurais passé au G2Elab, 5 années dont 3 en thèse.
5 années de travail dans un cadre vraiment agréable grâce à tous ceux qui composent ce laboratoire. Et même si aujourd'hui c'est avec plaisir que je poursuis un nouveau projet, je ne peux que me rendre compte de la chance que j'ai eu et que je vais forcément regretter un peu.

Il faut tout d'abord que je remercie Bertrand Raison de m'avoir ouvert la porte du G2Elab. Il faut croire que j'ai eu la chance de toquer au bon endroit lorsque je cherchais un stage de deuxième année. J'ai pu ainsi revenir après un séjour à l'étranger et travailler avec Bertrand en attendant le début du financement de ma thèse.

Ensuite il faut que je remercie Bertrand en tant qu'encadrant de thèse. Lorsque j'ai dit que c'était un encadrant "unique", je ne disais pas que c'était mon unique encadrant, mais bien qu'il n'y en avait pas deux comme lui ! Et en cela je me considère chanceux. Avoir Bertrand comme directeur de thèse c'est travailler mais toujours dans la bonne humeur. Avec sa rigueur et son efficacité Bertrand m'a toujours poussé un peu plus de l'avant. Bien sûr travailler avec Bertrand c'est aussi se faire vanner (lorsqu'on le mérite bien sûr), mais encore dans la bonne humeur. Et le summum: se faire vanner en latin ! oui même en 2015.

Je remercie sincèrement Bertrand pour cet accompagnement de qualité, tout au long de mon travail, ce qui participera aux très bons souvenirs que j'aurais de cette période de ma vie.

Je souhaite remercier tous les membres du jury et plus particulièrement les rapporteurs, Jean-Claude Maun et Jean-Claude Vannier pour l'intérêt qu'ils ont porté à mon travail.

Merci bien sûr à toutes les personnes du G2Elab, que ce soit les "pré-doctorants", doctorants, post-doctorants, enseignants-chercheurs, services administratifs, services techniques, services informatiques qui font du G2Elab un laboratoire vraiment agréable. Séminaires, pots de thèse, barbecues d'équipe, matchs de foot et autres évènements (organisés entre autres par OPLAT) rythment agréablement l'année.

Merci aux collègues/amis qui ont été présents à un moment ou à un autre au labo et avec qui j'ai toujours passé du bon temps. Josselin, Pierre, une petite partie de coinche?

Merci à Jean-Louis (responsable officieux de la benne), Archie (super la légende du rat crevé dans la double cloison, je ne l'oublierai pas), Justine, Rémi (VLAN !... tiens voilà Rémi), c'est à dire ceux de la première heure. Merci à Victor, Aurélien et Clémentine d'avoir avec moi réussi à occuper le bureau chacun sur des plages horaires (très) différentes.

Merci à vous 3, à Manue (sympa la confrontation de génération: "moneo" contre "ticket de RU en bois"), à G (acronyme de Gaspard), et Archie de finir vos thèses après moi pour que je vous nargue un peu. Tiens, Archie je vois que t'es dans les deux catégories, "première heure" et "laissé derrière"...

Je souhaite aussi remercier tous les "étrangers" du labo qui nous font découvrir de belles choses à travers leurs cultures et tout spécialement Mariam et José.

Pendant ces 5 ans j'ai tout de même passé plus de temps en dehors du labo que dedans. Et si j'ai tant apprécié vivre ici c'est surtout grâce à tous mes amis proches, qui sauront se reconnaitre, et à Elsa bien sûr. Merci de participer à me rendre heureux au quotidien ! C'est indispensable !

Pour finir je veux remercier toute ma famille qui m'a toujours aidé et soutenu dans tous mes projets, et surtout mes parents pour m'avoir permis de venir étudier à Grenoble et en être arrivé là aujourd'hui. Je peux dire que j'ai toujours été heureux et que je ne regrette rien de ces 10 dernières années, bien au contraire !

Contents

List of Figures

List of Tables

General Introduction

Contents

Abstract

This introduction presents the general state of development of distribution networks. The Greenlys project, frame of the work presented in this thesis, is introduced as well as the data, on which our work is based, that we obtained throughout the partnerships in this project. The thesis outline will conclude this introduction.

1 State of the developments in distribution networks

For a long time distribution networks have been operated in a very simple and practical way. The diversity of the situations: rural network, urban network, overhead lines, underground cables, very different territories and climatic conditions, always lead to an adapted operation of each distribution network. The only developed equipment was mainly analogical and dedicated to ensure the safety of the network and its users.

Even though the distribution network was operated live, not many data was available, unlike the transmission network where the securing operations are much more developed.

New challenges of today for network operators are mainly to develop an intelligent and sustainable energy management. These challenges bring all the different actors to work together in order to re-think the whole electrical network and specifically the distribution networks which lags behind.

Even though distribution networks have been upgraded through time and that new digital equipment replace the historical analogical one, the distribution networks today do not possess the correct equipment to allow a full response to those new challenges. It is in this context that the notions of “smartgrid”, and “Advanced Distribution Automation” functions, emerged, referring to a connected network in terms of information flow but also operating orders which will possess the necessary advanced distribution tools to allow the development of new operation methods, the integration of new technologies, and by these means the response to the complicated energy challenges that we will face.

2 The Greenlys project

The work presented in this thesis is part of the Greenlys project[1], “the first full scale Smart Grid demonstration project".

This project is financed through a program of investments for the future[2] which allocates financing through various call for interests. The French Environment & Energy Management Agency[3] makes many call for interests concerning the four programs within its competencies: technological demonstration platforms in renewable energy and green chemistry, smartgrids, circular economy and vehicles of the future. Greenlys is one of them.

Greenlys, which started in 2012 and will end in 2016, has been set up by a consortium of partners, major stakeholders in the French electricity market with complementary skills: Électricité Réseau Distribution France (ERDF), the project leader, GDF Suez, Gaz Électricité de Grenoble (GEG), Schneider Electric, Grenoble Institute of Technology (Grenoble INP), Atos Worldgrid, Réseau de Transport d’Électricité (RTE), Alstom, the

[1] www.greenlys.fr

[2] “Investissements d’avenir” from the “Commissariat général à l’investissement” - www.gouvernement.fr/investissements-d-avenir-cgi

[3] ADEME - Agence de l’Environnement et de la Maîtrise de l’Energie - www.ademe.fr

CEA national solar energy institute (CEA INES), Rhône-Alpes Énergie Environnement (RAEE), Hespul and the CNRS LEPII-EDDEN (Economy of sustainable development and energy) laboratory.

The G2Elab[4] (Grenoble Electrical and Engineering Laboratory), which is part of Grenoble INP[5], participates in many divisions of the project.

The division in which this work fits in is "Distribution network performance and agility: the self-healing network".

3 Network data

The two Distribution System Operator (DSO) part of Greenlys (ERDF and GEG) both provided us with complete data concerning parts of their network. This data made it possible to conduct complete network simulations with the minimum of unknown parameters, therefore allowing simulations the closest as possible to real situations.

One of the DSO also provided us with real fault measurements which occurred on the same feeders that we obtained data from. However, as our work concentrates on developing a new fault localization method based on smartgrid networks with the available technology (in terms of signal measurements and communication) that goes with it, and despite the numerous signals which the DSO records, the data unfortunately did not include all the needed information in order to test our method on these real measurements.

However, the provided data was used in order to perform simulations using models the closest as possible to reality. Therefore the results throughout our work are obtained with simulated faults that are close to reality.

4 Thesis outline

The first chapter of this thesis aims at presenting the state of the art of the various fault localization methods existing in general and more specifically for distribution networks. We also present the outline of the new method that we develop in the rest of the document.

The second chapter presents a fault localization method which is based on the actual equipment of most distribution networks, and locates which section or area of the network is faulty. It is not a precise fault distance computation algorithm. However, based on a probabilistic process, the method shows how to use efficiently the already available data in order to compute faulty section detection with a high success rate despite possible equipment failures.

[4] www.g2elab.grenoble-inp.fr

[5] Grenoble Institute of Technology

Chapter three describes in details the theory of the proposed precise fault localization method. It details the different stages of the methods, the conditions as well as the limits.

The last chapter presents the results that we obtain applying our method on simulated real networks. We analyze the different performance, depending of the method parameters, the fault situations or the type of network, as well as the perspectives of improvements.

The thesis is finally ended by a general conclusion.

Chapter I

Fault Localization State of the Art and Thesis Objectives

Contents

Abstract

We present in this first chapter a state of the art of the research in the field of electrical network fault localization. To cope with the historical development of fault localization, a general fault localization state of the art is first detailed, mainly focused on transmission network dedicated solutions, before presenting a more specific state of the art concerning adaptations of fault localization methods to the distribution network. Finally the outline of the goals and obstacles which will meet the method developed in this thesis is presented.

1 Introduction

When first considering the electrical network fault localization research field, one will first find developed methods and techniques which are designed to identify and isolate a zone or area. It is indeed the first concern of a Transmission System Operator (TSO) or Distribution System Operator (DSO) under a fault situation to know which area is faulty and which switches should be operated in order to isolate the fault from the rest of the network.

This concern has therefore brought the different actors to develop simple, robust and easy to implement solutions, such as impedance relays for transmission networks, or fault current detectors for distribution networks. However, if some of these solutions can quickly locate a faulty area, the precise localization which is done off-line (once the fault is isolated from the network) is often very time consuming and require dedicated equipment and methods.

Consequently, other methods which concentrate on trying to locate precisely the faults have been developed. They are a bit more complex than the faulty area localization methods, but have the advantage of locating the faulty section or area, therefore allowing a quick and efficient switch operation to isolate it, and at the same time give a precise location of the fault. It is this kind of method which is proposed in this thesis and that is developed in the following state of the art.

2 General fault localization state of the art

Note: the methods presented in this state of the art concern on-line fault localization method meaning techniques that are processed while the fault is still occurring and while the feeder is still powered, opposed to off-line techniques which are designed to locate the fault once the feeder is disconnected.

Fault localization is a research topic which of course appeared at the same time as the development of electrical networks. As these networks were developed throughout two main levels: transmission and distribution, fault localization research was concentrated on the most critical one: the transmission network. Nowadays technologies that are used for fault localization on the transmission network are still technologies developed more than ten years ago, even if they have of course been improved since. We describe in the following paragraphs the evolution and the different techniques of fault localization on transmission networks.

The first fault localization technique was of course the visual inspection of the lines and equipment, thus being very time consuming. Therefore new methods based on measurements and computations emerged quickly. The first one is probably the use of a current ratio (between one terminal ground current and the total ground current) [Lantz, 1962], but this method is not robust to resistive faults. Other methods such as frequency-modulated radar techniques were also used [Stevens et al., 1972].

Quickly, new fault localization methods were developed, this time using the measurements and analysis of traveling waves produced by the fault appearances. Finally, with the development of protection relays based on the network reactance computation, fault loop impedance computation methods were consequently elaborated. Generally, the first method development were using two-end terminal techniques, which needed communication between both ends, but often evolved in more complex version using only one-end terminal data.

The following list presents chronologically non exhaustively different fault localization methods.

- **Fault localization using fault generated traveling waves**
  These methods consist in detecting in the measured currents and voltages fast traveling waves produced by unusual electrical events such as a fault. Also used for fast detecting relays [Chamia and Liberman, 1978], it is used as soon as the early 80's [Crossley and McLaren, 1983] to locate faults.

  This fault localization method uses the comparison of the time travel of the different surges generated by the fault. When a fault occurs, one surge will travel in direction of the relay, while another one will travel in the other direction to another relay. It is the time difference between the detection of these two surges (which can be done by monitoring electrical variables or as mentioned below by applying a wavelet transform to the signals) at the relays which allows to determine the fault distance. However, despite the "simple" topology of a transmission network, the reflections of the fault surges at different "nodes" of the network and the travel speed of the waves can considerably complicate the fault localization. The wavelet transform theory [Magnago and Abur, 1998] is based on the traveling wave theory but instead of analyzing relaying signals, it applies a wavelet transformation to the measured signals in order to identify the high frequency components of the fault transients.

- **Fault localization by computing the fault loop reactance**
  Reactance computation is a technique which is already used by protection relays. These relays are tuned to protect a certain zone. In order to know whether the fault is inside or outside the protected zone, the reactance of the network during the fault is computed. The results will then be interpreted depending on the reactance value and are linked to different time delay.

  It is this reactance that can be expressed as a distance when knowing the conductors characteristics. However this method shows some imprecision which are dealt with in [Wiszniewski, 1983] where the authors add the estimation of the fault resistance. Fault loop impedance methods have later been developed for distribution networks as we will see in section 3.2.

- **Fault localization by directly computing the fault distance**

This method was developed in 1982 [Takagi et al., 1982]. It consists in developing network equations and expressing the fault distance using data from one terminal only. This method makes two assumptions which are proper to transmission networks (see appendix B). [Adu, 2001] proposes a variation of this method.
We will describe in more details this method throughout the thesis.

3 Current fault localization methods for distribution networks

3.1 Introduction and transmission versus distribution networks

Fault localization procedures are probably as various as are the distribution networks around the world. A complete fault localization procedure is made of a fault detection stage, a fault isolation stage in order to protect the rest of the network and finally a fault localization stage which is necessary in order to repair the network before returning to normal operation.

For example, the french DSO, ERDF, uses three functions: fonsynt, fonloc and fonrep, during its entire fault procedure, which are centralized and performed at the local operation center. The fonsynt function analyzes and identifies the type of fault, then the fonloc function operates the circuit breaker, gathers fault indicators information and locates the fault, and finally the fonrep funtion is used to reconfigure the network and restore the energy supply to a maximum of clients.

More generally, each of these stages will be particular to the network on which the fault occurs. Fault detection, for example, is affected by the type of neutral grounding of the substation's transformer. A protection plan is usually defined for each network and each fault type (single or multiphase), depending of its installations, voltage characteristics and others in order to isolate the faulty part from the rest of the network. The fault localization stage is affected by many characteristics: transformer neutral grounding, topology, type of loads, conductor characteristics, type of faults, etc, which makes it difficult to perform a good and precise fault localization, especially when there is a unique measurement point at the head of the feeder.

In most cases, at least in French networks, it is actually not really a fault localization but a faulty section localization which is done. Indeed the method is mostly based on the information given by fault indicators which are located in strategical nodes of the network, most of the time nodes which also possess a manual or remote trigger switch. As it will be described in chapter II, these fault indicators only detect the presence of a fault current which indicates a fault location downstream or upstream of the fault indicator (some fault indicators can also detect the direction of the fault current).

The fault localization method that are presented in the following state of the art are methods which use the measurements of the electrical characteristics in one or multiple points of the network, and which base the fault localization on the analysis of these measurements. These methods can be opposed to the methods performing faulty section or

area localization, such as the method described previously and using fault indicators information.

- Differences between distribution and transmission networks

Historically, fault localization methods have been first developed for transmission networks. Indeed the transmission network is more critical since a major fault can affect a very big area, many industrial and residential costumers and can even lead to economical consequences for a region, state or country. Furthermore, distribution networks are usually sparsely equipped in monitoring equipment. For all these reasons, research on fault localization methods for the distribution networks is not as mature, and is still in development stage.

The meshed structure of the transmission network is opposed to the radial configuration of the distribution network. On the transmission network, power flows on a line can be in both directions, depending of the loads. Therefore the methods developed for the transmission network need to use information retrieved from both ends of a line.

Furthermore, a transmission line between two nodes is often very long and made of only one continuous conductor, thus limiting the number of needed equipment in order to localize faults. The distribution network is completely different: its radial configuration is made for a power flow from top to bottom, it often possesses many nodes and laterals, and has smaller distances with many different conductors. The consequence is a network which is more complicated to monitor, and it is therefore harder to localize faults.

3.2 State of the art for distribution networks

Concerning fault localization on distribution network, different approaches exist. A method developed in Finland in 1994 [Jarventausta et al., 1994] uses fuzzy sets in order to determine the network sections which have the most possibilities of enduring a fault. This method, not based on a fault distance computation, uses knowledge such as topology of the network and its environment, considering that most faults occur due to weather conditions.

In 1997 another technique is published [Zhu et al., 1997]. This quite complete method computes a fault distance in an iterative way. It first estimates the remaining load current downstream the fault point by using a radial power flow algorithm and subtracts it to measured phase current in order to estimate the fault current. Then the fault distance is computed, as well as the fault resistance. This process is done iteratively until a convergence criteria is met. Subject to uncertainties (system modeling, phasor estimation,...) the authors also develop a probabilistic extension to their method in order to improve the results.

[Welfonder, 1998] proposes another method which is developed specifically for distribution networks with a compensated neutral. This method consist of two parts: a propagation method of the voltage and currents measured at the head of a feeder, and

a localization process using the propagated measurements at the head of each section of the network, at different frequencies than the classical 50 Hz due to the particular type of neutral grounding (compensated neutral). This approach necessitates the estimation of the fault resistance, and computes the fault distance using a polynomial equation and a fault loop impedance approach.

Other methods have been published in the years two thousand. All developing new approaches: one based on a direct circuit analysis [Choi et al., 2004] particularly efficient for unbalanced systems, another based on the frequency response and the analysis of transients at the initial fault moment [Bogdashova and Kachesov, 2005]. The last one is more a faulty section localization method [Pham, 2005] as it does not compute a fault distance but uses the data from fault indicators to compute probabilities of the network sections to be faulty.

Some more specific works focus on the detection of high impedance faults [Masa, 2012] or the special case of arc type faults [Elkalashy et al., 2007]. These type of works are useful for a full understanding of the complexity of fault situations and will help in developing complete fault localization methods adapted to a large range of situations.

However, the most documented methods are the following: the computation of the fault loop impedance which is then transformed in a distance, and the direct computation of the fault distance using the network equations.

- **Fault loop impedance computation methods**
  As described in section 2, these methods compute the impedance of the loop created by the fault by using the imaginary part of an electrical network equation. This impedance can then be compared to the per unit length impedances of the lines and cables of the network in order to determine a distance.

  [Wiszniewski, 1983] published a paper on this method for transmission networks. It has since been adapted for distribution networks [Saha et al., 2001] by combining the fault loop impedance computation with a feeder impedance computation, section by section, in order to find a match between the two values, and therefore locate the fault.
  In [Penkov, 2006], the author uses a fault loop impedance method and analyzes the impact of distributed generation unit on this fault localization method for various fault types and neutral grounding types. The author also concentrates on discriminating zones, rightly stating that computing a fault distance on radial distribution networks is not enough to locate precisely the fault.

  Other works compare this method with a fault distance computation method about the effect of the load current [Karnik et al., 2011] or their effectiveness on non-homogeneous networks [Kulkarni et al., 2011].
  More recent works [Das et al., 2011] introduce complementary approaches such as using fault current profiles from fault simulations at different nodes of the network

which are to compare with the measured fault current in order to locate the fault.

- **Fault distance computation**
  The first fault distance computation method was proposed in 1982 for the transmission network [Takagi et al., 1982] and later reviewed [Adu, 2001].
  Based on the network equations expressing the phase voltages and symmetrical components voltages [Karnik et al., 2011] at the measuring point in function of the networks elements, the method allows the computation of the fault distance with a minimum of information. The authors evaluate the effect of the load current on this method, while [Kulkarni et al., 2011] evaluates the effect of the non-homogeneous character of most distribution networks.

3.3 Method summarization table

Table I.1 presented here summarizes the different fault localization mentioned in the previous sections.

	Traveling Waves		Impedance based methods		
	Relay measurements	Wavelet transform	Positive reactance	Loop reactance	Takagi equation
References	[Crossley and McLaren, 1983]	[Magnago and Abur, 1998]	[Saha et al., 2001] [Das et al., 2011] [Karnik et al., 2011]	[Karnik et al., 2011]	[Takagi et al., 1982]
Particularities	use of relay measurements to detect fault surges and estimate the distance knowing the speed travel	computes a wavelet transform on the measured signal to detect fast surges and estimate the distance knowing the speed travel	uses the positive reactance computation to estimate the fault distance	uses a loop impedance computation to estimate the fault distance	computes the fault distance from voltage and current measurements
+			simple	simple	takes into account the load current
-	needs a high sampling rate	needs a high sampling rate	makes a lumped-load assumption	neglects the load current	needs a homogeneous network for good performance; makes a lumped-load assumption
Equations			$x = \frac{\mathrm{Im}\left(\frac{V}{I_S}\right)}{\mathrm{Im}(z_1)}$	$x = \frac{\mathrm{Im}\left(\frac{V}{3.I_0}\right)}{\mathrm{Im}\left(\frac{2.z_1+z_0}{3}\right)}$	$x = \frac{\mathrm{Im}\left(V_a.{I_f}_{est}{}^*\right)}{\mathrm{Im}\left(z_1.I_{tot}.{I_f}_{est}{}^*\right)}$

Table I.1: Summary of the various fault localization methods presented throughout this chapter

4 The need of an improved method

4.1 Goals

The new method developed in our work is based on a fault localization method for the transmission network. Our goal is to adapt the method to the specific particularities of distribution network in order to create a tool which brings effectiveness, speed and precision in fault localization on distribution networks.

An effective method is a method which possesses a high success rate. A fault localization algorithm which is too often wrong is probably worse in term of effectiveness when considering the useless on field work which will result from the wrong localizations.

Speed in fault localization is a main objective for many reasons. First of all it is necessary to recover power to all customers as fast as possible. But it cannot be done without numerous steps: localization of the exact fault location, remote and manual switch operations in order to reduce the black-out zone, maintenance and finally complete power recovery for the black-out zone. However all these steps cannot be done effectively without a quick access from the expert to precise information concerning the fault location. The goal is therefore to develop an algorithm that can deliver an analysis of the fault situation and propose possible fault locations in a few minutes on the basis of measurements performed only at the head of the feeder.

The precision of the localization is also very important and of course the developed method aims to give fault localization results as precise as possible. However, the precision depends on many parameters that are not always inherent to the method, such as for example: input data precision, topology of the network, fault resistance. The desired precision can also vary depending of the DSO's needs concerning the localization. For example a DSO with switches every 300 meters on its network might not necessarily need a precision in the order of a meter.

Beyond these general goals, the method that we develop in our work also aims in solving specific problems related to the particularities of a distribution network, listed below:

- the strong heterogeneity of the line/cable types (conductor section, electrical characteristics...)
- the radial structure of most distribution feeders
- the tapped loads
- the few data available about the state of the network operation and the loads status
- a unique measurement point

Apart from the fault localization method that we will develop in this thesis, part of our work also concentrates on improving a faulty section localization method (see chapter II), based on the existing equipment available and already installed on most distribution networks nowadays: fault indicators which indicate if an abnormal current (therefore due

to a fault situation) has been detected.

Our goal by developing such a method is to provide another solution to the fault localization problem, which is not based on new equipment, or advanced distribution tools, but rather on doing better with what is already available.

4.2 Obstacles

Many obstacles will need to be overcome in order to succeed in developing such a method. As the different works presented in this chapter show, the developed fault localization method are often specifically dedicated to solving one particular problem, which will be enough for some distribution networks, but not for all.

The obstacles to developing a more general method are therefore numerous. First of all, we can draw the attention on the type of neutral grounding of the transformer of the network substation. Indeed, compensated neutral grounding do not lead to the same electrical phenomena than impedant neutral grounding. The differences are major, in terms of fault current amplitude and dominant frequencies for example, and will hardly be managed by a unique method.

The unknown fault resistance, or maybe impedance, is also a fault parameter which should be overcome by the method. This factor is strictly uncontrollable and is also poorly known. Most of the research considers a resistive fault, even if the special case of arc faults, which show a very specific time depending impedance, have also been studied [Elkalashy et al., 2007].

Another concern is the complex radial topology of most distribution networks, which necessitates another approach than the classical unique observation point like in transmission fault localization systems.

5 Conclusion

As the presented state of the art show, there are a certain number of methods or variations of methods that have been developed in the field of fault localization for distribution network. Most of the time concentrated on one particular problem, no general or universal method has yet been developed, and considering the great variety of distribution networks around the world it is without any doubt a great challenge.

Chapter II

Probabilistic Fault Localization Method Using Fault Indicators States

Contents

Abstract

We develop in this chapter a probabilistic fault localization method based on remotely retrieved fault indicator states. We will describe the current use of fault indicators before developing the probabilistic method. The method will then be applied to a simple test case in order to clarify its mechanism. Advanced developments and analysis are then detailed before showing some results as well as performances.

1 Introduction

Fault indicators (FI) are part of the protection scheme of a distribution network. A fault indicator is an equipment which is used during the fault localization process. FIs have been designed to be able to detect the flow of a fault current on the line or cable where they are installed. They work with a basic current threshold logic which considers that the current flow is not normal but due to a fault situation when its value passes the threshold value.

The logic of the FIs is always based on a current threshold. However, some models called "directional FI" can also detect the direction of the current flow, which therefore need to know the voltage. However it is almost always an estimation of the voltages and currents by the measurements of the magnetic and electric fields issued from the conductors. When using non-directional FIs it is the observation of the next upstream and downstream FIs which can give the direction of the fault current flow and therefore the fault location.

Let us consider that non-directional FIs have 2 states: no fault current detected / fault current detected. Directional FIs will therefore have 3 states: no fault current detected / upstream fault current detected / downstream fault current detected. During the fault localization process, the states of the FIs need to be retrieved in order to analyze the fault current flow in the feeder.

They are two types of FIs, the communicating FIs and the non-communicating FIs. The state of the communicating FIs can be retrieved remotely and is used by the operation scheme in order to quickly isolate the faulty section from the rest of the network. The non-communicating FIs use a light signal on site, therefore a maintenance crew has to physically move on field to retrieve the FI state. In France, communicating FIs are often associated to a remote switch, meanwhile non-communicating FIs can be associated to a manual switch. The FI state information is therefore used in two steps: communicating FIs are used for an automatic faulty zone isolation, and non-communicating FIs are used for a finer fault isolation by on field expert.

2 Reliability problems of fault indicators responses

Fault indicators are equipment which are not meant to be used frequently. Most models are battery powered and do not detect a fault current for years. However it is important that FIs work properly when a fault occurs, and it is generally once a fault occurs that the malfunctioning of a FI is detected. This aspect can be critical for the fault localization process. As previously said, most FIs models need to be retrieved on field. This means that technicians need to check each FI starting from the substation and going downstream along the feeder and its laterals. As long as the FIs state is "fault current detected" the technician keep going downstream. Logically the fault location should be somewhere between the last FI with a "fault current detected" state and the following FI with a "no fault current detected" state. Of course if there are laterals starting somewhere between

these two FIs, they need to be checked too (see figure II.1).

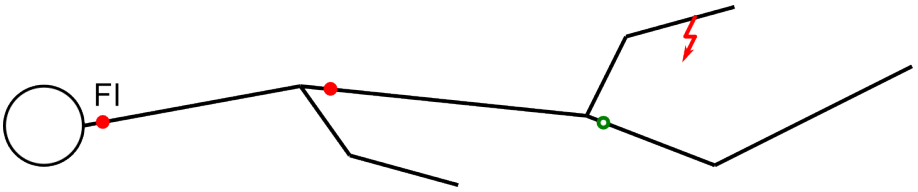

Figure II.1: Fault on a lateral between two FIs

The fact that FIs can have failure weakens this reasoning. Indeed it is possible that a defective FI misleads the technicians looking for the fault location (see figure II.2). In order to avoid these cases, the technicians are often forced to check all the FIs of the feeder, which is even more time consuming.

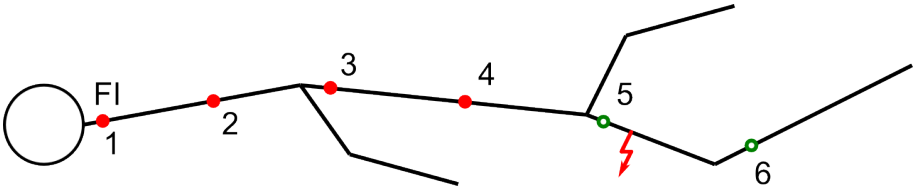

Figure II.2: Defective FI misleading experts on the real fault location

3 Probabilistic method

This method is developed in a specific context. We previously stated that the actual method, consisting of experts going on field and retrieving FI states manually, is limited since it is very time consuming. The future context will consist of new equipment which will be able to communicate remotely state. It is therefore on this smart grid context with communicating FIs that the method we developed is based.

3.1 Signature matrix of the FIs of a network

Considering a network with FIs we can divide it in sections, each section being bordered by one upstream FI and one downstream FI (except for the last section). This means that for each section there is a number of FIs that has detected a fault current and the rest that has not detected anything. We can therefore say for each section there is a sort of "signature" made of all the FIs states. And thinking the other way around, that for a given FI "signature" there is a corresponding faulty section.

We will first describe how the signature matrix is built. Considering "non directional" FIs, which possess only 2 states:

- 0: no fault current detected
- 1: a fault current is detected

"Directional" FIs will have 3 states:

- 0: no fault current detected
- 1: a downstream fault current is detected
- -1: an upstream fault current is detected

To build the signature matrix we will consider each section and look which FIs are on the fault current path. These FI's will be in state 1 (or -1 when the fault current is flowing upstream) and the others in state 0. The cases with upstream fault current detected can occur only if there is a distributed generation unit on the feeder and that it contributes to the fault current.

Let us consider the network of figure II.3 which has 6 sections which correspond to 6 different possible fault zones. Each zone has its corresponding signature.

For a fault on section n°3 for example, the FIs n°1, 2 and 3 will see a fault current flow, and FIs n°4, 5 and 6 will not see the fault current. We will therefore write that the signature of a fault on section n°3 is:

- $S_3 = [1\ 1\ 1\ 0\ 0\ 0]$

A signature can therefore be built for each section of the network. Regrouping all the signatures of each section together gives us a signature matrix (see table II.1) which gives for each possible faulty section the corresponding FI signature.

			Fault Indicator number					
			1	**2**	**3**	**4**	**5**	**6**
Number of faulty line	**Without DGU**	**1**	1	0	0	0	0	0
		2	1	1	0	0	0	0
		3	1	1	1	0	0	0
		4	1	1	1	1	0	0
		5	1	1	1	1	1	0
		6	1	1	1	1	1	1
	With DGU	**1**	1	-1	-1	-1	0	0
		2	1	1	-1	-1	0	0
		3	1	1	1	-1	0	0
		4	1	1	1	1	0	0
		5	1	1	1	1	1	0
		6	1	1	1	1	1	1

Table II.1: Signature Matrix of the simple 6 sections network, without or with presence of DGU

Cell colors are only here to help visualizing the signature matrix content

If we consider the same network but with the presence of a Distributed Generation Unit (DGU) between FIs n°4 and n°5, on a fault occurrence on section n°3 the FI n°4 will be in state -1 due to the upstream fault current that it will detect. The corresponding

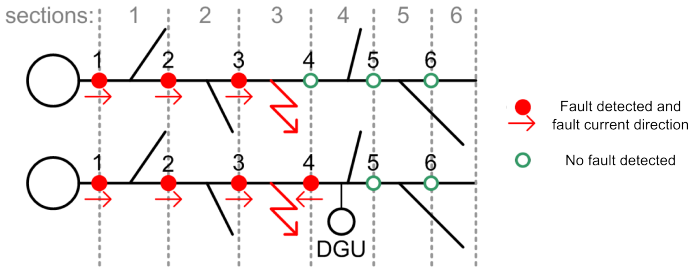

Figure II.3: Simple network (with and without DGU) with FIs seeing a fault on section n°3

fault signature of section n°3 for such a network is S_3 = [1 1 1 -1 0 0].

A fault localization algorithm could hence use such a fault signature matrix in order to instantly determine the faulty section depending of the network FIs states. However, as stated previously, the failure of this kind of equipment is not rare, and it would result in a fault signature which does not belong to the fault signature matrix.

Example of a fault signature which does not belong to the signature matrix:

- S_{fault} = [1 0 1 1 0 0] → FI n°2 is defective. Even if this signature is not in the signature matrix, it is quite easy to guess which FI is defective
- S_{fault} = [1 1 1 0 0 0] → FI n°4 is defective. For this signature, it is impossible to know that it is S_4 with a defective FI because the signature corresponds exactly to another existing signature, S_3.

3.2 Reasons of data corruption

We have been talking in the previous paragraphs of defective FIs which consequently corrupt the fault signature. But in a context of remotely retrieved information, data corruption can occur at various levels of the communication system. The probabilistic method developed in the following is therefore very interesting as it makes the fault localization process robust to data corruption of any kind.

3.3 Definition of functioning rates and probability coefficients

The proposed probabilistic method is based on various computations made from FI functioning rates and probability coefficients.

3.3.1 Functioning rates

Let us define the following rates:

- functioning rate of a FI: α, it is the probability that when its state is read the FI is functioning; (1-α) is therefore the probability that when its state is read the FI does not function.

- correct functioning rate of a FI: β, it is the probability that the FI is working correctly (meaning in its correct state for a given situation). (1-β) is therefore the probability that the FI is in a wrong state (not the state is should be considering the given situation).

A non-directional FI state has only two values (0 or 1), so for each correct state, there can be only one wrong state.

In the following, unless stated, α and β are equal to 0.95 (see appendix A for more details).

3.3.2 Probability coefficient associated to directional FIs

Directional FIs are slightly different. Indeed their state can take 3 values (0,1 or -1), which means that for each state there is one correct state and two wrong states. We can introduce new probability coefficients that will distribute wrong state probabilities between each two wrong states:

- ε: probability that when not working properly a FI is in state 1 instead of state 0 (1-ε) being the probability that the FI is in state -1 instead of 0
- ε': probability that when not working properly a FI is in state 1 instead of state -1 (1-ε') being the probability that the FI is in state 0 instead of -1
- ε": probability that when not working properly a FI is in state -1 instead of state 1 (1-ε") being the probability that the FI is in state 0 instead of 1

In the following, unless stated, ε is equal to 0.5, and ε' and ε'' are equal to 0.3 **(see appendix A for more details).**

3.4 State probabilities table

Now that state probabilities have been defined, we can compute for each possible situation the probabilities for a FI to be in one or another state. There are two main situations: the FI functions or does not. In the case that the FI functions there are two or three sub-situations (depending if the FI is directional or not): there is no fault, there is a downstream fault, there is an upstream fault. These cases are summarized in tables II.2 and II.3, and examples below show how the tables are filled.

State probabilities			FI's state	
			0	1
Situation	The FI does not function		$1-\alpha$	0
	The FI functions	Fault	$\alpha.(1-\beta)$	$\alpha.\beta$
		No fault	$\alpha.\beta$	$\alpha.(1-\beta)$

Table II.2: State probabilities of non-directional FIs

Using the probabilities defined in 3.3.1 and 3.3.2, we can define the state probabilities such as in the examples below.

Example for non-directional FIs:

Situation: the FI does not function → correct state = 0
State probabilities:

- $P(0) = (1 - \alpha)$, as defined, $(1 - \alpha)$ is the probability that the FI does not function
- $P(1) = 0$, since it does not function, the probability to be in state 1 is zero.

Situation: the FI functions and there is a fault → correct state = 1
State probabilities:

- $P(0) = \alpha.(1 - \beta)$, as defined, $(1 - \beta)$ is the probability that the FI does not function correctly. In order to be in state 0 when there is a fault, the FI functions (α) but not correctly $(1 - \beta)$.
- $P(1) = \alpha.\beta$

Example for directional FIs:

Situation: the FI does not function → correct state = 0
State probabilities:

- $P(0) = (1 - \alpha)$
- $P(1) = 0$
- $P(-1) = 0$

Situation: the FI functions and there is a downstream fault → correct state = 1
State probabilities:

- $P(0) = \alpha.(1 - \beta).(1 - \varepsilon')$, the FI functions and should be in state 1, therefore the probability that it is in state 0 is the probability that it functions (α) but not correctly $(1 - \beta)$ and also that the wrong state is 0 and not -1 (which corresponds to $(1 - \varepsilon')$, see 3.3.2)
- $P(1) = \alpha.\beta$
- $P(-1) = \alpha.(1 - \beta).\varepsilon'$

State probabilities			FI's state		
			0	1	-1
Situation	The FI does not function		$1 - \alpha$	0	0
	The FI functions	Downstream fault	$\alpha.(1 - \beta).(1 - \varepsilon')$	$\alpha.\beta$	$\alpha.(1 - \beta).\varepsilon'$
		Upstream fault	$\alpha.(1 - \beta).(1 - \varepsilon'')$	$\alpha.(1 - \beta).\varepsilon''$	$\alpha.\beta$
		No fault	$\alpha.\beta$	$\alpha.(1 - \beta).\varepsilon$	$\alpha.(1 - \beta).(1 - \varepsilon)$

Table II.3: State probabilities of directional FIs

By doing this for every situation possible, we can build the state probabilities table for non-directional and directional FIs.

3.5 Conditional probabilities table

Once state probabilities have been defined, we can define conditional probabilities. We will thereafter discuss about actual states and ideal states:

- the actual state is the state of the FI at a given time
- the ideal state is the state in which should be the FI for a given situation

The conditional probabilities will give us the probabilities for an FI to be in a given actual state knowing its ideal state : P(actual state/ideal state).

To compute the conditional probabilities, we will use the state probabilities tables II.2 and II.3. The method is simple: for a given actual state, we add the state probabilities of the two main situations (FI does not function and FI functions) since these two situations are disjointed sets. For the situation where the FI functions, we use the probability corresponding to the ideal state.

Examples: Let us compute the following conditional probabilities for directional FIs using II.3

$P(0/0)$ = probability of the FI to be in state 0 knowing that it should be in state 0

- the FI does not function: $1-\alpha$
- the FI functions / there is no fault: $\alpha.\beta$

$\rightarrow P(0/0) = 1-\alpha+\alpha.\beta$

$P(1/0)$ = probability of the FI to be in state 1 knowing that it should be in state 0

- the FI does not function: 0
- the FI functions / there is no fault: $\alpha.(1-\beta).\varepsilon$

$\rightarrow P(1/0) = 0+\alpha.(1-\beta).\varepsilon = \alpha.(1-\beta).\varepsilon$

The conditional state probabilities tables (Tables II.4 and II.5 for non-directional FIs, and tables II.6 and II.7 for directional FIs) are filled with the same reasoning for each combination actual state/ideal state.

		Ideal state	
		0	1
Actual State	0	$1-\alpha+\alpha.\beta$	$1-\alpha+\alpha.(1-\beta)$
	1	$\alpha.(1-\beta)$	$\alpha.\beta$

Table II.4: Conditional state probabilities table for non-directional FIs

These conditional state probabilities have been defined for the state of one FI. But we now need to consider the entire signature of the FIs of the network. We will define R as the response signature, meaning a signature composed of the states of the FIs during the

		Ideal state	
		0	1
Actual State	0	0.9525	0.0975
	1	0.0475	0.9025

Table II.5: Conditional state probabilities table for non-directional FIs - numerical values

fault. S_i will refer to the ideal signature of the FIs for a fault on section i. Therefore instead of defining the probability $P(actualstate/idealstate)$, we will define $P(R/S_i)$.

The $P(R/S_i)$ will be the sum of all the $P(actualstate/idealstate)$ for each of the FIs composing the signature R.

		Ideal state		
		0	1	-1
Actual State	0	$1-\alpha+\alpha.\beta$	$1-\alpha+\alpha.(1-\beta).(1-\varepsilon')$	$1-\alpha+\alpha.(1-\beta).(1-\varepsilon'')$
	1	$\alpha.(1-\beta).\varepsilon$	$\alpha.\beta$	$\alpha.(1-\beta).\varepsilon''$
	-1	$\alpha.(1-\beta).(1-\varepsilon)$	$\alpha.(1-\beta).\varepsilon'$	$\alpha.\beta$

Table II.6: Conditional state probabilities table for directional FIs

		Ideal state		
		0	1	-1
Actual State	0	0.95250	0.08325	0.08325
	1	0.02375	0.90250	0.01425
	-1	0.02375	0.01425	0.90250

Table II.7: Conditional state probabilities table for directional FIs - numerical values

3.6 Probabilities computation

We previously have computed the conditional probability P(R/Si), which corresponds to the probability of the signature response to be R knowing that it should be Si. However, this is not the probability that interests the distribution system operator. Indeed the DSO does not know Si since he does not know where is located the fault, but knows R, since it knows the states of the FIs. The probability that the DSO therefore wants to compute is P(Si/R) which translates into the probability that the fault is on section i knowing that the response signature is R.

In order to compute this probability, we will introduce in the following lines the various needed probabilities:

- $P(S_i)$: the probability that section i is faulty
- $P(S_i, R)$: the probability that section i faulty and that the response signature is R

- $P(R/S_i)$: the probability that the response signature is R knowing that section i is faulty
- and finally the probability that we want to compute, $P(Si/R)$: the probability that section i is faulty knowing that the response signature is R

We will need to use the following general probabilities formulas:

$$P(S_i, R) = P(S_i/R).P(R) = P(R/S_i).P(S_i) \tag{II.1}$$

$$P(R) = \sum_{S_i} P(S_i, R) = \sum_{S_i} P(R/S_i).P(S_i) \tag{II.2}$$

We can therefore obtain the following formula for $P(Si/R)$:

$$P(S_i/R) = \frac{P(R/S_i).P(S_i)}{P(R)} = \frac{P(R/S_i).P(S_i)}{\sum_{S_i} P(R/S_i).P(S_i)} \tag{II.3}$$

The equation can be simplified when considering the following hypothesis:
every section has the same probability to be faulty, therefore all $P(S_i)$ are equal and $P(S_i) = P(S)$

The equation then becomes:

$$P(S_i/R) = \frac{P(R/S_i)}{\sum_{S_i} P(R/S_i)} \tag{II.4}$$

Of course this hypothesis is debatable, the sections varying in length, age and electrical characteristics, they do not have the same probability of being faulty. However we will work for now with this hypothesis and introduce later section probabilities depending of their parameters. Observing equation II.4 shows that $P(S_i/R)$ can be computed with all the $P(R/S_i)$ which are known.

4 Application on a simple test case

In the following lines we will use the previously described probabilistic fault localization method on a simple test case. The goal is to see on a practical case how the method works.

4.1 Case description

Let us consider the very simple distribution network depicted in figure II.4. This network consists of a main feeder with a few laterals. It possesses 6 FIs which divide the network in 6 sections. We will consider two cases, one with a Distributed Generation Unit (DGU) as well as directional FIs and one without DGU and with non-directional FIs.

We consider a fault on section n°3 and that the response signature, constructed with the states of all the FIs of the network during the fault, is $R = [111000]$. In this example, no FI is faulty, they are all in their correct state for this fault situation.

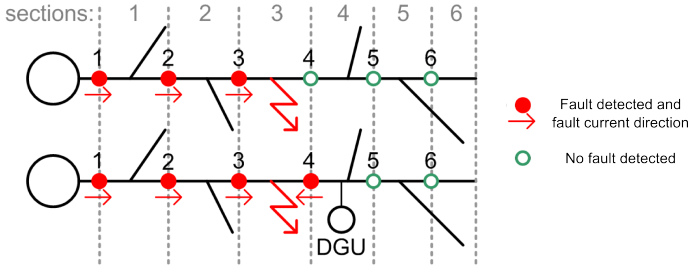

Figure II.4: Simple network (with and without DGU) with FIs seeing a fault on section n°3

R	[111000]		
Section i	S_i	$P(R/S_i)$	$P(S_i/R)$
3	[111000]	0.63524	0.89068
4	[111100]	0.05552	0.07785
2	[110000]	0.01672	0.02344
5	[111110]	0.00485	0.00680
1	[100000]	0.00044	0.00062
6	[111111]	0.00042	0.00059
0	[000000]	0.00001	0.00002

Table II.8: $P(S_i/R)$ results for the simple 6 sections network without DGU with a fault on section n°3

1. **Build the signature matrix for the network in both cases**
   This is the first step. It is necessary, before making any computation, to know all the possible fault signatures of the network. Since the network has 6 sections, there will be only 6 fault signatures, noted from S_1 to S_6. The signature matrix is shown in table II.1 in section 3.1.
2. **Compute all the $P(R/S_i)$ probabilities**
   For each signature S_i we can compute the probability $P(R/S_i)$. The results are presented in column n°3 of tables II.8 and II.9.
3. **Compute all the $P(S_i/R)$**
   Once all the $P(R/S_i)$ have been computed, we can compute the probabilities that interest us: $P(S_i/R)$. Classifying these probabilities from the highest to the lowest, we sort sections from the most possibly faulty to the least possibly faulty (see tables II.8 and II.9).

Table II.8 shows the results obtained for the simple 6 sections network without DGU for a fault on section n°3. We can see that the algorithm gives section n°3 as the most probably faulty section with a probability of 0.89. The second most probably section is section n°4 with a much lower probability of 0.08.

Looking at the three first most probably faulty section, we can see that the algorithm gives three sections that are consecutive (sections n°2, n°3 and n°4), therefore giving a

R	[1 1 1-1 0 0]		
Section i	S_i	$P(R/S_i)$	$P(S_i/R)$
3	[1 1 1-1 0 0]	0.60189	0.96775
2	[1 1-1-1 0 0]	0.00950	0.01528
4	[1 1 1 1 0 0]	0.00950	0.01528
5	[1 1 1 1 1 0]	0.00083	0.00134
1	[1-1-1-1 0 0]	0.00015	0.00024
6	[1 1 1 1 1 1]	0.00007	0.00012
0	[0 0 0 0 0 0]	0.0000003	0.0000005

Table II.9: $P(S_i/R)$ results for the simple 6 sections network with DGU with a fault on section n°3

great hint on which part of the network the fault seems to be located.

Table II.9 shows the results obtained for the simple 6 sections network with DGU for a fault on section n°3. Again the algorithm gives section n°3 as the most probably faulty with a probability of 0.97. We can note that the algorithm does not determine which section between sections n°2 and n°4 is the next most probably faulty section, but gives them equiprobably faulty.

4.2 Limits

We will now describe a few limitations of this method. Some of them are inherent to the method itself and can be overcome, some other depend of the FI equipment of the network.

- **Cases of equiprobability of sections to be faulty**
  In some cases (see table II.9), the algorithm can find more than one section as the most probably faulty. This is due to the fact that both parameters ε' and ε'' are equal. Consequently, as it can be seen in table II.6 and II.7, $P(0/1) = P(0/-1)$. Therefore, considering the following fault signatures as an example:
  - S_3 =[1 1 1 0 0-1-1]
  - S_7 =[1 1 1 0 0 1-1]
  - R =[1 1 1 0 0 0-1]

  we see that $P(S_3/R) = P(S_7/R)$. This means that for the response signature R, the algorithm will find that S_3 and S_7 are equiprobably faulty, and therefore will not be able to give a unique solution.

  To avoid these possible equiprobabilities, it is possible to not consider that all $P(S_i)$ are equal, and define section probabilities. This solution is presented in section 5.

- **Sections fault signatures resemblances and differences**

		Fault Indicator number											
		1	**2**	**3**	**4**	**5**	**6**	**7**	**8**	**9**	**10**	**11**	**12**
Number of faulty line	**1**	1	0	0	0	0	0	0	0	0	0	0	0
	2	1	1	1	0	0	0	0	0	0	0	0	0
	3	1	1	1	1	1	0	0	0	0	0	0	0
	4	1	1	1	1	1	1	1	0	0	0	0	0
	5	1	1	1	1	1	1	1	1	1	0	0	0
	6	1	1	1	1	1	1	1	1	1	1	1	0

Table II.10: Signature Matrix of the simple 6 sections network, with two FIs per section

In the simple network previously described we considered the presence of one FI per section. The consequence is that for each section its fault signature has only one difference with the previous and next section.

Let us look at the following fault response signature R, for a fault on section n°4, which contains an error (FI n°4) due to a defective FI for example:

- S_3 =[1 1 1 0 0 0]
- S_4 =[1 1 1 1 0 0]
- R =[1 1 1 0 0 0]

Since the defective FI is the last 'one' of the signature, the response signature R is strictly identical to the fault signature of the upstream section, S_3.

The more sections fault signatures are different, the less they can be mistaken in case of corrupted data. Let us imagine the same six sections simple network as before, but with two FIs per section (one at each end). Table II.10 shows the matrix signature of such a network.

An error in the response signature R is not enough to make a mistake between two correct fault signatures. The robustness of the signatures to corrupted data is therefore higher.

- **Choice of the values of the parameters α, β, ε, ε' and ε''**
  In order to seize the importance of the choice of the values of these parameters, an analysis has been made on two different levels:
  1. interactions between the parameters and consequences of the chosen values
  2. the consequences of the difference between the parameters values used in the algorithm and the "real" parameters values (of the equipment on the network)

  This work is detailed in appendix A.

5 Considering sections characteristics

When developing the method in section 3.6, we made an hypothesis stating that all $P(S_i)$ are equal, which can be translated into "every section of the network has the same probability of fault occurrence". A section being defined by all the lines/cables between two consecutive FIs, consequently they vary in length, conductor types and conductor ages. Therefore every section will have a different probability of being faulty, $P(S_i)$, and the following equation will be used for the probabilities computations:

$$P(S_i/R) = \frac{P(R/S_i).P(S_i)}{\sum_{S_i} P(R/S_i).P(S_i)} \tag{II.5}$$

In the following lines we show one way of computing the $P(S_i)$. However it should be considered as an example only, each Distribution System Operator should use its own parameters depending of the particularities of their network.

We can consider that each parameter is independent and that a probability coefficient can be associated to each one of them. The probability of a section to endure a fault event can be defined as the average value of these coefficients.

- We can define a length coefficient for each conductor i as: $\frac{l_i}{L_{tot}}$, l_i being the length of the conductor, L_{tot} being the sum of the length of all conductors
- We can define a conductor type coefficient (0.8 for a cable and 1.2 for a line for example) for each section i as: $\frac{t_i}{T_{tot}}$, t_i being a coefficient depending of the type of the conductor, and T_{tot} being the sum of the conductor type coefficients of all conductors
- We can define an age coefficient for each conductor i as: $\frac{a_i}{A_{tot}}$, a_i being the age of the conductor, A_{tot} being the sum of the ages of all conductors

We can therefore define the probability of a conductor to be faulty as:

$$P(S_i) = \frac{\alpha_1.\frac{l_i}{L_{tot}} + \alpha_2.\frac{t_i}{T_{tot}} + \alpha_3.\frac{a_i}{A_{tot}}}{\alpha_1 + \alpha_2 + \alpha_3} \tag{II.6}$$

The coefficients α_1, α_2 and α_3 can be used in order to dispatch the dominance of each parameter in the total probability.

Most of the time, sections will be composed of more than one conductor. Considering that a section i is made of n conductors, we will therefore use the following equation:

$$P(S_i) = \frac{\alpha_1.\frac{\sum_{j=1}^{n} l_j}{L_{tot}} + \alpha_2.\frac{\sum_{j=1}^{n} t_j}{T_{tot}} + \alpha_3.\frac{\sum_{j=1}^{n} a_j}{A_{tot}}}{\alpha_1 + \alpha_2 + \alpha_3} \tag{II.7}$$

In table II.11 we provide an example with parameters (length, type coefficient and age) chosen arbitrarily and with $\alpha_1 = \alpha_2 = \alpha_3 = 1$.

Results obtained when considering section characteristics are shown throughout Case 2 in section 7.2.

i	length (km)	$\frac{l_i}{L_{tot}}$	type coefficient	$\frac{t_i}{T_{tot}}$	age (years)	$\frac{a_i}{A_{tot}}$	$P(S_i)$
1	0.2	0.0930	1.2	0.188	10	0.118	0.133
2	0.15	0.0698	0.8	0.125	15	0.176	0.124
3	0.3	0.1395	1.2	0.188	14	0.165	0.164
4	0.75	0.3488	1.2	0.188	11	0.129	0.222
5	0.45	0.2093	1.2	0.188	20	0.235	0.211
6	0.3	0.1395	0.8	0.125	15	0.176	0.147
Total	$L_{tot} = 2.15$	1.0	$T_{tot} = 6.4$	1.0	$A_{tot} = 85$	1.0	1.0

Table II.11: Weighting of the $P(S_i)$ of each section in regards of length, type and age parameters (chosen randomly for the example)

6 Detection of faulty fault indicators

6.1 Minimum probability of a correct response signature

We will now observe which case gives the minimum event probability that corresponds to a correct response signature (i.e. a response signature identical to one of the signatures of the signature matrix of the network). We will therefore compute each $P(R_i/S_i)$ for $R_i = S_i$ for the previous network without DGU. The results are displayed in table II.12.

														$P(R_i/S_i)$
R_1	1	0	0	0	0	0	S_1	1	0	0	0	0	0	**0.70757**
R_2	1	1	0	0	0	0	S_2	1	1	0	0	0	0	**0.67043**
R_3	1	1	1	0	0	0	S_3	1	1	1	0	0	0	**0.63524**
R_4	1	1	1	1	0	0	S_4	1	1	1	1	0	0	**0.60189**
R_5	1	1	1	1	1	0	S_5	1	1	1	1	1	0	**0.57030**
R_6	1	1	1	1	1	1	S_6	1	1	1	1	1	1	**0.54036**

Table II.12: $P(R_i/S_i)$ results for $R_i = S_i$

We can see that for R_6 and S_6, $P(R_6/S_6) = 0.54036$, which is the lowest "event probability" for an event which has a correct response signature (here R_6). This is mathematically explained by the following facts:

- $P(0/0) = 1 - \alpha + \alpha.\beta > P(1/1) = \alpha.\beta$ since $\alpha \leq 1$
- $P(0/0) = 1 - \alpha + \alpha.\beta > P(-1/-1) = \alpha.\beta$ since $\alpha \leq 1$

Looking at the conditional state probabilities in tables II.5 and II.7 we can see that all the other probabilities: $P(0/1), P(1/0), P(0/-1), P(-1/0)$, and $P(1/-1)$ have lower numerical values. Therefore, mathematically, a response signature which has an error and does not correspond to any existing S_i will always be lower than the lowest $P(R_i/S_i)$ which corresponds to the signature S_i which has the most ones and/or minus ones. In the above case it is S_6.

$P(R_6/S_6) = 0.54036$ is the lowest "event probability" corresponding to an event with a correct response signature. Therefore, when a fault occurs and we retrieve a response signature R, by computing every $P(R/S)$ and comparing it to the lowest "event probability" described above, we can immediately detect if the FIs response signature contains errors or not.

Consequently, considering that for a unique k, $P(R_k/S_k)$ is the lowest "event probability", for any fault giving the response signature R, if there is a $P(R/S_i)$ such as $P(R/S_i) > P(R_k/S_k)$, it means that R does not contain any error. Otherwise, if every $P(R/S_i)$ is inferior to $P(R_k/S_k)$, the signature R contains an error.

In the results presentation, the probability corresponding to the lowest event probability will be called **boundary probability** while the maximum $P(R/S_i)$ for a given event and response R will be called **probability of the event**.

6.2 Finding faulty FIs

We just presented a method which allows to detect if the response signature R of a fault event contains errors or not. If the algorithm concludes that R contains errors, it is then very easy to find them.

Indeed, once field experts have confirmed which section is faulty they know the fault signature S_i, corresponding to the faulty section, that they should have received. It is therefore very simple to compare this signature with the real signature R received and identify which FIs are not in the state that they should have been.

Example with the simple 6 sections network in figure II.4: experts confirm that the fault occurred on section n°3. The fault signature associated to this section is:

- S_3 =[111000];

Let us assume that the response signature of the FIs following the fault event was:

- R =[011000]

Comparing these two signatures show that in R, FI n°1 is not in state 1 as it should be considering S_3. FI n°1 can therefore be considered as faulty.

It is important to note that even without confirmation by field experts, looking at the first probably faulty sections and comparing their signatures S_i to R gives a good idea of the possibly faulty FIs.

7 Results and performances

In this section we will apply the presented method on a special network designed in order to be representative of the different cases that the algorithm can face. Results will

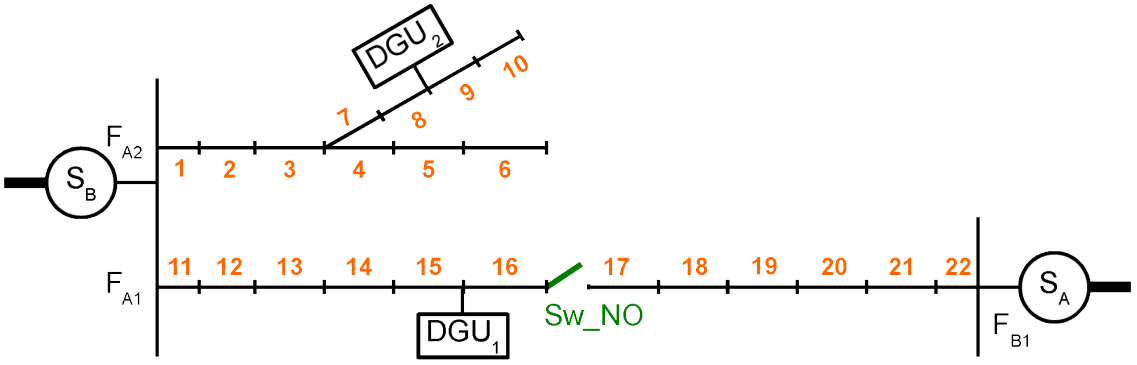

Figure II.5: Network

		FI number																					
		1	2	3	4	5	6	7	8	9	10	11	12	13	14	15	16	17	18	19	20	21	22
Section number	1	1	-1	-1	0	0	0	-1	-1	0	0	0	0	0	0	0	0	0	0	0	0	0	0
	2	1	1	-1	0	0	0	-1	-1	0	0	0	0	0	0	0	0	0	0	0	0	0	0
	3	1	1	1	0	0	0	-1	-1	0	0	0	0	0	0	0	0	0	0	0	0	0	0
	4	1	1	1	1	0	0	-1	-1	0	0	0	0	0	0	0	0	0	0	0	0	0	0
	5	1	1	1	1	1	0	-1	-1	0	0	0	0	0	0	0	0	0	0	0	0	0	0
	6	1	1	1	1	1	1	-1	-1	0	0	0	0	0	0	0	0	0	0	0	0	0	0
	7	1	1	1	0	0	0	1	-1	0	0	0	0	0	0	0	0	0	0	0	0	0	0
	8	1	1	1	0	0	0	1	1	0	0	0	0	0	0	0	0	0	0	0	0	0	0
	9	1	1	1	0	0	0	1	1	1	0	0	0	0	0	0	0	0	0	0	0	0	0
	10	1	1	1	0	0	0	1	1	1	1	0	0	0	0	0	0	0	0	0	0	0	0
	11	0	0	0	0	0	0	0	0	0	0	1	-1	-1	-1	-1	0	0	0	0	0	0	0
	12	0	0	0	0	0	0	0	0	0	0	1	1	-1	-1	-1	0	0	0	0	0	0	0
	13	0	0	0	0	0	0	0	0	0	0	1	1	1	-1	-1	0	0	0	0	0	0	0
	14	0	0	0	0	0	0	0	0	0	0	1	1	1	1	-1	0	0	0	0	0	0	0
	15	0	0	0	0	0	0	0	0	0	0	1	1	1	1	1	0	0	0	0	0	0	0
	16	0	0	0	0	0	0	0	0	0	0	1	1	1	1	1	1	0	0	0	0	0	0
	17	0	0	0	0	0	0	0	0	0	0	0	0	0	0	0	0	1	1	1	1	1	1
	18	0	0	0	0	0	0	0	0	0	0	0	0	0	0	0	0	0	1	1	1	1	1
	19	0	0	0	0	0	0	0	0	0	0	0	0	0	0	0	0	0	0	1	1	1	1
	20	0	0	0	0	0	0	0	0	0	0	0	0	0	0	0	0	0	0	0	1	1	1
	21	0	0	0	0	0	0	0	0	0	0	0	0	0	0	0	0	0	0	0	0	1	1
	22	0	0	0	0	0	0	0	0	0	0	0	0	0	0	0	0	0	0	0	0	0	1

Table II.13: Signature matrix of the network designed to test the method's performance
Cell colors are only here to help visualizing the signature matrix content

be analyzed and we will study the performances of the method

The network shown in figure II.5 possesses two substations S_A and S_B. Substation A has two feeders, F_{A1} and F_{A2}, while substation B has only one, F_{B1}. The two feeders F_{A1} and F_{B1} are connected by a normally open switch (Sw_NO) making it possible for one substation to backup the other one in case of a fault on one of these two feeders. The other feeder of substation A is not connected to another backup substation, but has a lateral secondary line. Two Distributed Generation Unit (DGU) are connected to this network, one on F_{A1}, and one on the lateral of F_{A2}.

We will consider that the network is only equipped by one FI per section, located on the upstream side of the section. Table II.13 shows the signature matrix for the 22 sections of this network.

7.1 Results for various situations

We will develop here the results obtained with the algorithm for some particular situations. But we will first recall the needed inputs of the algorithm and the outputs that are produced.

- **Inputs:**
  - Signature matrix of the network corresponding to its topology on fault occurrence
  - [optional] Characteristics of the sections: length, conductor type, age
  - Fault response signature of the FIs of the network
- **Outputs:** the output is a script containing the following information
  - Boundary event probability to identify a signature without errors
  - Event probability
  - List of section classified from most probably to least probably faulty
  - Analysis of the possibly defective FIs

The four following cases are presented in order to illustrate the different situations which the algorithm can face. In theses cases, the sections probabilities to be faulty have not been used, instead the simplified equation II.4 is used to compute the results.

1. **Case 1: fault on section n°4 - No data corruption in the response signature**

   Let us consider a fault on section n°4, and a response signature R made of the 22 FIs actual states without any errors. We will therefore have:

   - R =[111100-1-100000000000000]

   The following script is the output of the algorithm for the signature matrix of table II.13 and the response signature R above.

```
****
  Minimum probability to identify a perfect signature
  (also called boundary probability): 0.23502
  Probability of this event : 0.24804
  Section 4: P(S4/R) = 0.89111
  Section 5: P(S5/R) = 0.077884
  Section 3: P(S3/R) = 0.02345
****
  Most probable faulty line : 4
****
  Analysis of potentially defective FIs:

  Analysis of the first probable answer:
  Section 4: P(S4/R) = 0.89111
  No FI is faulty.
```

```
Analysis of the second probable answer:
Section 5: P(S5/R) = 0.077884
FI n°5 faulty on line n°5
  Wrong answer of FI: 0
  instead of: 1
```

We see here an example of a perfect response signature not containing any errors. The algorithm therefore identifies section n°4 as the most probably faulty. Section n°5 is the second most probably faulty section, but with a much lower probability.

2. **Case 2: fault on section n°7 - Dysfunction of one FI**

We will now consider a fault on section n°7. Furthermore we will use a response signature R which contains an error, the dysfunction of FI n°7 which results in the FI being in state 0 instead of state 1:

- R =[1110000-100000000000000]

The following script is the output of the algorithm:

```
****
  Minimum probability to identify a perfect signature
  (also called boundary probability): 0.23502
  Probability of this event : 0.024148
  Section 3: P(S3/R) = 0.4697
  Section 7: P(S7/R) = 0.4697
  Section 4: P(S4/R) = 0.041052
  [...]
****
  Most probable faulty lines: 3 or 7
****
  Analysis of potentially defective FIs:

  Analysis of the first probable answer:
  Section 3: P(S3/R) = 0.4697
  FI n°7 faulty on line n°7
    Wrong answer of FI: 0
    instead of: -1

  Analysis of the second probable answer:
  Section 7: P(S7/R) = 0.4697
  FI n°7 faulty on line n°7
    Wrong answer of FI: 0
    instead of: 1
```

First of all we can see that the event probability is lower than the boundary probability, which means that the response signature R contains at least one error and

does not correspond to any fault signature of the signature matrix.

The algorithm finds two sections as the most probably faulty, meaning that both sections have the same probability to be faulty. This is due to the fact that we present here results obtained with equation II.4 and not equation II.5. We introduce here the notion of "doubt" since the algorithm finds more than one section as most probably faulty (see performance results in 7.2).

For the first two probable answer, a 'defective FI analysis' is made. The analysis of section n°3 as the faulty section shows that if this section is really faulty, then the FI n°7 is defective and should have been in state **-1** instead of **0**.
When considering the second probable answer, section n°7, the analysis shows that if this section is really faulty, then the FI n°7 is defective and should have been in state **1** instead of **0**.

We see through this example that the algorithm can not always give a unique solution (see section 5 to see how to avoid this). However sections n°3 and n°7 are consecutive, which is already a good information on where the fault seems to be located. Furthermore the first two probable answers give the FI n°7 as defective, which is what was simulated by giving the input R =[1110000-100000000000000] to the algorithm.

3. **Case 3: fault on section n°7 - Incoherent functioning of one FI**

We will finally consider a fault on section n°7 and will use a response signature R which contains an incoherent error, the dysfunction of FI n°7 which results in the FI being in state 1 instead of state 0:

- R =[1110101-100000000000000]

The following script is the output of the algorithm:

```
****
  Minimum probability to identify a perfect signature
  (also called boundary probability): 0.23502
  Probability of this event : 0.0065274
  Section 7: P(S7/R) = 0.91597
  Section 5: P(S5/R) = 0.048034
  Section 3: P(S3/R) = 0.014463
  [...]
****
  Most probable faulty line: 7
****
  Analysis of potentially defective FIs:

  Analysis of the first probable answer:
  Section 7: P(S7/R) = 0.91597
```

```
FI n°5 faulty on line n°5
  Wrong answer of FI: 1
  instead of: 0

Analysis of the second probable answer:
Section 5: P(S5/R) = 0.048034
FI n°4 faulty on line n°4
  Wrong answer of FI: 0
  instead of: 1
FI n°7 faulty on line n°7
  Wrong answer of FI: 1
  instead of: -1
```

The event probability is again much lower than the boundary probability identifying a perfect signature. We therefore immediately know that the response signature contains an error.

The algorithm finds section n°7 as faulty with a high probability compared to the second and third proposed section. The analysis of this answer shows that if this section is really faulty, then the FI n°5 is defective and is in state **1** instead of the correct state **0**.

If we take a look at the second most probable answer, section n°5, we see that if this section is really faulty, then two FIs are defective. FI n°4 is in state **0** instead of state **1** and FI n°7 is in state **1** instead of **-1**.

4. **Case 4: fault on section n°9 - Incoherent functioning of one FI misleading the algorithm**

In this last example we will consider a fault on section n°9 and will use a response signature R which contains an error: the dysfunction of FI n°9 which results in the FI being in state 0 instead of state 1. R =[11100011000000000000000].

The following script is the output of the algorithm:

```
****
  Minimum probability to identify a perfect signature
  (also called boundary probability): 0.23502
  Probability of this event : 0.26178
  Section 8: P(S8/R) = 0.89116
  Section 9: P(S9/R) = 0.077889
  Section 7: P(S7/R) = 0.023452
  [...]
****
  Most probable faulty line : 8
****
```

```
Analysis of potentially defective FIs:

Analysis of the first probable answer:
Section 8: P(S8/R) = 0.89116
No FI is faulty.

Analysis of the second probable answer:
Section 9: P(S9/R) = 0.077889
FI n°9 faulty on line n°9
  Wrong answer of FI: 0
  instead of: 1
```

The algorithm gives section n°8 as the most probably faulty section. Section n°9 is the second answer. In this case the "corrupted" response R corresponds to the existing fault signature S_8, therefore the algorithm finds a perfect match, and of course section n°8 turns out as the most probably faulty.

However, despite this wrong result from the algorithm, we can make the following comments:

- the algorithm is not totally wrong as it finds a section which is adjacent to the faulty section
- this problem is due to the small difference (only one state) between two signatures of two consecutive sections, and can be addressed by increasing the signatures differences (see section 4.2)

We see through these examples that the algorithm gives an instantaneous state of the situation and the most probable scenarios: faulty sections and defective FIs if there are any. The immediate knowledge of the most probable fault situation is a very useful information in order to conduct effective on field maintenance. The expert can now focus on a prioritized area, with a great chance to quickly find the fault location and conduct the necessary operations.

7.2 Performances

In order to evaluate the algorithm we also developed a method to measure and analyze the algorithm performances. With the lack of real fault data, the only evaluation possible here is the evaluation of the robustness of the algorithm to corrupted response signatures.

In order to simulate fault events we will need to simulate response signatures. Each section of the network (22 in total) will therefore be simulated as faulty. For each section we will make 10000 response signature draws. Each FI state of the signature will be drawn following the density function defined by the conditional probabilities (table II.7).

Remark: the choice of 10000 signature draws is a compromise between results precision and computing time. With another 10000 draws, the results will differ slightly, however the precision is good enough for a one digit after decimal number.

The following example shows how the signature draws are made:

1. Let us consider section n°6 and its fault signature S_6 =[111111-1-1000000000000000].

2. We can create 10000 response signatures R_6 based on the following procedure:
   - compute all the conditional probabilities based on the chosen α, β, ε, ε' and ε'' parameters (see table II.7 for our case)
   - for each ideal FI state, create the density function based on the conditional probabilities
     Example with FI n°1 of S_6:
     - ideal state = 1
     - $P(1/1) = 0.90250$, $P(-1/1) = 0.01425$ and $P(0/1) = 0.08325$
     - make a random draw of the actual state of FI n°1 using this distribution (on 10000 draws, we will have a total of 9025 **1**, 142.5 **-1** and 832.5 **0**).

3. We can finally input each of the 10000 response signatures created to the algorithm

For each response signature input, we observe the solution of the algorithm and classify it. Considering that we use the algorithm without weighting the probabilities of the sections depending of their characteristics, there will be the three following results' class:

- **success**: the faulty section is the most probably faulty section suggested by the algorithm (see "Case 1" and "Case 3" in 7.1)
- **failure**: the faulty section is not the most probably faulty section suggested by the algorithm (see "Case 4" in 7.1)
- **doubt**: the faulty section is part of the equiprobably faulty sections suggested by the algorithm (see "Case 2" in 7.1)

Remarks on the method:

- for each section we realize 10000 response signature draws
- the signature is limited to the FIs of the concerned feeder (when the signature matrix contains more than one feeder)
- all the FI states of the signature are drawn using the density function

The robustness results are presented for two different cases. The first one uses the simple equation II.4 to compute the solution, therefore with every $P(S_i)$ equal. The second one uses equation II.8, with $P(S_i)$ defined for each section depending of the sections length and conductor type:

$$P(S_i) = \frac{\frac{\sum_{j=1}^{n} l_j}{L_{tot}} + \frac{\sum_{j=1}^{n} t_j}{T_{tot}}}{2} \tag{II.8}$$

1. **Case 1: Robustness results with equal $P(S_i)$ for all sections**
   Figure II.6 shows the robustness results of the algorithm using the robustness evaluation method described above. The section probabilities to be faulty are all equal,

therefore the algorithm finds, for a certain amount of cases, more than one probably faulty section. We can see that the mean success on the 10000 response signatures draws is of 85.5 %. The minimum success rate being 76.1 % for fault n°3, and the maximum success rate being 94.7 % for fault n°22. The results are summarized in table II.14.

There are two ways of interpreting the "doubts" answers depending of how the DSO looks at it:

- "doubts" can be seen as positive answers since the correct faulty section is among the faulty sections suggested by the algorithm. The algorithm has then a mean "success+doubts" of 91.8 %.
- the DSO only consider a unique solution as a positive answer, therefore "doubts" are not considered as positive. The DSO might prefer the solution with defined $P(S_i)$ for every section which results in the quasi impossibility to have "doubts" (see 5 and the following "Case 2" results)

8.3 % mean failures explanation: all failures are due to the fact that the drawn response signature R is corrupted and strictly identical to an existing fault signature different from the fault signature of the concerned fault. The only solution to this problem is to increase the signatures differences between two consecutive fault signatures in order to limit the possible mistakes. This solution is presented in 4.2.

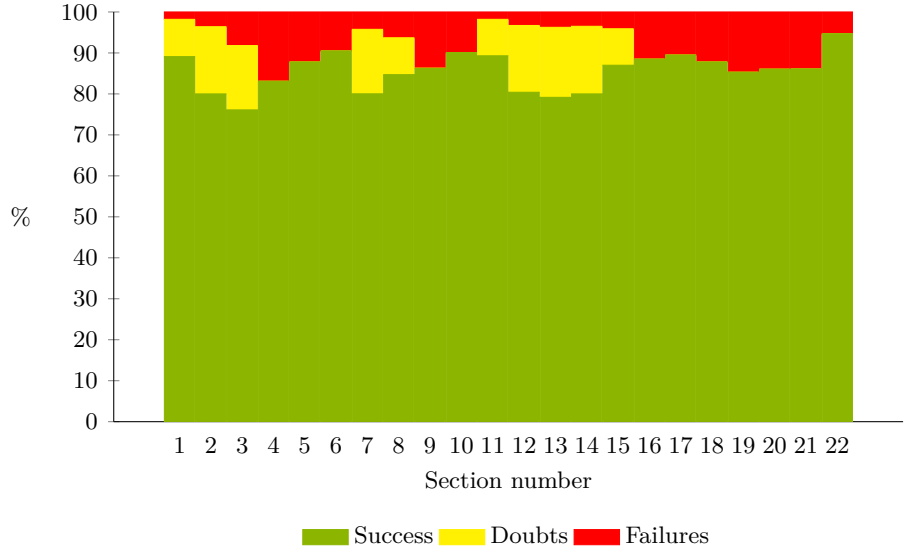

Figure II.6: Case 1 robustness results of the algorithm for the network shown in figure II.5

Mean success: 85.5 %, doubts: 6.2 % and failures: 8.3 %

	Success	Doubts	Failures
Max.	94.9 %	17.3 %	16.4 %
Mean	85.5 %	6.2 %	8.3 %
Min.	75 %	0 %	1.5 %

Table II.14: Results summary for case 1

2. **Case 2: Robustness results with a defined $P(S_i)$ for each section**
In figure II.7, the shown results are obtained with the same robustness evaluation method as previously. However this time the section probabilities to be faulty are weighted depending of the sections characteristics with equation II.8. The consequence is that the chances that the algorithm finds sections equiprobably faulty are slim, in our case the algorithm never finds sections equiprobably faulty, therefore the mean doubts rate is 0 %. Consequently, the mean rates of success and failures both increase respectively up to 88.4 % and 11.6 %, some doubts being transformed in success and others into failures. The results are summarized in table II.15.

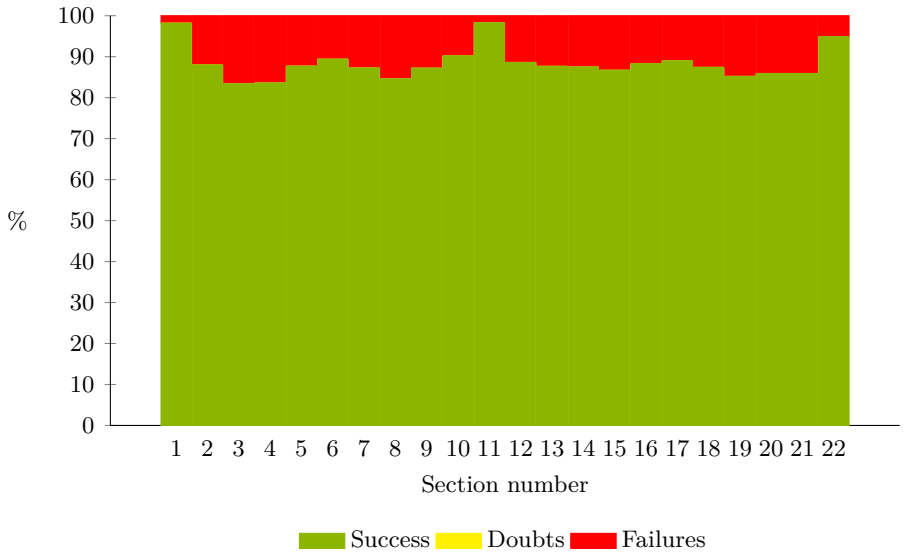

Figure II.7: Case 2 robustness results of the algorithm for the network shown in figure II.5
Mean success: 88.4 %, doubts: 0 % and failures: 11.6 %

	Success	Doubts	Failures
Max.	98.3 %	0 %	16.6 %
Mean	88.4 %	0 %	11.6 %
Min.	83.4 %	0 %	1.7 %

Table II.15: Results summary for case 2

8 Conclusion

The work presented in this chapter was done in the context of development of new fault localization methods especially taking into account the smart-grid evolutions of distribution networks.

The initial problem is the limitations that faces today fault localization techniques, as reminded in section 2. The developed method is based on the use of fault indicators (FIs) which already equip most of distribution networks, and on the smart-grid evolution, especially in terms of FI state communication.

The method presented is defined as probabilistic since it is based on probability definitions of the possible FIs states, and probability computations using the expected FIs states depending of fault locations (see section 3.1) and the real retrieved FIs states during a fault (see section 3.6).

The presented results show that the performance of the method is quite good and robust to FI failures with a mean success to identify the faulty section over 85 % for the network used in our work. Furthermore, when the algorithm gives the wrong section as faulty, it often gives a section close to the real faulty section, thus still giving a good indication to the DSO on where is the faulty area.

Another aspect of the method is a positive side-effect which results from a conclusion that can be made when the algorithm finds the correct faulty section based on a FI signature which contains errors: in this case it means that the algorithm has identified one or more FI failures. This is precious information for the DSO as it helps maintaining the equipment while still finding the correct faulty section, which is not possible at the time with classic techniques.

This method can therefore bring many improvements, without needing great investments, to the faulty section localization techniques. Furthermore, this method can be associated to a fault distance computation algorithm in order to make a complete and precise fault localization algorithm.

Chapter III

Fault Localization Method

Contents

Abstract

We develop in this chapter a fault localization method which localizes the fault in terms of distance to the head of the feeder. We will describe the principle of the method and its origins before adapting it to the particularities of distribution networks. New approach for particular networks or special faults will also be presented.

1 Introduction

The fault localization method developed and presented in this chapter is based on the fault distance computation. This type of computation is a hard task as it depends of so many factors. For example it can depend of the precision of measurements, the knowledge and precision of the network characteristics, which are factors which can be handled up to a certain point. But it also depends of unknown factors such as the fault characteristics, its resistance, its type, etc.

Fault localization techniques which are at an advanced stage are designed for transmission networks which consist of much more "simple" network, due to their long lines without tapped loads, with the same cable/line type. However the meshed nature of transmission networks brings specific problems to fault localization since fault currents can flow downstream as well as upstream.

The particularities of distribution networks, which are their radial nature, tapped loads and unknown real time consumption, various types of cables/lines, bring the need to adapt the existing fault localization method as they do not work as is.

2 Fault localization using the Takagi method

2.1 Principle developed by Takagi

As introduced in Chapter I, an equation to compute the fault distance on a line of a transmission network was developed in 1982 by T.Takagi [Takagi et al., 1982]. This equation is based on the electrical equations of the loop formed by a single-phase to ground resistive fault (see figure III.1).

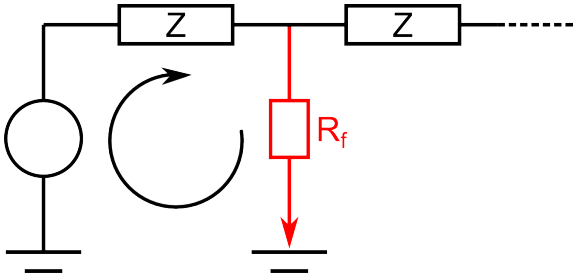

Figure III.1: Fault loop impedance

The main technical particularity of the method is to use currents and voltages from one terminal only, which is unusual for transmission networks. In [Takagi et al., 1982], the author describes the method using a single phase circuit with a fault. The technique is to separate the circuit in two equivalent circuits: the pre-fault load flow component and the fault current component (see figure III.2), which gives two equations describing the voltage (or current) at the fault point. By working around with the equations and making two mathematical assumptions (see appendix B for details), the author succeeds in providing

an expression of the fault distance depending of the following parameters: terminal voltage, terminal current, line impedance per unit length, and the difference between pre-fault terminal current and during-fault terminal current.

However this method has been developed for transmission networks. The particularities of these networks is to have long lines without any loads between two consecutive nodes. One of the approximations made by this method is to consider that all the loads are lumped beyond the fault point, which of course is not an acceptable approximation for distribution networks.

Figure III.2 shows the single phase circuit considered and the two equivalent circuits obtained using the superposition principle [Takagi et al., 1982, Ferracci, 1995].

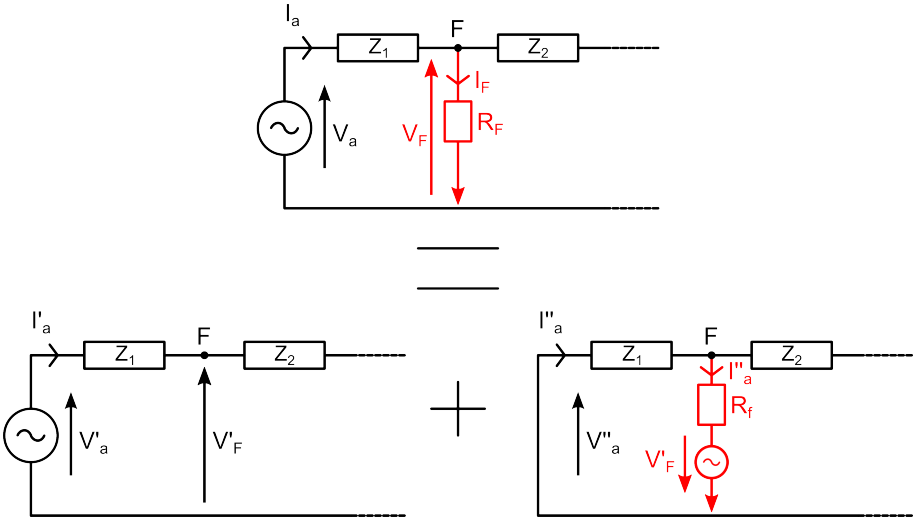

Figure III.2: Superposition principle on a single phase circuit enduring a phase to ground fault

As previously stated, one of the circuit corresponds to the pre-fault component, while the other corresponds to the fault component. The equation obtained with this approach is the following (the details on how to obtain this equation are presented in appendix B):

$$x = \frac{\mathrm{Im}\left(V_a.{I''}_a^*\right)}{\mathrm{Im}\left(z_1.I_a.{I''}_a^*\right)} \tag{III.1}$$

with the following terms:

- x fault distance
- V_a phase terminal voltage
- I_a phase terminal current
- ${I''}_a^*$ difference between pre-fault phase terminal current and during-fault phase terminal current
- z_1 line impedance per unit length

Below are the advantages of the method:

- few data is needed
- once the measurements are made, the computation is quick and simple (compared to an iterative method for example, see table I.1 in chapter I).

2.2 Adaptation to distribution networks

Recent works [Karnik et al., 2011] have developed the principle exposed by T.Takagi for distribution networks. The equation used to compute the fault distance is derived from the expression of the symmetrical components voltages at the terminal point of the network (see figure III.3).

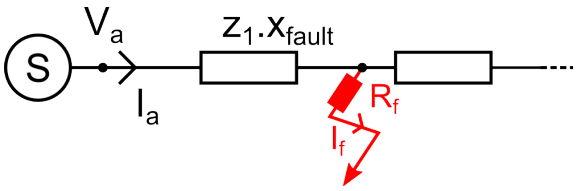

Figure III.3: Distribution network with a phase to ground fault

The symmetrical components voltages are the following:

$$\begin{aligned} V_1 &= I_1.Z_1 + V_{f1} \\ V_2 &= I_2.Z_2 + V_{f2} \\ V_0 &= I_0.Z_0 + V_{f0} \end{aligned} \tag{III.2}$$

with:

V_0, V_1, V_2	symmetrical components voltages at monitoring point
I_0, I_1, I_2	symmetrical components currents at monitoring point
Z_0, Z_1, Z_2	symmetrical components line impedance between monitoring and fault points
V_f	voltage at fault point

Summing the three lines in III.2 and taking $Z_1 = Z_2$ which is true for static equipment such as electrical lines gives:

$$V_a = V_f + (I_1 + I_2).Z_1 + I_0.Z_0 \tag{III.3}$$

Replacing V_f by $R_f.I_f$ and rearranging the other terms leads to this final equation:

$$V_a = Z_1.(I + I_0.\frac{Z_0 - Z_1}{Z_1}). + R_f.I_f \tag{III.4}$$

with $I_a = I_0 + I_1 + I_2$ and $V_a = V_0 + V_1 + V_2$.

In III.4 symmetrical components line impedances can be expressed by a distance term, x, and a per unit length impedance, z_i. We can furthermore define an impedance ratio term, K, to visually simplify the equation.

$$Z_0 = x.z_0,\ Z_1 = x.z_1 \ and \ Z_2 = x.z_2$$

therefore:

$$K = \frac{Z_0 - Z_1}{Z_1} = \frac{z_0 - z_1}{z_1}$$

Finally we can write the following equation:

$$V_a = x.z_1.I_{tot} + R_f.I_f \tag{III.5}$$

with $I_{tot} = I_a + I_0.K$.

Equation III.5 is the base equation of different fault loop impedance methods: the positive sequence reactance method and the Takagi method. Each method has its own way of dealing with the unknown variables of the equation. In [Takagi et al., 1982], the assumption that the fault current is the difference between the pre-fault current and the during-fault current at the monitored point (noted I''_a) is used in order to replace I_f. I''_a is a variable that can be computed from measurements.

The next step of the Takagi method is a way to eliminate the last unknown term of the equation, R_f. However one necessary assumption is to consider that the fault impedance is only resistive (therefore noted R_f) and does not contain a reactive part. Even if this assumption is generally considered, few studies have been conducted, to our knowledge, to justify it. Anyway, a way to eliminate R_f from the equation is to multiply both sides of the equation by the conjugate of I''_a, noted I''^*_a.

We can therefore write:

$$V_a.I''^*_a = x.z_1.I_{tot}.I''^*_a + R_f.I''_a.I''^*_a \tag{III.6}$$

Rearranging and taking the imaginary part of III.6 we obtain equation III.7 since R_f is real and the imaginary part of a complex multiplied by its conjugate is null.

The fault distance Takagi equation is therefore:

$$x = \frac{\mathrm{Im}\left(V_a.I''^*_a\right)}{\mathrm{Im}\left(z_1.I_{tot}.I''^*_a\right)} \tag{III.7}$$

3 Fault localization algorithm

3.1 Dealing with the network heterogeneity

One of the main difficulty of fault localization for distribution networks is to deal with the heterogeneity of the network regarding the type of conductors and the load distribution. It is very common that a distribution feeder contains several different types of conductors, often due to a decreasing conductor section as less and less loads are connected downstream.

Regarding equation III.7 it is clear that the network heterogeneity will be a problem when choosing the value of the per unit length impedance z_1. Solutions which consist in taking an average per unit length impedance or the value of the most present conductor have the advantage to be easy to implement but lead to a certain error [Kulkarni et al., 2011].

As already stated in section 2.1 the Takagi method makes the assumption that the loads of the network are lumped behind the fault point which is again an unacceptable approximation for distribution networks.

Considering that this method is well suited for an homogeneous network with load at the end of the line, the idea is to divide an heterogeneous network in sections which respect this criterion. Consequently, a section is defined by a line element with or without a load at the end such as in figure III.4. Each section is now compatible with the method without any assumptions.

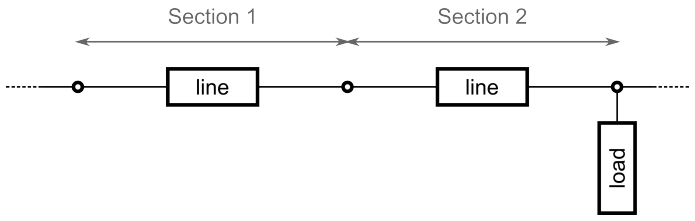

Figure III.4: Example of sections with and without presence of a load

It is important to consider that the loads are at the end of one section, and not at the beginning of the following one, since in order to compute a fault distance on a line section it is necessary to know the currents flowing only into the line.

In order to fully deal with the heterogeneity of the network, it is now necessary to obtain the voltages and currents of each phase at every upstream node of a section. Assuming that every section will be equipped with sensors is not a realistic solution considering the cost that it would represent. It is therefore necessary to find a way to estimate or compute voltages and currents at each section node. The solution developed in our work is based on the work of Till Wellfonder [Welfonder, 1998] and consists in propagating downstream the measures made at the head of the feeder.

- **Achieving voltage and current propagation**

  Considering three-phases distribution networks, each element (a line or a load) possess four (three phases and the ground) inputs and four outputs. Transforming each element into the three independent symmetrical components gives for each symmetrical component a quadripole element (two inputs and two outputs) (figure III.5).

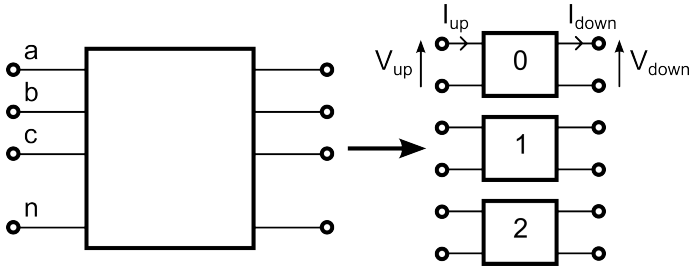

Figure III.5: Transformation of network elements into symmetrical components quadripoles

Using quadripoles to describe the network presents various advantages. It becomes first of all easier to browse through the network and it is easier to express input and output variables as a function of each other.

Two matrices can be defined, one for expressing outputs as a function of inputs (matrix B), and the other for expressing inputs as a function of outputs (matrix A):

$$\begin{bmatrix} V_{up} \\ I_{up} \end{bmatrix} = A. \begin{bmatrix} V_{down} \\ I_{down} \end{bmatrix} = \begin{bmatrix} a_{11} & a_{12} \\ a_{21} & a_{22} \end{bmatrix} . \begin{bmatrix} V_{down} \\ I_{down} \end{bmatrix}$$
$$and \tag{III.8}$$
$$\begin{bmatrix} V_{down} \\ I_{down} \end{bmatrix} = B. \begin{bmatrix} V_{up} \\ I_{up} \end{bmatrix} = \begin{bmatrix} b_{11} & b_{12} \\ b_{21} & b_{22} \end{bmatrix} . \begin{bmatrix} V_{up} \\ I_{up} \end{bmatrix}$$

Using the voltage and current measurements at the head of the feeder, it is possible to browse the feeder and to compute section by section the next downstream node voltages and currents using matrix B. However, the content of matrix B needs first to be defined for each element.

There will be one matrix A and one matrix B for each sequence of the symmetrical components: A_0, A_1, A_2, B_0, B_1 and B_2.

- **Defining the B matrix content for each element type**

A quadripole element can have series and parallel components. Series components will be considered as an impedance and noted Z while parallel components will be considered as an admittance and noted Y.

Let us consider a line element simply modeled by an impedance. There will be a voltage drop between the input and output but no change in the current. The quadripole and A and B matrix describing this element are shown in figure III.6.

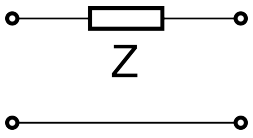

$$A = \begin{bmatrix} 1 & Z \\ 0 & 1 \end{bmatrix} \qquad B = \begin{bmatrix} 1 & -Z \\ 0 & 1 \end{bmatrix}$$

Figure III.6: A and B matrix of a serie impedance quadripole

Let us now consider a load element. The input and output voltage will be the same, but the output current will be equal to the input current minus the load current. The quadripole and A and B matrix describing this element are shown in figure III.7.

Using these two base elements it is simple to build the A and B matrix of a PI-model line element, shown in figure III.8.

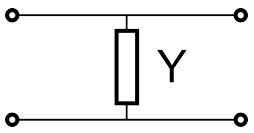

$$A = \begin{bmatrix} 1 & 0 \\ Y & 1 \end{bmatrix} \qquad B = \begin{bmatrix} 1 & 0 \\ -Y & 1 \end{bmatrix}$$

Figure III.7: A and B matrix of a parallel admittance quadripole

We will remind here that, for distribution networks, the length of each section is small enough in order to use a PI-model for the line elements without introducing substantial errors due to propagation which is not taken into account by this model (indeed, line pi-model are usually used to simulate lines over 50 km [Sabonnadière and Hadj-Said, 2007]).

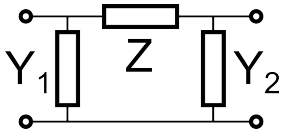

$$A = \begin{bmatrix} 1 + Y_2.Z & Z \\ Y_1 + Y_2 + Y_1.Y_2.Z & 1 + Y_1.Z \end{bmatrix} \qquad B = \begin{bmatrix} 1 + Y_1.Z & -Z \\ -Y_1 - Y_2 - Y_1.Y_2.Z & 1 + Y_2.Z \end{bmatrix}$$

Figure III.8: A and B matrix of a pi model line quadripole

- **Loads and lines aggregation when browsing through the network**

  We previously described how to model the different network elements (lines and loads) and how to compute the voltage and current at the downstream node of an element. The fault localization algorithm can now start with the voltage and current measurements at the head of the feeder and browse through the network, section by section (see III.4), in order to execute the fault distance computation.

  The browsing function of the algorithm can be very simple for an urban feeder composed of one straight line with tapped loads. However, when the network is a typical rural network with many junctions, each lateral must be aggregated into a load in order to be taken into account when browsing downstream the lateral.

  Figure III.9 shows a network with a main feeder (F, blue) and three laterals (L_1, red, L_2, green and L_3, orange). It is important to understand that during the fault localization process, the faulty branch is not known, therefore each branch has to be explored, and the upstream branches aggregated as loads. Below are a few examples to illustrate the method:

  – exploration of the branch upstream of node N_1

    $\Rightarrow$ no aggregation needed

– exploration of the branch between nodes N_1 and N_2

  ⇒ aggregation of L_3 in N_3 as a load

  ⇒ aggregation of L_1 (plus L_3 aggregated) in N_1 as a load

– exploration of the branch downstream node N_3

  ⇒ aggregation of L_3 in N_3 as a load

  ⇒ aggregation of L_2 in N_2 as a load

  ⇒ aggregation of part of F (below N_1) (plus L_2 aggregated) in N_1 as a load

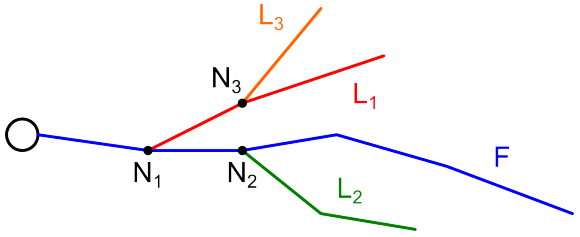

Figure III.9: Lateral to explore and aggregate

Figure III.10 shows a feeder with a lateral composed of four sections and two loads. When computing voltages and currents beyond node N_1, it is necessary to aggregate the lateral as a load in order to take into account the current that the lateral is consuming during the fault. The same load model is considered during the fault than under healthy functioning.

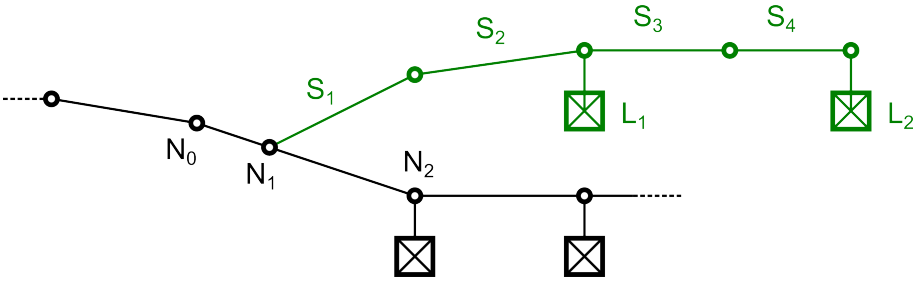

Figure III.10: Lateral (green) to aggregate in node N1 composed of four sections and two loads

The first step is to describe the lateral using quadripoles. Two types of elements compose the network: lines and loads. As shown in figure III.10, the lateral used in this example has four sections and two lines. The corresponding quadripoles (noted S_1 to S_4 for the sections and L_1, L_2 for the loads) can be seen in figure III.11. The goal is to aggregate all this quadripoles in one single "equivalent" quadripole (noted $Eq.$ in figure III.11).

Loads are elements described by a parallel impedance (see figure III.7). Therefore the tapped loads L_1 and L_2 which are connected in parallel can be inserted in series without transformations of any kind (figure III.12).

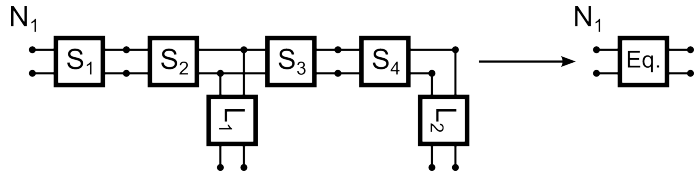

Figure III.11: Aggregation of the lateral as a single equivalent quadripole

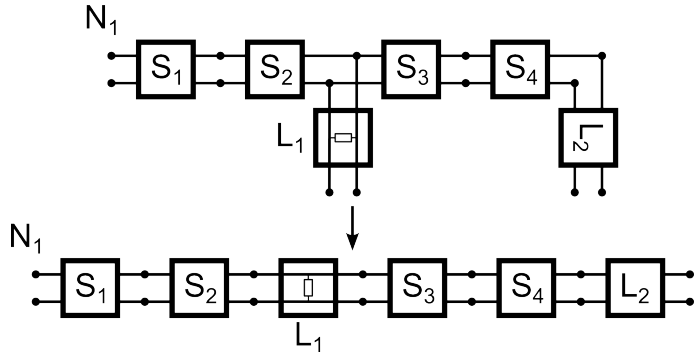

Figure III.12: Insertion in series of the tapped loads of the lateral

The advantages of having all quadripoles in series is that computing the equivalent quadripole is very easy using matrices multiplication. When propagating upstream measures downstream, the needed matrices are the matrices B. Therefore, in order to reduce computation time, only the matrices B can be computed. And if a matrix A is needed (as in next paragraphs) it is easy to compute it from the inverse of the B matrix.
To obtain an equivalent quadripole, the technique is to multiply the B matrices of each quadripole together, starting with the last quadripole B matrix since commutativity is not applicable here (because of the series elements composing the quadripole). The equivalent quadripole B matrix is therefore computed such as in the following equation concerning the lateral described previously:

$$B_{eq} = B_{L2}.B_{S4}.B_{S3}.B_{L1}.B_{S2}.B_{S1} \tag{III.9}$$

We now have computed the equivalent quadripole of the entire lateral connected in node N_1 of the feeder shown in figure III.10. When browsing downstream of node N1, the lateral must be taken into account and can be considered as a load, consuming part of the current of the feeder. However the equivalent quadripole B_{eq} matrix that we computed is not in the form of a parallel impedance such as:

$$B_{eq} \neq \begin{bmatrix} 1 & 0 \\ -Y & 1 \end{bmatrix}$$

it possesses four coefficients (b_{11},b_{12},b_{21} and b_{22}) which are different from 0 since they result from the multiplication of the B matrices of all the elements of the lateral.

In order to insert this equivalent element into the feeder as a load (such as the green lateral of figure III.10 in node N_1), it is necessary to compute its input impedance

(or admittance, Y_{eq}). The following equation gives the input admittance depending of the coefficients of the A_{eq} matrix of the element:

$$Y_{eq} = \frac{a_{eq\,21}}{a_{eq\,11}} \quad with \quad A_{eq} = B_{eq}^{-1}$$

The admittance Y_{eq} can be computed with the two coefficients of matrix A_{eq}, $a_{eq\,11}$ and $a_{eq\,21}$. The B matrix of the equivalent quadripole impedance corresponding to the aggregated lateral can therefore be built:

$$B = \begin{bmatrix} 1 & 0 \\ -\frac{a_{eq\,21}}{a_{eq\,11}} & 1 \end{bmatrix}$$

The quadripole corresponding to the green lateral of figure III.10 can finally be inserted in series in node N_1 of the feeder (see figure III.13) and the consumption of the lateral will therefore be taken into account when browsing downstream.

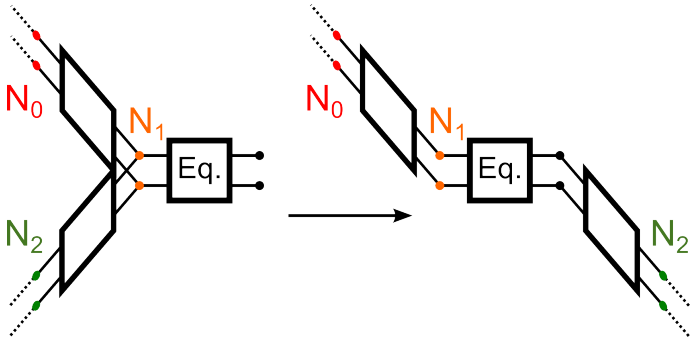

Figure III.13: Insertion of the lateral in the feeder

Note: This method of aggregation/insertion is of course valid at every level of junction and lateral, each sub-lateral needing to be aggregated and inserted as a load in its parent lateral (see figure III.9 and its description).

Throughout this section we developed the method used in order to use the fault localization algorithm presented in section 2.2. The method is divided into two seperate mechanisms:

1. the quadripole model used to aggregate loads and laterals from the branches extremities to the junction node
2. the propagation method which propagates to the downstream branches the voltages and currents measured at the head of the feeder

These mechanisms allow to execute a fault distance computation section by section knowing their input voltages and currents, and without making any other assumptions, therefore eliminating any errors due to approximate models.

3.2 Fault location computation

3.2.1 Analyzing the Takagi equation

The Takagi equation III.7, developed in section 2.2 and reminded below (III.10), can be applied to each section of the network as we browse downstream the feeder. However

this equation still makes an assumption which is the following: the fault current is considered equal to the difference between the faulty phase pre-fault current and post-fault current. The fault current in the equation can therefore be replaced by this current value which can be computed from the measurements at the head of the feeder.

$$x = \frac{\mathrm{Im}\left(V_a.{I''}_a^*\right)}{\mathrm{Im}\left(z_1.I_{tot}.{I''}_a^*\right)} \tag{III.10}$$

However, the consequences in the case that this assumption is wrong are not negligible. As it can be seen in III.11, if ${I''}_a^*$ and I_f are not exactly in phase, the term with R_f is not equal to zero. And ${I''}_a^*$ being present in every term, the error made by using this equation will be unacceptable.

$$\mathrm{Im}\left(V_a.{I''}_a^*\right) = \mathrm{Im}\left(x.z_1.I_{tot}.{I''}_a^*\right) + \underbrace{\mathrm{Im}\left(R_f.I_f.{I''}_a^*\right)}_{\neq 0 \rightarrow \text{error term}} \tag{III.11}$$

There are two options to solve this problem of inaccuracy:

- use another variable than ${I''}_a^*$ which is exactly in phase (we will note it I_{ph}) with I_f in order to exactly cancel the term with R_f:

$$\mathrm{Im}\left(V_a.{I_{ph}}^*\right) = \mathrm{Im}\left(x.z_1.I_{tot}.{I_{ph}}^*\right) + \underbrace{\mathrm{Im}\left(R_f.I_f.{I_{ph}}^*\right)}_{=0}$$

- estimate precisely I_f using another method, which by definition is in phase with itself, in order to exactly cancel the term with R_f:

$$\mathrm{Im}\left(V_a.{I_f}^*\right) = \mathrm{Im}\left(x.z_1.I_{tot}.{I_f}^*\right) + \underbrace{\mathrm{Im}\left(R_f.I_f.{I_f}^*\right)}_{=0}$$

The first option was first studied by analyzing the phase differences between the fault current and various other variables. The analysis was made for different distribution networks (rural and urban) and for various fault resistances. The work presented in appendix C details this first option and shows its limits. The second option is detailed in the following section 3.2.2.

The results that are presented in section 3 of chapter IV are obtained using three different currents in order to show the performance of each method.

3.2.2 Final fault localization equation

The fault current can be seen as the sum of the neutral grounding current and the line capacitive currents flowing through the healthy phases.

$$I_f = I_n + I_{c_{tot}} \tag{III.12}$$

This formulation is interesting since the neutral grounding current of the substation transformer can easily be monitored. The capacitive current $I_{c_{tot}}$ corresponds to the sum of all the "local" capacitive currents of all phases of the lines/cables on the network.

$$I_{c_{tot}} = I_{c_{a\ tot}} + I_{c_{b\ tot}} + I_{c_{c\ tot}}$$

It is by definition impossible to measure. However it can be estimated with various precision degrees.

For every distribution network, the capacitive currents of the feeders are given in their description. These capacitive currents correspond to the maximum total capacitive currents, $I_{c_{max}}$, that a healthy feeder will feed to a bolted fault located on another feeder near the substation. This maximum value will occur for the case where the residual voltage, $V_r = V_a + V_b + V_c$, is maximum.

The maximum theoretical value of V_r occurs with a 0Ω fault. When a bolted single phase fault occurs, the faulty phase voltage drops to 0V. The two other phases voltage increase to the phase-to-phase amplitude and have a phase-shift of 60° as can be seen on figure III.14.

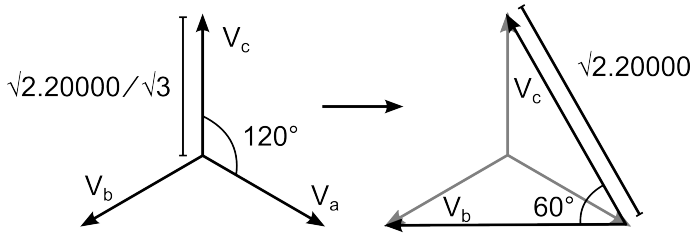

Figure III.14: Change of the phase-to-ground voltages under a bolted single phase fault to ground on phase a

Therefore, the reference value is computed in equation III.13 for .

$$V_{ref} = max\left(V_b + V_c\right) \tag{III.13}$$

$$= \sqrt{2}.20000.max\left(sin\left(\omega.t + \frac{\pi}{3}\right) + sin\left(\omega.t + \frac{2.\pi}{3}\right)\right) \tag{III.14}$$

$$= \sqrt{2}.20000.max\left(2.sin\left(\frac{2.\omega.t + \pi}{2}\right).cos\left(\frac{\frac{\pi}{3}}{2}\right)\right) \tag{III.15}$$

$$= \sqrt{2}.20000.\sqrt{3}.\underbrace{max\left(sin\left(\omega.t + \frac{\pi}{2}\right)\right)}_{=1} \tag{III.16}$$

$$V_{ref} = 48989\,V \tag{III.17}$$

Figure III.15 shows the circulation of the fault currents (see also [Ferracci, 1995]).

A simple way to estimate the capacitive current of the feeder is therefore to measure the residual voltage of the feeder and make a cross-multiplication using the maximum residual voltage and the maximum capacitive current in order to obtain the effective capacitive current of the feeder during the fault (see equation III.18).

$$I_{c_{tot}} = \frac{I_{c_{max}}.|V_r|}{|V_{ref}|} \tag{III.18}$$

Using III.12 and considering that the neutral grounding current and the total capacitive current are out of phase by 90 ° we can rearrange the equation and obtain the following

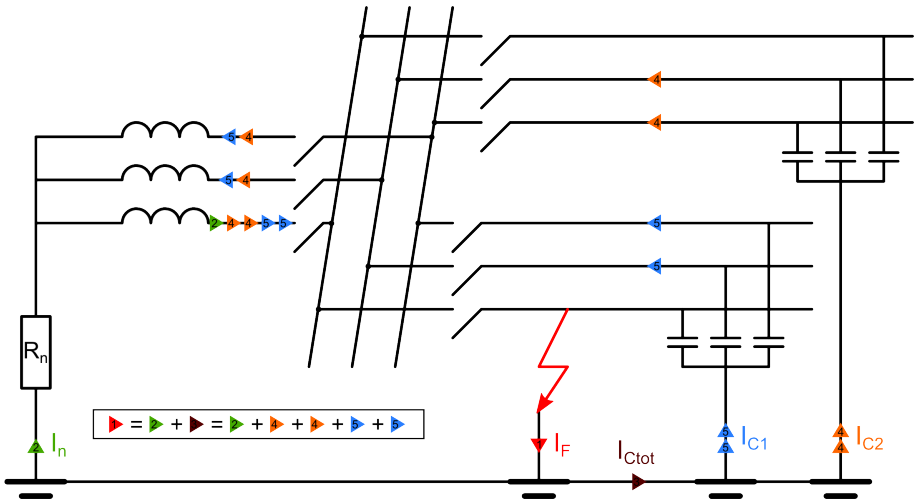

Figure III.15: Circulation of the fault current (I_f, red), into the neutral connection (I_n, green) and through the line capacitances of the faulty feeder (I_{c_1}, blue) and healthy feeder (I_{c_2}, orange), $I_{c_{tot}}$ (brown) being the total capacitive current

formula to compute the fault current phase and magnitude:

$$\begin{aligned} I_{f\ est} &= \sqrt{{I_n}^2 + {I_{c_{tot}}}^2} \\ \varphi_{I_{f\ est}} &= \arctan\left(\frac{I_{c_{tot}}}{I_n}\right) \end{aligned} \tag{III.19}$$

From now on, since the fault current is estimated (based on I_n measurements and DSO data about theoretical $I_{c_{tot}}$), we will note it $I_{f\ est}$.

Consequently, the final fault localization equation to use is the following:

$$x = \frac{\mathrm{Im}\left(V_a.{I_{f\ est}}^*\right)}{\mathrm{Im}\left(z_1.I_{tot}.{I_{f\ est}}^*\right)} \tag{III.20}$$

with $I_{f\ est} = \sqrt{{I_n}^2 + {I_{c_{tot}}}^2}.\exp^{j.(\varphi_{I_n}+\varphi_{I_{f\ est}})} = \sqrt{{I_n}^2 + {I_{c_{tot}}}^2}.\exp^{j.(\varphi_{I_n}+\arctan\left(\frac{I_{c_{tot}}}{I_n}\right))}$

3.2.3 Voltage and current measurements used in the equation

In equation III.20 the voltages and currents are expressed in a complex form. In order to use this method there is therefore a choice to make in order to transform the temporal values in complex values.

If using the Fourier Transform, the choice concerns three parameters:

- the starting time of the Fourier transform window
- the length of the Fourier transform window
- the frequency at which the signal is recovered

In the results presentation in chapter IV, the chosen parameters will be detailed.

3.3 Complete resumed flowchart of the method

This section presents a complete flowchart of the method in order to give a global view on what is done and when.

- **Offline operations - to do beforehand**

1. Build all the sections B matrix using the network data on the type, length of conductors and loads nominal active and reactive power[1]. This has to be done at each change in the topology of the network (change of the normally open switch for example, or change of a conductor). It is a slightly time consuming process which cannot be done "live", and does not need to, since changes in the topology of the network are not done on a daily scale.
2. Keep up to date the total capacitive current value of each feeder

- **Online operations - to do instantly when a fault is detected**

1. Retrieve the phase voltages and currents ($V_{a,b,c}$ and $I_{a,b,c}$)at the head of the feeder, and the neutral grounding current I_n
2. Compute the total capacitive current $I_{c_{tot}}$
3. Estimate the fault current using I_n and $I_{c_{tot}}$
4. Start the localization algorithm for $i = 1$
5. Compute the fault distance on section n°i
   - if the fault distance is $<$ to the section length: possible fault on this section
     5.1 if every upstream junction has been tested $\Rightarrow$ **go to step 6**
     otherwise $\Rightarrow$ increment i and go back to step 5
   - if the fault distance is $>$ to the section length: browse downstream to the next section
     5.1 Propagate the phase voltages and currents to the next section
     5.2 increment i and go back to step 5
6. **Return the list of the possibly faulty sections and their associated fault distances**

Note: let us draw the attention on step 6. In the case of radial distribution networks, the algorithm can find multiple solutions to a given fault situation. Indeed, a voltage/current couple measured at the head of the feeder can physically correspond to multiple fault locations. This is an important point to keep in mind when reading chapter IV presenting the results obtained with this method (see also section 3.4).

3.4 Recap of the precise working context of the method

Let us summarize here, now that the developed fault localization method has been completely detailed, the exact context in which this method is operational.

[1] It is important to note that the loads real time consumption is not known

The developed method is:

- a method for the distribution networks with the following characteristics:
  - three-phase or single-phase network
  - impedant neutral grounding of the substation transformer
  - urban or rural network which can possess laterals (or branches) connected to the main feeder
- a method for various fault situations:
  - resistive or bolted ground faults
  - single-phase to ground faults
  - three-phase to ground faults
- a method which needs few information:
  - global data:
    - network topology
    - maximum capacitive currents for each feeder of the substation
    - line characteristics (length, R,L and C per unit length)
    - loads characteristics (active and reactive power)
  - measurements at each fault occurrence:
    - phase voltages of the feeder
    - phase currents of the feeder
    - neutral current of the substation

This method is therefore well adapted to many distribution networks, and should cover many fault situations since single-phase to ground faults represent the majority of the fault situations of distribution networks.

However, it does not suit compensated neutral networks and will not be efficient for specific faults such as for intermittent faults with self reignition.

4 Localization of specific faults and for compensated neutral networks

4.1 Problematic of specific faults

The developed method, as described in section 3.4, does not suit all network configurations and fault situations. The most restrictive aspects are clearly the need of an impedant neutral grounding of the substation transformer and the handling of bolted or low resistance faults only.

We will explain now why this method is restricted to the previously cited cases and does not suit the following cases.

- **high resistance faults / compensated neutral / isolated neutral**:
  With these types of neutral connection to the ground or high fault resistances, the fault current during a phase to ground fault is very low since there is no loop possible

in the case of an isolated neutral (except with the conductors capacitances), or a very low fault current in the case of compensated neutral or high resistance fault with an impedant neutral grounding. This fact often introduces problems in detecting the fault, therefore locating the fault with such a small fault current becomes impossible with this method.

- **self reigniting arc faults**
  This type of faults creates a fault current which consists of two stages during a 0.02 s period. The first stage consists of the appearance of the electrical arc, and a corresponding "chaotic" fault current which principal component is not any more around 50 Hz. Then the electrical arc extinguishes itself which marks the start of the second stage. This stage corresponds to the building up of the voltage until that a new electrical strike appears. The cycle starts again at stage one.

  The characteristics of this particular type of fault currents is not compatible with the method which measures the voltages and currents on a period of 0.02 s and uses the Fourier transform to extract the 50 Hz component. Indeed, the two stage characteristic of the fault current jeopardizes the Fourier transform process and gives an unrealistic current which cannot be used correctly in fault distance computations.

4.2 Dealing with high resistance faults

The master student Antony Dasco Bartilomo worked during a few months on the specific case of high resistance single phase to ground faults. We develop in this section the work that he carried out in harmony with the work presented in this thesis.

The first developed idea concerns the estimation of the capacitive currents flows throughout the different phases of a distribution network feeder when it endures a phase to ground fault. Indeed, it is well known that during phase to ground faults, the possible current loops are the loop with the neutral grounding of the substation transformer and the loops with phase to ground line or cable capacitances. Therefore, knowing precisely these capacitive currents for a given fault situation can help in localizing correctly the fault, since it permits to estimate the fault impedance.

Secondly, the method proposes a way of localizing the fault location by analysing the evolution of the computed fault impedance. It is an iterative technique which uses the sign of the computed fault impedance to determine if the fault is located downstream or upestream. The method is described in details in the following sections.

4.2.1 Context of the method

The method is based on the same principles of the proposed fault localization algorithm presented in this thesis:

- measurements of the voltages and currents at the head of the feeder only
- propagation of the measurements throughout the nodes of the feeder

However, the proposed algorithm is based on another method for computing the fault distance. It is based on the computation of the fault impedance seen from the propagated point.

In the following sections, we detail how the fault current and the fault impedance are computed in order to perform the fault localization.

4.2.2 Fault current and fault impedance computations

The first step of the method is to compute the fault current. As described in section 3.2.2, the fault current can be seen as the sum of the neutral grounding current and the total capacitive currents of the network.

Starting the process from the measurement point, at the head of the feeder, it propagates the measures downstream, and knowing the electrical characteristics of each conductor section, computes the capacitive currents associated to each section under the studied fault situation.

When starting at the head of the feeder, the estimated fault current is considered equal to the neutral grounding current plus a first estimation of the total capacitive current, based on the measured voltage. There is therefore a substantial error since the voltages and currents will inevitably be different in other points of the network. As the algorithm progresses through the feeder, it updates the voltages and currents at each node, and therefore updates the estimation of the fault current by adding the capacitive currents computed at each section. The more the algorithm progresses downstream the feeder, the more the estimated fault current is accurate.

4.2.3 Fault localization

As the algorithm browses downstream the feeder, it computes the fault current which is needed for the computation of the fault impedance. When analyzing the network situation under a single phase to ground fault by using the symmetrical components networks, we can write the following equations at the fault point (for a fault on phase a):

$$\begin{gathered} I_1 = I_2 = I_0 = \frac{I_f}{3} \\ \text{and} \\ V_1 + V_2 + V_0 = 3.Z_f.I_0 \\ \text{therefore} \\ V_a = Z_f.I_f \\ \text{which gives} \\ Z_f = \frac{V_a}{I_f} \end{gathered} \tag{III.21}$$

The phase voltage is measured at the head of the feeder and then propagated up to the computation point where I_f is computed as described previously. It is consequently pos-

sible to compute the fault impedance Z_f.

The above equations are valid when computing Z_f exactly at the fault point. However, when browsing the feeder, the computations occur at each node. Therefore, if the fault is located between two nodes, the computed Z_f does not correspond exactly to the real Z_f.

To introduce this problem, let us assume that the measurements have been propagated at node N of figure III.16.

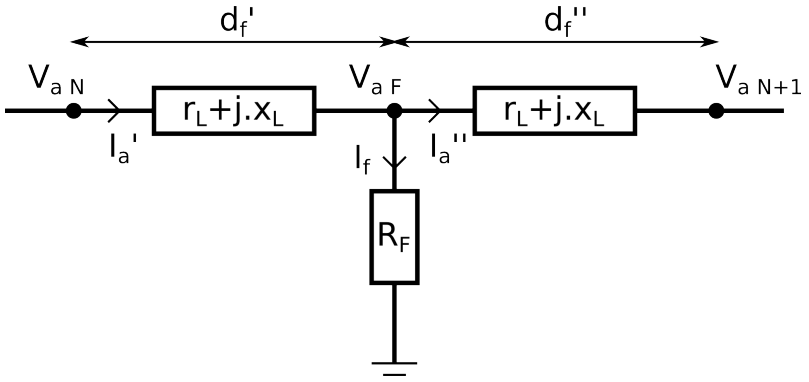

Figure III.16: Electrical diagram of the faulted phase

We can write the following equations:

$$\begin{aligned} V_{a\,N} &= I_a{}'.(r_L + j.x_L).d_f{}' + R_f.I_f \\ &= I_a{}'.(r_L + j.x_L).d_f{}' + R_f.(I_a{}' - I_a{}'') \\ &= I_a{}'.(r_L.d_f{}' + R_f + j.x_L.d_f{}') \underbrace{-R_f.(I_a{}'')}_{I_a{}''\ \text{neglected}} \end{aligned}$$

$$Z_f = \frac{V_{a\,N}}{I_f} = (r_L.d_f{}' + R_f) + j.(x_L.d_f{}') \tag{III.22}$$

Note: In these equations the following assumptions are made:

- the capacitive currents of the analyzed section are not taken into account, but considering that the different sections of a distribution networks are small, this assumption should not impact much the results
- the faulty phase current upstream of the fault, $I_a{}'$, is considered equal to the fault current I_f, and the downstream faulty phase current is consequently neglected

Looking at equation III.22, we can see that as long as node N is located upstream of the fault point F, the distance $d_f{}' > 0$ and the imaginary part of Z_f is positive. When N and F points are the same, $d_f{}' = 0$ and $Z_f = R_f$.

The same computation can be done when placing ourselves downstream the fault point, at node N+1 for example. When the algorithm arrives at point N+1 it has not found the

fault point F yet and propagates the voltages and currents from N to N+1 (see figure III.17).

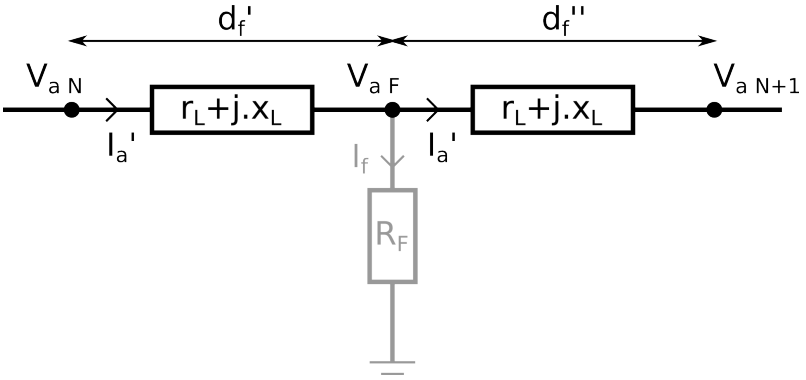

Figure III.17: Electrical diagram of the faulted phase with propagation in N+1 without "seeing" the fault point

We can therefore write the following equations:

$$\begin{aligned} V_{a\,N+1} + I_a^{'}.(r_L + j.x_L).d_f^{''} &= R_f.I_f \\ V_{a\,N+1} &= R_f.I_f - I_a^{'}.(r_L + j.x_L).d_f^{''} \\ &= I_f.(R_f + r_L.d_f^{''} - j.x_L.d_f^{''}) \\ Z_f = \frac{V_{a\,N+1}}{I_f} &= (R_f - r_L.d_f^{''}) + j.(-x_L.d_f^{''}) \end{aligned} \tag{III.23}$$

Looking at equation III.23, we can see that as long as node N+1 is located downstream of the fault point F, the distance $d_f^{''} > 0$ and the imaginary part of Z_f is negative. When N+1 and F points are the same, $d_f^{''} = 0$ and $Z_f = R_f$.

Therefore observing the sign of the computed $Z_f = \frac{V_N}{I_f}$ gives an information on where we are located compared to the fault point F. As long as the imaginary part of Z_f is positive, we are located upstream the fault point. When the imaginary part becomes negative, we have passed the fault point.

The complete iteration steps of the method can therefore be summarized to the following:

- propagation of the measured voltages and currents to the next downstream node
- computation of the fault current using the known upstream capacitive currents and estimating the remaining downstream capacitive currents participating to the fault
- computing the fault impedance Z_f thanks to the propagated voltage and the computed fault current
- determining if the fault is located upstream or downstream the computation point depending of the sign of the imaginary part of the computed fault impedance

Starting at the head of the feeder with voltage and current measurements, the above steps are repeated until that a change of sign of the imaginary part of Z_f is observed. When the change of sign occurs, the fault location has been found.

The first level of the method processes these iterative steps for each node. But once one section has been found as faulty, the method can again be processed on the section. Indeed the section can be divided in a number of sub-sections and the algorithm can progress from one sub-section to another just like it does at the node level. The precision of the fault localization can therefore be increased by dividing the found faulty sections in smaller sub-sections, but it also increases the algorithm computation time. A compromise has to be done depending of the desired objectives.

4.2.4 Notes on the method and perspectives

This method is interesting for many reasons, but first let us remind the context in which it can be applied.

The method can be applied to heterogeneous distribution networks, radial or not, and with an impedant neutral grounding of the substation transformer. It is based on the measurements of voltages and currents at the head of the feeder, and the propagation of these measures through the feeder to each node in order to perform a fault localization on each homogeneous section of the feeder.

The localization performed is based on:

- the fault current estimation as the sum of the neutral grounding current and the capacitive currents, which are estimated and then updated throughout the propagation
- the fault impedance computation, thanks to the estimated fault current and the propagated voltage
- finally the fault localization is done by analyzing the sign of the imaginary part of the fault impedance

But it is important to keep in mind the assumptions made during the localization process:

- the fault is considered purely resistive, which guarantees the independance of the observed imaginary part of the computed fault impedance regarding the fault resistance therefore providing a fault localization robust to high fault resistances
- during the fault impedance computation, the line capacitance of the section on which the localization is made are not taken into account. But the usually small length of the sections ($< 1\,\text{km}$) allow to make this assumption without much consequences

The results shown in the master thesis of Dasco Bartilomo A. [Dasco, 2014] have been obtained on a small part of a real heterogeneous distribution network (see IV). The first results are encouraging and confirm that the method should now be tested with a complete long and radial heterogeneous distribution network. The sensitivity to non purely resistive

faults should also be tested in future works.

Finally, this method could be interesting in the case of compensated neutral grounding distribution networks as it takes into account the capacitive part of the fault current which is the major part of a fault current on such a distribution network.

4.3 Dealing with a specific fault: self reigniting electric arc

As stated previously, this type of fault is very particular as it consists of two different stages which occur one after another during a 50 Hz period. Each stage corresponding to a different electrical state: electric arc burning and then arc extension and building up of the voltage until the next electric arc.

The student Maximin Blanc did an intership supervised by Raison B. (director of this thesis) and me and worked specifically on the subject of self reigniting electric arc in 2013 [Blanc, 2013].

Part of his work consisted in developing an arc model in order to be able to simulate these type of faults.

The opportunity was given by one of the Greenlys project partner (see section 2) which provided us with various real fault measurements on multiple feeders. One of the fault occurrence corresponded exactly to a self reigniting electric arc fault. Therefore, high quality measurements (sampling frequency of 6400 Hz) were available in order to compare it with simulated arc faults (see figures III.18 and III.19).

In order to produce an arc model, his work was based on different arc model previously developed. The model developed by Blanc M. is tuned in order to obtain a simulated arc fault the closest to the real arc fault measurement. The final arc model reproduces quite accurately the real arc fault. It is a base model which the parameters can be tuned in order to simulate different types of arc faults.

The model equation is the following and defines the variation of the electric arc conductance during time:

$$\tau.\frac{dg}{dt} = G(t) - g(t) \tag{III.24}$$

with g being the conductance of the electric arc, G being the stationary conductance of the arc, and τ the electric arc time constant.

Tuning the different parameters which characterize G and τ, Blanc M. shows that it is possible to recreate the fault measurements by modeling and simulation (see figures III.20 and III.21).

However, the development of the method is still ongoing as for now a manual tuning of both the electric arc parameters and the fault location needs to be done in order to

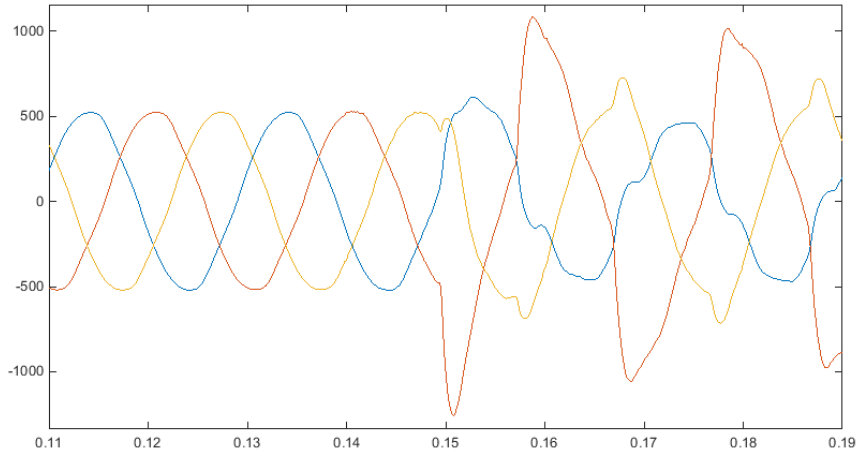

Figure III.18: Phase currents during arc fault

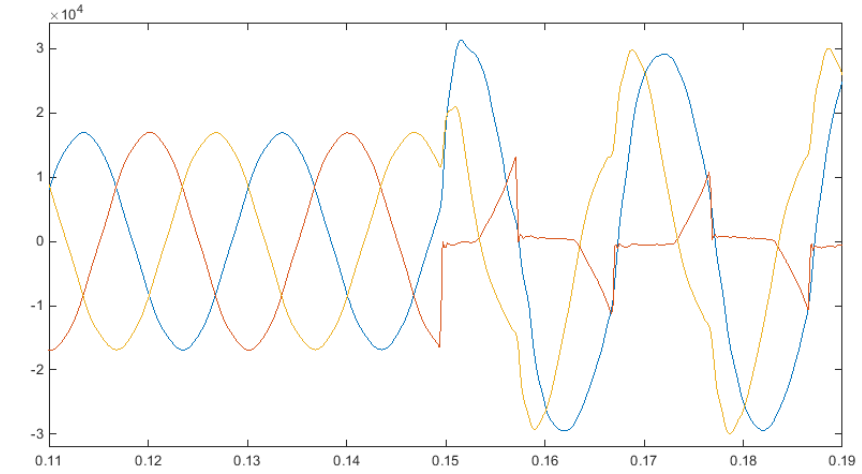

Figure III.19: Phase voltages during arc fault

recreate the fault measurements.

Note: In the PhD thesis [Masa, 2012] the author develops a fault detection method for high impedance faults and arc faults. The characterization of these types of fault is developed and high impedance faults and arc faults are also tested throughout laboratory test. The author therefore manages to develop a complete high impedance fault detection method.

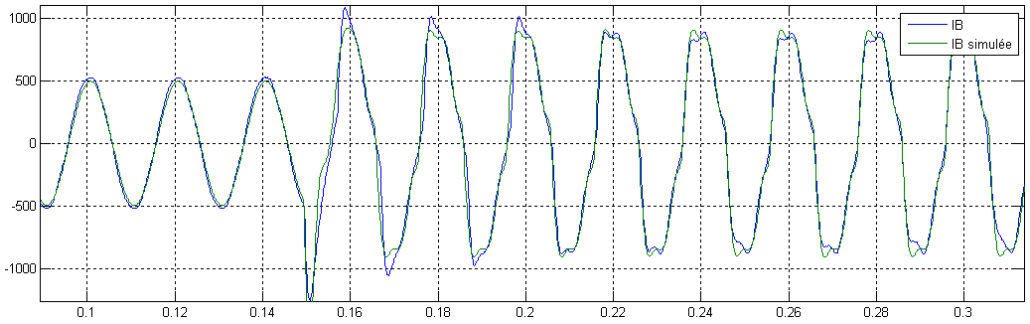

Figure III.20: Phase b currents, measured (blue) and simulated (green)

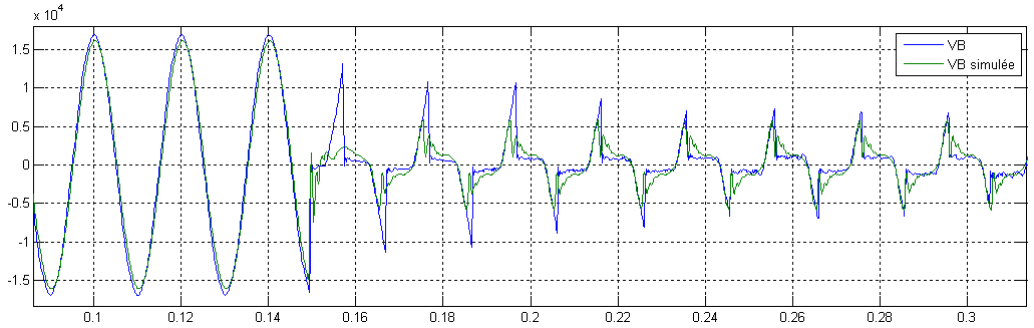

Figure III.21: Phase b voltages, measured (blue) and simulated (green)

5 Conclusion

The method presented in this chapter is a complete precise fault localization method which, from few voltages and currents measurements at the head of the main feeder, can browse downstream the feeder, propagating the measurements from node to node, taking loads and line/cable characteristics into account, and finally computing a fault localization on each homogeneous section.

The algorithm output is therefore one or more (for a radial network) distances and the associated sections that are found to possibly be faulty.

The fault distance computation principle, based on a transmission network dedicated solution (the Takagi equation), needs a current in phase with the fault current in order to express the fault distance independently of the unknown fault resistance. In our method we propose to estimate the fault current, which by definition is in phase with itself.

In order to process the fault distance computation on each homogeneous section of the network, the method proposes to use the quadripoles model of the networks elements (line/cable and loads). This method allows to easily propagate the initial voltage and current measurements made at the head of the feeder, throughout the feeder and taking into account the various voltage drops, current consumptions by the loads or sub-feeders, etc. The method necessitates to know the precise topology of the networks and the electrical characteristics of the different elements, but in comparison the alternative of monitoring each node of the network is much more complicated and onerous.

In the last part of this chapter, we have also exposed a few lead on possible solutions for special cases which cannot be treated by the proposed method.

Chapter IV

Results of Fault Localizations on Simulated Networks

Contents

Abstract

We develop in this chapter the results obtained with the fault localization algorithm. The two simulated networks, the simulation details and parameters are first presented. The simulated faults characteristics and locations are then described. Results of fault localizations on the two networks on the basis of simulations and real fault measurements are finally detailed, as well as a sensitivity analysis of the localization process for these cases.

1 Introduction

The fault localization method presented in chapter III was tested on simulated networks throughout the entire development phase. Many different networks were used depending of the advancement of the development. Starting with unrealistic very simple networks, which were made more complex as the different parts of the algorithm were improved (measurements propagation, radial network browsing, fault distance computation, ...), the final fault localization algorithm has been tested on simulations corresponding to real urban and rural networks.

The networks simulations were conducted with the software "ATPDraw"[1] which is a graphical preprocessor to the Alternative Transients Program (ATP) version of "Electromagnetic Transients Program" (EMTP)[2].

The measurements resulting from the simulations were then converted to the ".mat" format of Matlab® in order to be processed by the algorithm which was developed using this software.

The following sections will detail the real networks used and the precise characteristics of the simulation in order to give a detailed context. Finally the results and performances of the fault localization algorithm will be presented.

2 Real networks simulated and simulation details

2.1 Simulation parameters of ATPDraw / EMTP

During the development process, the simulated networks contained many nodes and lines of interest, and the number of monitored variables was important (voltage and currents for each phase). Therefore the simulation time was reduced to a minimum, even though as a final application, the needed number of monitored variables is much lower (7 variables: 3 voltages and 3 currents at the head of the feeder, plus the neutral grounding current).

Below are the time milestones during the simulations:

- $t = 0.00\,s$ start of the simulation
- $t = 0.03\,s$ fault occurence
- $t = 0.06\,s$ end of simulation

The choice of these milestones was done in the goal of having at least one pre-fault period, as well as both transient and steady state fault signals.

The ATPDraw software simulation parameters to set are the "time step of the simulation" (in seconds) and the "saving frequency of the simulation data to the output file" (in

[1] www.atpdraw.net
[2] www.emtp.org

number of time steps). Setting the time step to $1e^{-7}\,s$ is a good compromise which gives a good precision of the simulation results and a simulation time of a few minutes only for the biggest networks.

Setting the saving frequency to 10 gives output data which is sampled at a time step of $1e^{-6}\,s$, therefore reducing by 10 the size of the matrices manipulated by the algorithm, which is enough for the algorithm precision and again reduces the software time computation.

This simulation context is the context used for all the results presented in the following sections of this chapter.

2.2 An urban distribution network

One of the available networks provided by Electricité Réseau Distribution France (ERDF, the main french Distribution System Operator) is a feeder of an urban distribution substation. The substation feeds ten feeders connected to two different busbars which can be rescued by another substation.

The Distribution System Operator (DSO) gave us access to detailed information about one of the feeder:

- topology
- electrical characteristics of the sections
- substation diagram
- detailed loads characteristics: nominal active power, nominal reactive power, type of customers

Unlike transmission networks, distribution networks are most of the time constituted of different types of cables/lines. The network is therefore divided into sections which can differ one from another but can each be considered homogeneous. Concerning the electrical characteristics of the sections, the provided database only contained the following elements:

- the positive sequence resistance R_1
- the positive sequence reactance X_1
- and the zero sequence capacitance C_0

The lines being passive elements, the negative sequence components are equal to the positive sequence components. However, the three missing elements R_0, X_0 and C_1 had to be determined. To do so, we compared electrical characteristics of different lines/cables given by manufacturers in order to logically fill the blanks. Therefore, R_0 and X_0 were determined this way.

Note: Concerning C_1 we considered that for cables the positive sequence value is identical to the zero sequence value. This consideration was made in agreement with some manufacturers data which give the same value for both C_1 and C_0 for cables. However, this is a complex and discussed point (in [Tziouvaras, 2006, Herraiz et al., 2009] for example the authors discuss the estimation of the zero sequence impedance of high voltage

underground cable) and should be considered as an assumption that should be closely studied.

Concerning lines, the values are known to be different for C_1 and C_0, and we therefore used the manufacturers data.

An example in table IV.1 illustrates this principle (with DSO data in blue and manufacturer data in yellow) used to complete the electrical characteristics of each line or cable.

Cable 150mm²	**DSO data**	**Manufacturer data**	**Merged data**
R_1 (ohm/km)	0.2	0.2	0.2
R_0 (ohm/km)	-	1.04	1.04
X_1 (ohm/km)	0.1	0.117	0.1
X_0 (ohm/km)	-	1.66	1.66
C_1 (nf/km)	-	205	179
C_0 (nf/km)	179	205	179
Line 75mm²	**DSO data**	**Manufacturer data**	**Merged data**
R_1 (ohm/km)	0.435526	0.4413	0.435526
R_0 (ohm/km)	-	0.583	0.583
X_1 (ohm/km)	0.35	0.35	0.35
X_0 (ohm/km)	-	1.582	1.582
C_1 (nf/km)	-	10.1	10.1
C_0 (nf/km)	5	5	5

Table IV.1: Example of DSO data (blue) and manufacturers data (yellow) merged for the line/cable models used in the simulation

The general characteristics of the studied feeder are the following:

- a single branch of a total length of 10.662 km
- presence of cable conductors only
- 7 different types of cables
- loads total active power: 3166 kW
- loads total reactive power: 1266.4 kVar
- type of loads: 7 HTA[3] loads and 26 HTA/BT[4] substations
- characteristics of the sections:
  - total number of sections: 81
  - minimum section length: 10 m
  - maximum section length: 623 m
  - mean section length: 132 m

Figure IV.1 shows the studied feeder. The substation located in the upper right corner of the figure powers the feeder constituted of a single branch (more than 10 km long) which

[3]"Haute Tension A" (meaning "Medium Voltage") corresponds to a voltage level of 20 kV
[4]"Basse Tension" meaning "Low Voltage" corresponds to a voltage level of 400 V

feeds 7 HTA loads and 26 HTA/BT substations (both represented in brown). The normally open switch (in red) is located logically at the end of the feeder. And two normally closed switch (in blue), used for possible reconfiguration schemes during fault situations divide the feeder in three parts.

Figure IV.1: Urban network studied with the representation of the substation, loads and normally open and closed switches

	I_{cap} (in A)		I_{cap} (in A)
Feeder 1	22.5	Feeder 6	26.6
Feeder 2	37.6	Feeder 7	31.8
Feeder 3	19.4	Feeder 8	54.2
Feeder 4	7.8	Feeder 9	59.1
Feeder 5	?	Feeder 10	?

Table IV.2: Urban network - Maximum capacitive currents for each feeder feeding a fault on another feeder (data missing for feeders n°5 and n°10)

The substation of this feeder also powers nine other feeders. Therefore in order to conduct a correct fault localization procedure, it is important to know the capacity of each feeder to supply a capacitive fault current to a fault located on another feeder. Table IV.2 gives the maximum capacitive fault current of each feeder (except for two feeders where the DSO data is missing).

2.3 A rural distribution network

The DSO (ERDF) also gave us data concerning a rural distribution network. The type of the provided data is the same as presented in section 2.2. The same merging method was used to complete the missing information about the lines/cables electrical characteristics.

The feeder, being in a rural zone, does not have the same characteristics than the urban feeder previously described. The general characteristics of this feeder are detailed below:

- a main feeder of a total length of 21.507 km
- three long lateral sub-feeders between 2.545 km and 6.933 km and many other lateral sub-feeders from a few hundred meters to one or two kilometers
- presence of overhead lines (93.7%) and cables (6.3%) conductors
- 4 different types of lines and 3 different types of cables
- loads total active power: 2809 kW
- loads total reactive power: 1124 kVar
- type of loads: 3 HTA loads and 97 HTA/BT substations
- characteristics of the sections:
  - total number of sections: 253
  - minimum section length: 13 m
  - maximum section length: 2013 m
  - mean section length: 300 m

Figure IV.2 shows the rural feeder. The substation located in the lower left corner powers the main feeder and its numerous lateral branches. This network feeds 3 HTA loads and 97 HTA/BT substations. Due to its radial configuration with many branches, this feeder possesses 5 normally open switches which allow 5 different power backup connections. Furthermore, the feeder possesses 3 strategically distributed normally closed switches. This feeder therefore has some capacity of reconfiguration in order to minimize the out of power zone during a fault.

The substation of this feeder powers five feeders. The maximum capacitive current of each feeder is given in table IV.3. This maximum capacitive current is the maximum current due to the capacitances of the conductors that a feeder would supply to a fault on another feeder.

	I_{cap} (in A)
Feeder 1	15
Feeder 2	23
Feeder 3	12
Feeder 4	15
Feeder 5	17

Table IV.3: Rural network - Maximum capacitive currents for each feeder feeding a fault on another feeder

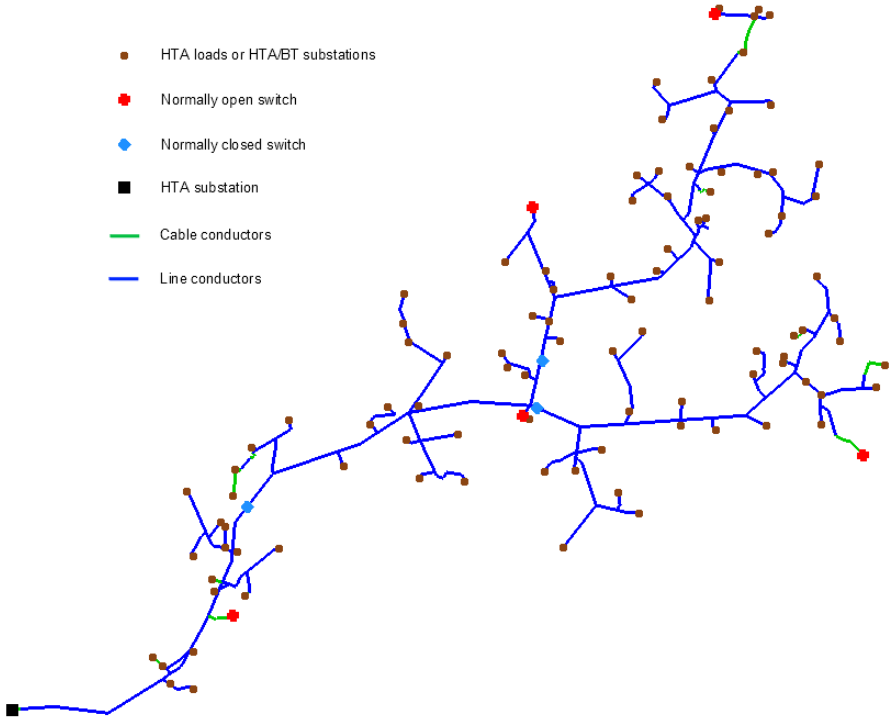

Figure IV.2: Rural network studied with the representation of the substation, loads and normally open and closed switches

2.4 The fault simulation

Our work concentrates on single-phase to ground fault, in agreement with the statistics which give this type of fault as the most present on distribution networks ($> 60\,\%$) [Jecu, 2011]. Therefore, the simulated faults are the same for both the urban and rural feeders. However, the method that we develop works also for three-phase faults (see section 2 of appendix B.

Fault statistics on the french networks shows that more than $80\,\%$ of single phase fault resistances are between 0 and 80 Ohm. We therefore decided to test the following fault resistances:

$$0.0001\,\Omega \quad 1\,\Omega \quad 5\,\Omega \quad 10\,\Omega \quad 15\,\Omega \quad 20\,\Omega \quad 40\,\Omega \quad 80\,\Omega$$

In the rest of the document we will write "$0\,\Omega$" even though for programming purposes the real simulated fault value is $0.0001\,\Omega$. The distribution of the fault resistances tested is not linear in order to really observe the differences between bolted faults and low resistance faults.

2.5 Simulated fault locations

2.5.1 Position of the faults

In an electrical network faults can occur in various places: junctions, conductors, switches, etc. In our modeling of the network, the only component of the model are the

nodes and the lines/cables. However only the lines/cables are physically modeled. Nodes are perfect connection points.

Therefore it has been decided to place the faults in the middle of the sections that were chosen to simulate a fault on. All simulated faults in our work are placed in the middle of a homogeneous conductor section.

2.5.2 Urban network

The urban network is constituted of a single main feeder. At first, about thirty fault locations were chosen. Finally only five fault locations have been retained without losing genericity in terms of fault situations and at the same time allowing more synthetic results. For each location, the fault point is chosen in the middle of the concerned section. Table IV.4 shows the distances of each fault location to the head of the feeder.

Fault	F1	F2	F3	F4	F5
Distance (m)	2083.5	4178.0	5750.5	7981.5	10127.5

Table IV.4: Fault distances on the urban feeder

Figure IV.3 shows the faulty sections and the associated fault locations.

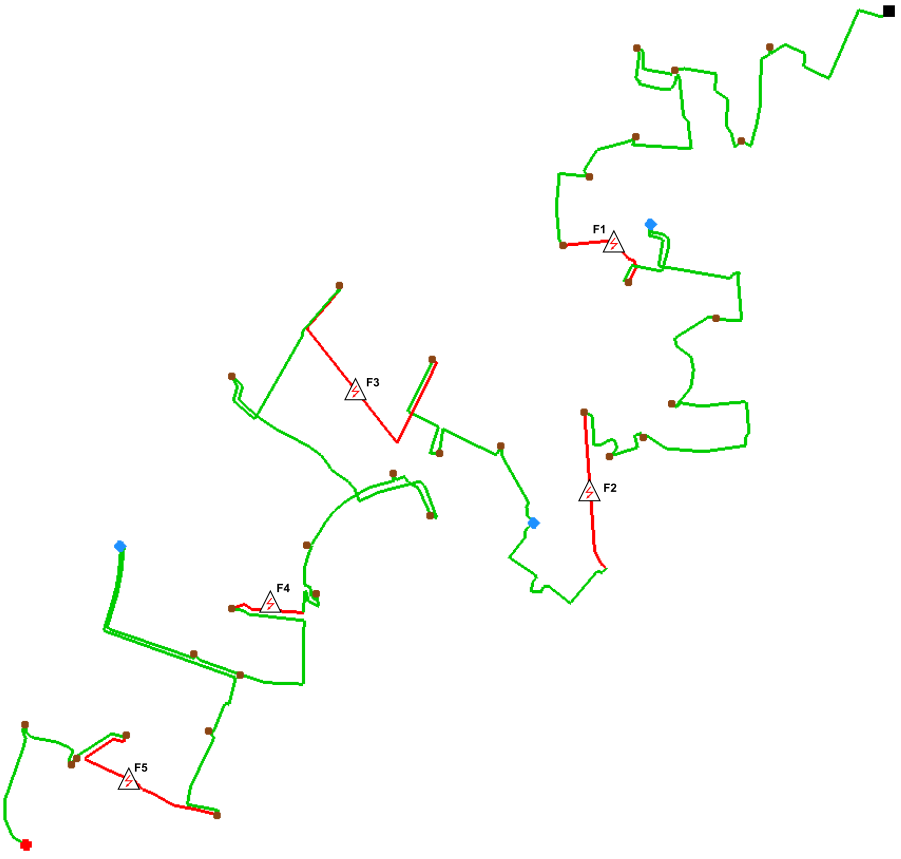

Figure IV.3: Faulty sections (red) with the associated fault locations (triangle) and the fault names of the urban network (complete figure legend in figure IV.1)

2.5.3 Rural network

The rural network is constituted of a main feeder and many lateral sub-feeders (see section 2.3). Eight fault locations have been chosen, four located on the main feeder (F1 to F4) and four located on lateral sub-feeders (L1 to L4). For each location, the fault point is chosen in the middle of the concerned section. Table IV.5 shows the distances of each fault location to the head of the feeder.

Fault	F1	F2	F3	F4
Distance (m)	5067.5	10564.5	16540.5	21140.5
Fault	L1	L2	L3	L4
Distance (m)	17361.5	20138	10815.5	14378.5

Table IV.5: Distances of the faults on the main feeder (F) and the laterals (L) of the rural network

Figure IV.4 shows the faulty sections and the associated fault locations.

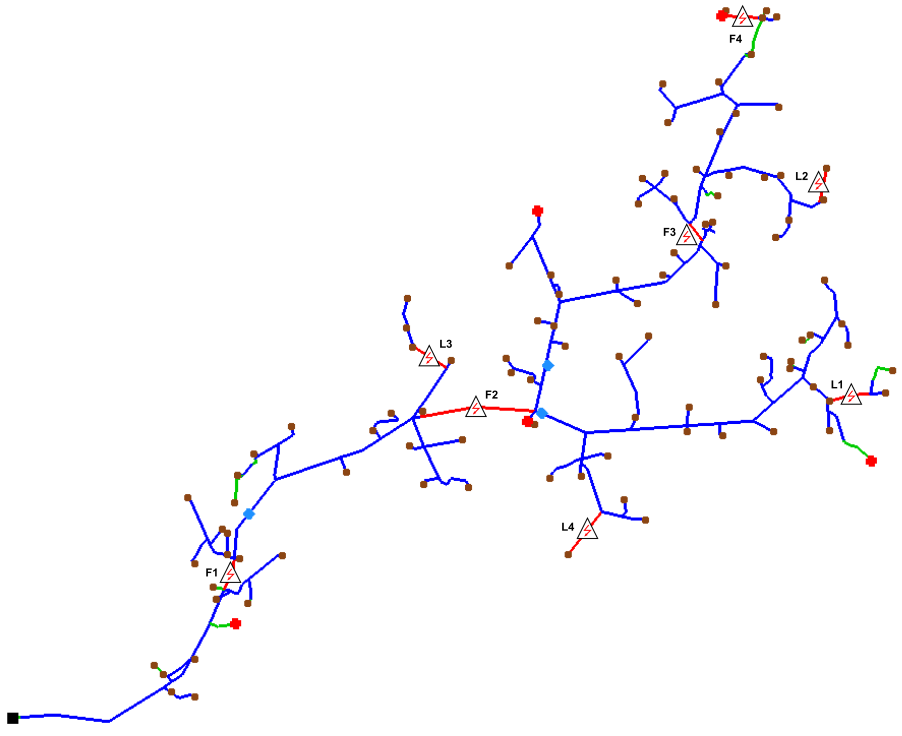

Figure IV.4: Faulty sections (red) with the approximate fault locations (triangle) and the fault names of the rural network (complete figure legend in figure IV.2)

3 Fault localization results and performances

It is first necessary to remind how these results have been obtained and explain what exactly is shown in the following figures and graphs.

First of all, we can summarize below the context in which these results have been obtained:

- data of real networks (topology/cable characteristics/loads/...) are used (see previous sections)
- these networks are simulated in ATPDraw/EMTP
- the location of the faults are predetermined
- the studied fault resistances vary from 0 to 80 Ω
- the simulation results of the different fault configurations (location and fault resistance) are processed within Matlab to perform the fault localization computation

3.1 Foreword about the voltage and current measurements

As stated in chapter III, the voltage and current measurements need to be transformed into symmetrical components phasors values in order to use the described localization method.

We used the Fourier Transform and studied the signals at their dominant frequency which is the 50 Hz component. The Fourier Transform parameters used are the following:

- **window starting time:** we chose to make the window start as soon as possible, therefore the window starts **0.01 s** after the occurrence of the fault

- **window length:** we chose to have a short window of one period, therefore **0.02 s**

The choices of a window starting right after the fault occurrence (and not waiting for the steady state) and having a short window of one period only were made in the goal of having a method that can analyze in live the fault data and give a fault localization as fast as possible. Even though the technical aspects of such a method have not been studied, it is obvious that the measurements of the voltages and currents needs to be done as soon as possible and as short as possible.

Furthermore, the classical protection scheme possess breakers which operates in 200 ms for the quickest. Therefore, after these 200 ms, the network topology is modified. The measurements need therefore to be done before these topology modifications.

Another technique consists in using a sliding Fourier transform, with the same window length. However, considering that we use the 50 Hz content only which does not vary much during the transient period of the fault, the sliding Fourier transform does not change the results.

3.2 Foreword about the fault distance results

The fault localization algorithm output for a given fault situation is the distance from the head of the feeder (or measurement point) to the fault. However, in order to interpret more easily the results, it is more relevant to express the result in terms of error between the real fault location and the computed fault location.

Figure IV.5 shows two fault distance computation results and their associated errors compared to the real fault distance. If the error is negative, the algorithm found a distance smaller than the real fault distance. On the contrary, if the error is positive, the found distance is bigger than the real fault distance.

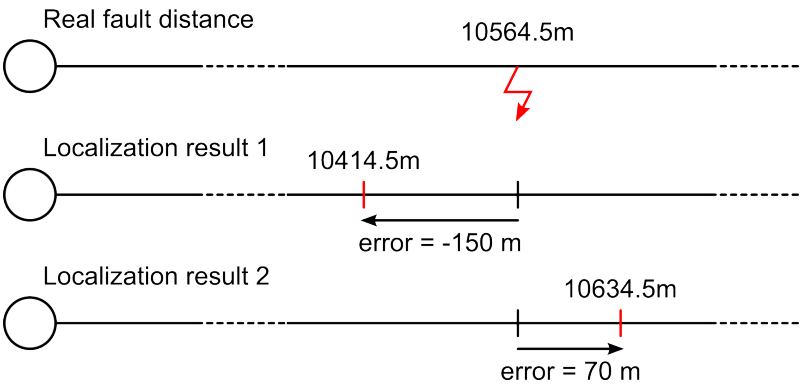

Figure IV.5: Example of two results and their associated errors compared to the real fault distance

All the results will therefore be expressed in terms of error between the real fault distance and the proposed fault distance by the algorithm.

3.3 Foreword about the faulty section results

The algorithm is of course also able to give the faulty section associated to the found fault distance, and when it finds more than one fault location, it gives all the faulty section associated to each fault location. The interpretation of the performance of the results is made according to the following criteria:

- **success** - if the real faulty section is among the faulty sections found by the algorithm, the result is considered as a success
  → **table cell in green**

- **half-success** - if the real faulty section is adjacent to one of the faulty sections found by the algorithm, the result is considered as a half-success
  → **table cell in yellow**

- **failure** - if the real faulty section is not among nor adjacent to the faulty sections found by the algorithm, the result is considered as a failure
  → **table cell in red**

These criteria are illustrated in figure IV.6.

These results can be hard to interpret correctly since the length of each section plays an important role in the result classification.

Example: if a small section of 20 m is between the real faulty section and the faulty section found by the algorithm, the result will be considered as a failure, despite a possible distance error of 30 m.

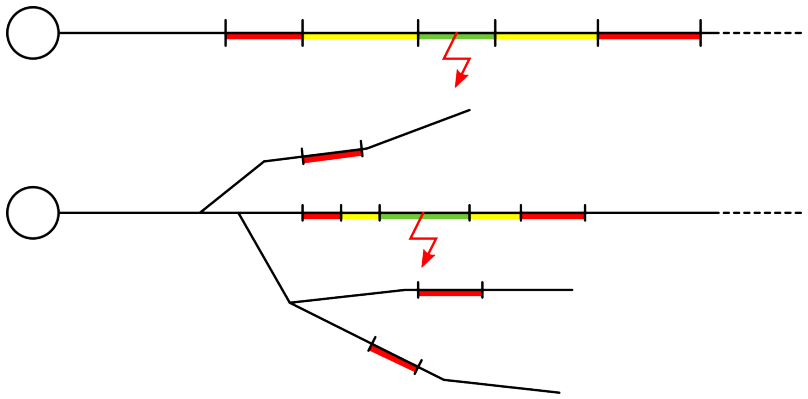

Figure IV.6: Classification of the results in term of section localization

For this reason, after having shown the two different result presentations (fault distance and faulty section) separately, they will finally be crossed with each other.

Note: it is important to understand that a section is defined as a homogeneous conductor, and that each physical end of a conductor defines the end of one section and the beginning of another section. Therefore there can be many sections between two operating switches on a network.

3.4 Foreword about the case of radial networks and multiple solutions

In case of a radial network, which contains branches, it is possible that the algorithm finds more than one fault location. Indeed, a voltage/current couple measured at the head of the feeder, can physically correspond to more than one situation. The more the feeder possesses sub-feeders, the higher are the chances for the algorithm to find multiple solutions.

The fault distance results that are presented in the following sections are therefore not computed the same way when there is a single solution or multiple solutions.

- Single solution
  - the error is the difference between the found fault distance and the real fault distance

Table IV.6 illustrates this error computation case.

- Multiple solutions - it depends of the section localization results (see section 3.3)
  - correct section found: the error is computed with the found fault distance of the correct section
  - adjacent section(s) found: the error is computed with the average of the found fault distance(s) of the found section(s) adjacent to the real faulty section
  - wrong section(s) found: the error is computed with the average of all found fault distance(s) of the found section(s)

Correct section	S_f			
Correct distance	x_f			
Found sections	correct	adjacent	wrong	
	S_1	S_2	S_3	S_4
Found distances	x_{s1}	x_{s2}	x_{s3}	x_{s4}
Error	$x_{s1} - x_f$	$x_{s2} - x_f$	$x_{s3} - x_f$	$x_{s4} - x_f$
Final error	$x_{s1} - x_f$			

Table IV.6: Computation example of the error displayed in the results in the case of a single solution

Table IV.7 and IV.8 illustrates the different computations of the error as described above.

Correct section	S_f				
Correct distance	x_f				
Found sections	correct	adjacent		wrong	
	-	S_1	S_2	S_3	S_4
Found distances	-	x_{s1}	x_{s2}	x_{s3}	x_{s4}
Error	-	$x_{s1} - x_f$	$x_{s2} - x_f$	$x_{s3} - x_f$	$x_{s4} - x_f$
Final error		$avg((x_{s1} - x_f) + (x_{s2} - x_f))$			

Table IV.7: Computation example of the error displayed in the results in the case of multiple solutions including adjacent sections

Correct section	S_f				
Correct distance	x_f				
Found sections	correct	adjacent	wrong		
	-	-	S_1	S_2	S_3
Found distances	-	-	x_{s1}	x_{s2}	x_{s3}
Error	-	-	$x_{s1} - x_f$	$x_{s2} - x_f$	$x_{s3} - x_f$
Final error			$avg((x_{s1} - x_f) + (x_{s2} - x_f) + (x_{s3} - x_f))$		

Table IV.8: Computation example of the error displayed in the results in the case of multiple solutions composed only of wrong sections

Note: Of course this way of presenting the results is possible retrospectively since for a real fault occurrence we do not know where is located the fault. It is therefore important to keep in mind that concerning radial networks, this method should be associated to an area discrimination method in order to find the real solution among the multiple solutions given by the algorithm (in [Penkov, 2006] the author presents various criteria that can help discriminating the real faulty zones among the proposed solutions).

Therefore the presented results aim in showing the performance that this method could reach when associated to a discrimination method of the faulty area.

Note: Some results presented without this "treatment" are shown in appendix F.

3.5 Urban network

The urban network described in section 2.2, corresponds to a unique feeder with no laterals. It is an underground feeder with mainly cable conductors.

3.5.1 Simulated faults

a) **Current used: $\mathbf{I''_a}$ - difference between post and pre fault currents**

Let us remind below the equation used in the algorithm in order to compute the fault distance and obtain the following results (see 2.2).

$$x = \frac{\mathrm{Im}\left(V_a.I''^{*}_a\right)}{\mathrm{Im}\left(z_1.I_{tot}.I''^{*}_a\right)} \tag{IV.1}$$

	F1 2.08 km	**F2** 4.18 km	**F3** 5.75 km	**F4** 7.98 km	**F5** 10.12 km
0 Ω	2	1	3	29	44
1 Ω	-37	-86	-95	-107	-136
5 Ω	-62	-280	-393	-534	-711
10 Ω	14	*-347*	*-592*	*-866*	-1179
15 Ω	124	-346	-670	-1070	-1517
20 Ω	*294*	-271	-683	-1177	-1692
40 Ω	951	*190*	-446	-1238	*-2043*
80 Ω	2047	*973*	*349*	-852	*-2049*

Table IV.9: Results with I''_a - Error in meters for the five different fault locations and for the eight different fault resistances - results in *italic* correspond to a special case due to the algorithm behavior

As it can be seen in table IV.9, the results globally worsen as well as with the increase of the fault resistance than with the increase of the fault distance. The maximum error occurs for a 80Ω fault in F5: 2049m.

Note on results in *italic*: the algorithm propagates the measured voltage and current at the beginning of each homogeneous section and tries to locate the fault on the considered section:

- the computed fault distance is $<$ to the length of the section
  $\rightarrow$ the section is faulty
- the computed fault distance is $>$ to the length of the section
  $\rightarrow$ the algorithm propagates the voltage and current to the next section
- the computed fault distance is < 0
  $\rightarrow$ the algorithm propagates the voltage and current to the next section

What happens in the case of the fault situations where the algorithm does not find an answer is the following:

1. the computation on section N gives a fault distance $>$ to the length of the section
2. the algorithm propagates the voltage and current to the section $N+1$
3. the computation on section $N+1$ gives a fault distance < 0
4. the algorithm propagates the voltage and current to the section $N+2$ and continues on finding fault distance < 0
5. the algorithm reaches the end of the network without finding any faulty section

Table IV.10 shows as an example the case of the fault situation F2 - 10 Ω. When performing a fault localization on section N, the algorithm finds a distance greater than the 121m of the section and therefore propagates the voltage and current to the next section. But the fault localization performed on this new section, $N+1$, gives a negative result. The algorithm therefore continues downstream without ever finding any faulty section.

	Section N	Section $N+1$
Section length (m)	121	100
Computed fault distance (m)	143.97	-3.78
Total fault distance (m)	$x + 143.97$	$x + 121 - 3.78 = 117.22$
Mean fault distance (m)	$x + 130.60$	

Table IV.10: Fault distance computation of two consecutive sections in the case of the fault situation F2 - 10 Ω using equation IV.1 and considering x as the length between the head of the feeder and the beginning of section N

However, in order that the algorithm still provides an answer in those particular cases, the fault localization result is computed differently: the algorithm computes the average between the two fault distance computed on the two consecutive section. In the case of the example detailed in table IV.10, the final fault distance is therefore $x + 130.6$, x being the distance between the head of the feeder and the beginning of section N.

Figure IV.7 shows the mean distance error (in absolute value) on all fault locations for each fault resistance. However, the eight fault locations simulated show a strong diversity in terms of distance or load power flow for example. Therefore the standard deviation is also depicted on figure IV.7 and illustrates explicitly the non linear evolution of the results with the increase of the fault resistance and fault distance.

Conclusion: The use of the current I''_a is based on a statement which is true for transmission networks but is inexact for distribution networks. The consequences of this approximation is clearly seen in the results presented here: bad performance of the algorithm and strong disparities.

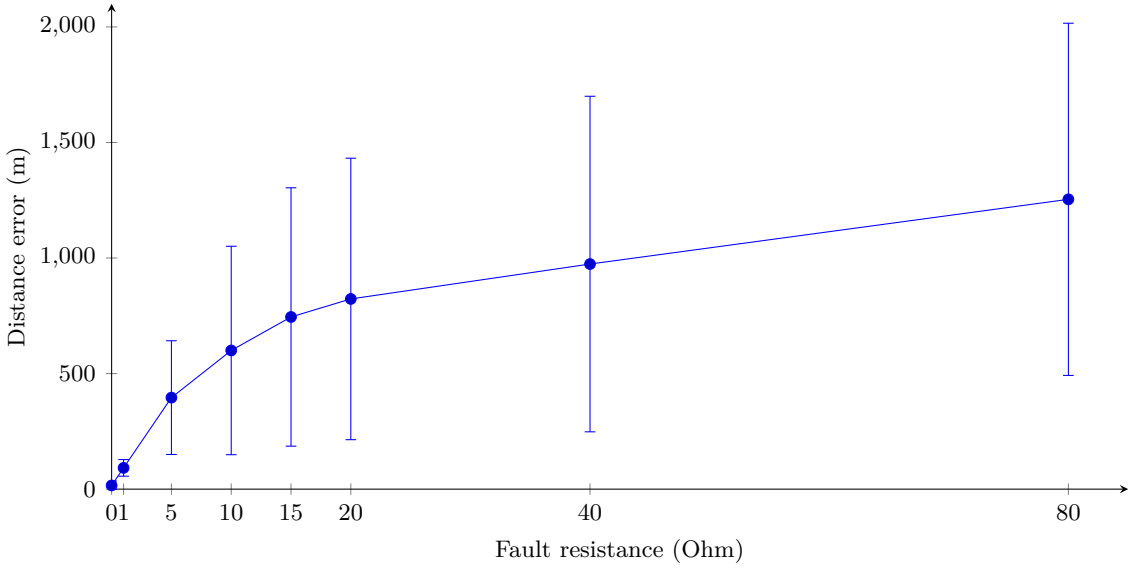

Figure IV.7: Results with I''_a - Mean distance error (m), in absolute value, on all fault locations for each fault resistance and the standard deviations associated

b) **Current used: $\mathbf{I_a}$ - phase current during the fault**

Let us remind below the equation used in the algorithm in order to compute the fault distance and obtain the following results (see 2.2).

$$x = \frac{\mathrm{Im}\left(V_a.{I_a}^*\right)}{\mathrm{Im}\left(z_1.I_{tot}.{I_a}^*\right)} \tag{IV.2}$$

	F1 2.08 km	**F2** 4.18 km	**F3** 5.75 km	**F4** 7.98 km	**F5** 10.12 km
0 Ω	-20	-39	-10	47	63
1 Ω	297	205	179	143	99
5 Ω	1416	1014	889	*505*	228
10 Ω	2575	1949	1725	761	*204*
15 Ω	3325	2910	2086	1080	*302*
20 Ω	4213	*3342*	2506	1506	*410*
40 Ω	*6147*	*4946*	3374	*2342*	*914*
80 Ω	*8240*	*5913*	*5102*	*2238*	*2226*

Table IV.11: Results with I_a - Error in meters for the five different fault locations and for the eight different fault resistances - results in *italic* correspond to a special case due to the algorithm behavior

The results obtained with equation IV.2, with the current I_a, and presented in table IV.11 are different from the results obtained with the current I''_a. Indeed, this time the fault distance is always over estimated except for a few low fault resistance cases.

Some results are again displayed in *italic* for the same reasons as the one explained in section 3.5.1 a).

Figure IV.8 illustrates these results. The evolution appears to be a little bit more linear than in the previous case, but the amplitude of the errors is much bigger. The maximum error occurs for a 80 Ω fault in F1: 8240 m.

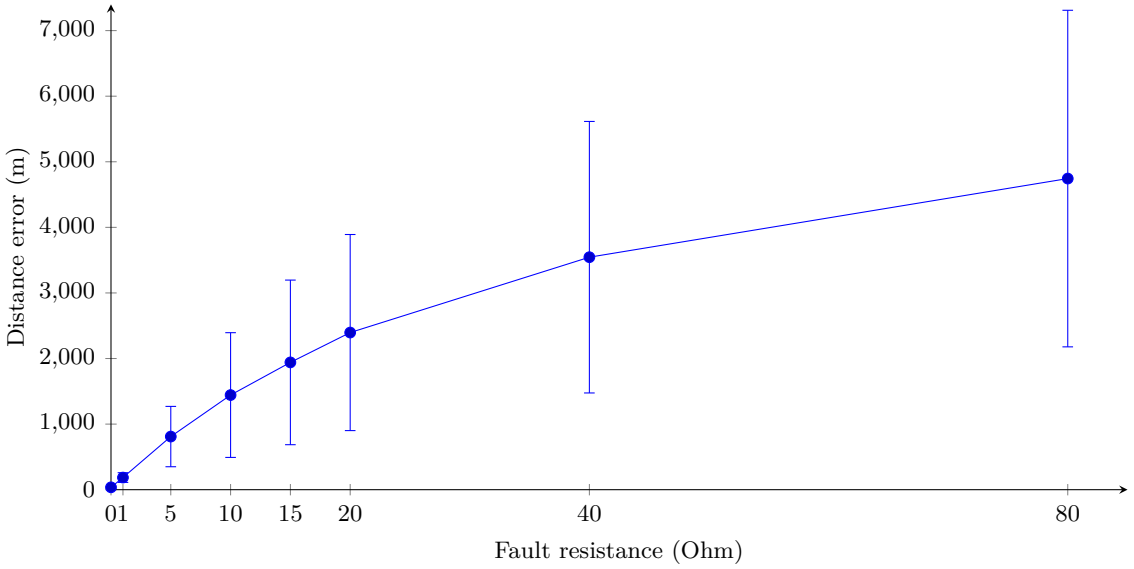

Figure IV.8: Results with I_a - Mean distance error (m), in absolute value, on all fault locations for each fault resistances and the standard deviations associated

Conclusion: The use of the current I_a in the computations corresponds to the approximation of considering that the fault current matches the phase current during the fault. This assumption is theoretically not valid, and in practice introduces errors with an unacceptable order of magnitude.

c) **Current used: $\mathbf{I_{f\ est}}$ - estimated fault current**

Let us remind below which equation is used in the algorithm in order to compute the fault distance and obtain the following results (see 2.2).

$$x = \frac{\mathrm{Im}\left(V_a.{I_{f\ est}}^*\right)}{\mathrm{Im}\left(z_1.I_{tot}.{I_{f\ est}}^*\right)}$$
$$\text{with } I_{f\ est} = \sqrt{{I_n}^2 + {I_{c_{tot}}}^2}.\exp^{j.\left(\varphi_{I_n} + \arctan\left(\frac{I_{c_{tot}}}{I_n}\right)\right)} \tag{IV.3}$$

The results shown in table IV.12 follow a different pattern than the one presented in the two previous cases. This time the fault distances are almost always under estimated. The maximum error occurs for a 80 Ω fault located in F1: 2385 m.

However, observing figure IV.9 shows that the evolution of the error with the in-

	F1 2.08 km	**F2** 4.18 km	**F3** 5.75 km	**F4** 7.98 km	**F5** 10.12 km
0 Ω	1	-7	0	37	57
1 Ω	-31	-36	-24	10	29
5 Ω	-153	-147	-123	-88	-72
10 Ω	-306	-283	-248	-202	-183
15 Ω	-461	-417	-369	-313	-286
20 Ω	-617	-550	-488	-420	-387
40 Ω	-1223	-1068	-952	-842	-781
80 Ω	*-2385*	-2075	-1868	-1679	-1589

Table IV.12: Results with $I_{f\ est}$ - Error in meters for the five different fault locations and for the eight different fault resistances - results in *italic* correspond to a special case due to the algorithm behavior

crease of the fault resistance and distance is quite linear, and that furthermore the standard deviation is much smaller than in the two previous case.

In this case, there is only one result displayed in *italic* which corresponds again to the algorithm behavior presented previously (see section 3.5.1 a)).

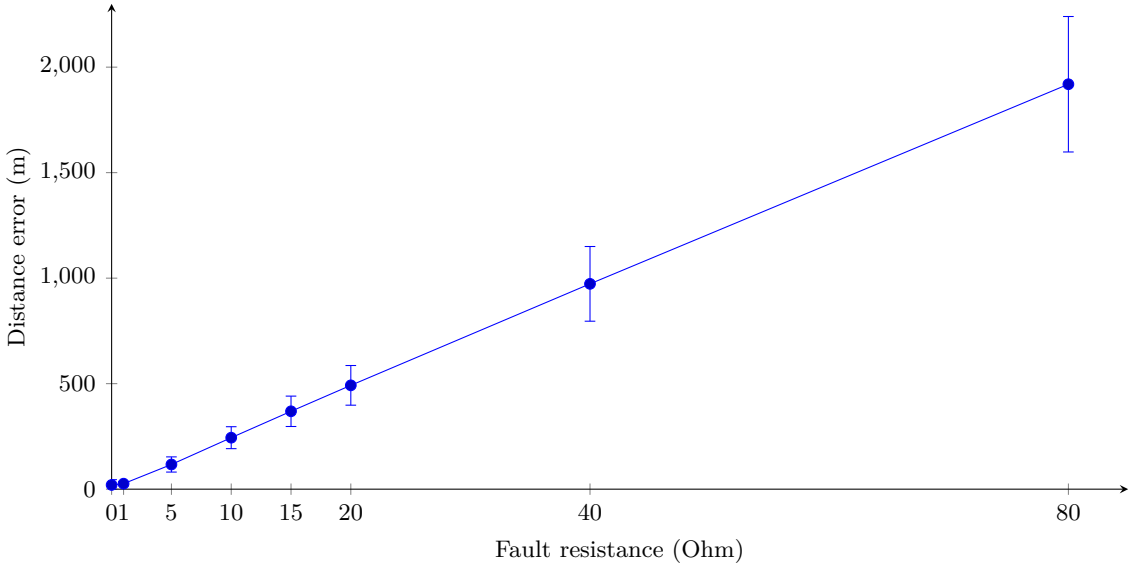

Figure IV.9: Results with $I_{f\ est}$ - Mean distance error (m), in absolute value, on all fault locations for each fault resistances and the standard deviations associated

Conclusion: The use of the current $I_{f\ est}$ in the computations seems to be the most relevant. Indeed it gives results which show a low standard deviations, traducing more consistency and a dependency to a lower number of variables. Even though at high fault resistances it gives results slightly worse than with the use of current I''_a, at low fault resistances the improvement of the results is significant.

Note: in appendix D we present the graphic illustrations of the results presented

in table IV.12. The results are plotted for each fault location and for each fault resistance.

d) **Summary of the results**

Now that the results of each cases have been presented, figure IV.10 shows the superposition of the three previous figures (IV.7, IV.8 and IV.9) in order to compare the different results on a graph with the same scale.

Now that the fault distance results have been detailed, we can add the section results (see section 3.3). Both results (fault distance and section localization) are therefore presented in the same table for each case (see tables IV.13, IV.14 and IV.15).
As a reminder (see section 3.3), below is the color code used to present the section localization results:

	success	real faulty section among the faulty sections found by the algorithm
	half-success	real faulty section adjacent to one of the faulty sections found by the algorithm
	failure	real faulty section not among nor adjacent to the faulty sections found by the algorithm

As stated previously, the section localization results are difficult to interpret. They do not seem so good when looking at the tables color, but some comments need to be made in order to explain these relatively bad results.

First of all, it is important to act that the global quality of the results depends on

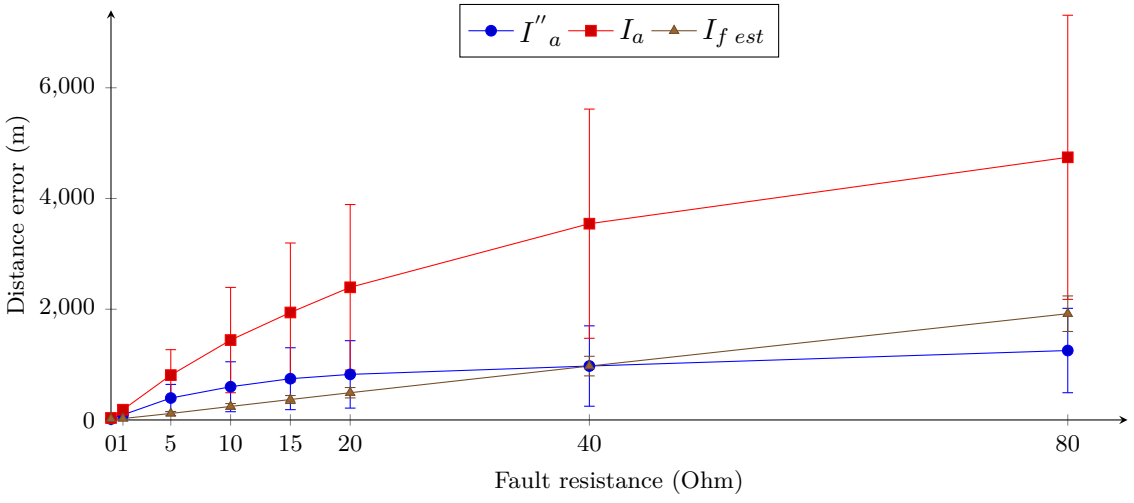

Figure IV.10: Superposition of the results for I''_a, I_a and $I_{f\ est}$ - Mean distance error (m), in absolute value, on all fault locations for each fault resistances and the standard deviations associated

	F1 2.08 km	**F2** 4.18 km	**F3** 5.75 km	**F4** 7.98 km	**F5** 10.12 km
0 Ω	2	1	3	29	44
1 Ω	-37	-86	-95	-107	-136
5 Ω	-62	-280	-393	-534	-711
10 Ω	14	*-347*	*-592*	*-866*	-1179
15 Ω	124	-346	-670	-1070	-1517
20 Ω	*294*	-271	-683	-1177	-1692
40 Ω	951	*190*	-446	-1238	*-2043*
80 Ω	2047	*973*	*349*	-852	*-2049*

Table IV.13: Cross results (distance and section) for the urban network using current I''_a

	F1 2.08 km	**F2** 4.18 km	**F3** 5.75 km	**F4** 7.98 km	**F5** 10.12 km
0 Ω	-20	-39	-10	47	63
1 Ω	297	205	179	143	99
5 Ω	1416	1014	889	*505*	228
10 Ω	2575	1949	1725	761	*204*
15 Ω	3325	2910	2086	1080	*302*
20 Ω	4213	*3342*	2506	1506	*410*
40 Ω	*6147*	*4946*	3374	*2342*	*914*
80 Ω	*8240*	*5913*	*5102*	*2238*	*2226*

Table IV.14: Cross results (distance and section) for the urban network using current I_a

the length of the faulty section and the ones surrounding it. Faults located in other places will bring different results. Indeed, the smaller are the sections lengths, the harder it is for the algorithm to find the correct faulty section.
Case F4 - 10 Ω in table IV.15 illustrates this problem: the error is of 202 m and the found faulty section is not the real faulty section, nor adjacent to it, it is therefore a "failure" result. However, case F3 - 20 Ω which has a bigger error, 488 m, finds a faulty section adjacent to the real faulty section, it is therefore a "half-success". Clearly the topology of the network influences the section localization results.

Below is a reminder of a few characteristics which help in visualizing the topology of this urban network and therefore in interpreting the results:

- minimum section length: 10 m
- maximum section length: 623 m
- mean section length: 132 m

Conclusion: the results obtained with the estimated fault currents present the best consistency in terms of evolution of the error with the increase of the fault resistance and of correct section localization. For faults up to 10 Ω the error made on the fault distance computation is always under 306 m.

	F1 2.08 km	**F2** 4.18 km	**F3** 5.75 km	**F4** 7.98 km	**F5** 10.12 km
0 Ω	1	-7	0	37	57
1 Ω	-31	-36	-24	10	29
5 Ω	-153	-147	-123	-88	-72
10 Ω	-306	-283	-248	-202	-183
15 Ω	-461	-417	-369	-313	-286
20 Ω	-617	-550	-488	-420	-387
40 Ω	-1223	-1068	-952	-842	-781
80 Ω	*-2385*	-2075	-1868	-1679	-1589

Table IV.15: Cross results (distance and section) for the urban network using current $I_{f\ est}$

3.6 Rural network

The rural network, described in section 2.3, corresponds to a long feeder with many lateral sub-feeders (or branches). The topology of this network is therefore interesting for testing the robustness of the algorithm on a strongly radial network.

3.6.1 Simulated faults

a) **Current used: $\mathbf{I''_a}$ - difference between post and pre fault currents**

The equation used in this case is the same as equation IV.1 for the urban network in section 3.5.1 a), it uses the current I''_a.

	F1 5.07 km	**F2** 10.56 km	**F3** 16.54 km	**F4** 21.14 km	**L1** 17.36 km	**L2** 20.13 km	**L3** 10.82 km	**L4** 14.38 km
0 Ω	-8	-5	-6	-26	-66	-46	-2	-46
1 Ω	-123	-224	304	-270	-330	-296	-292	-332
5 Ω	502	-805	1142	1243	1122	1111	1048	1188
10 Ω	773	1399	1860	2007	1834	1836	1657	1762
15 Ω	881	1686	2355	2598	2347	2433	1738	2134
20 Ω	896	1930	2653	3040	2762	2873	2043	2551
40 Ω	591	2404	3615	4197	3714	4101	2587	-3566
80 Ω	212	-892	4297	5435	4612	4926	3647	-4340

Table IV.16: Results with I''_a - Error in meters for the eight different fault locations and for the eight different fault resistances

Table IV.16 shows the fault distance results. The errors made by the algorithm quickly increase over 1000 m, the maximum error being 5435 m for the case F4 - 80 Ω.

The evolution of the results with the increase of the fault resistance shown in figure IV.11 possesses the same characteristics as the results for the urban network (see figure IV.7), but with a greater amplitude of the error.

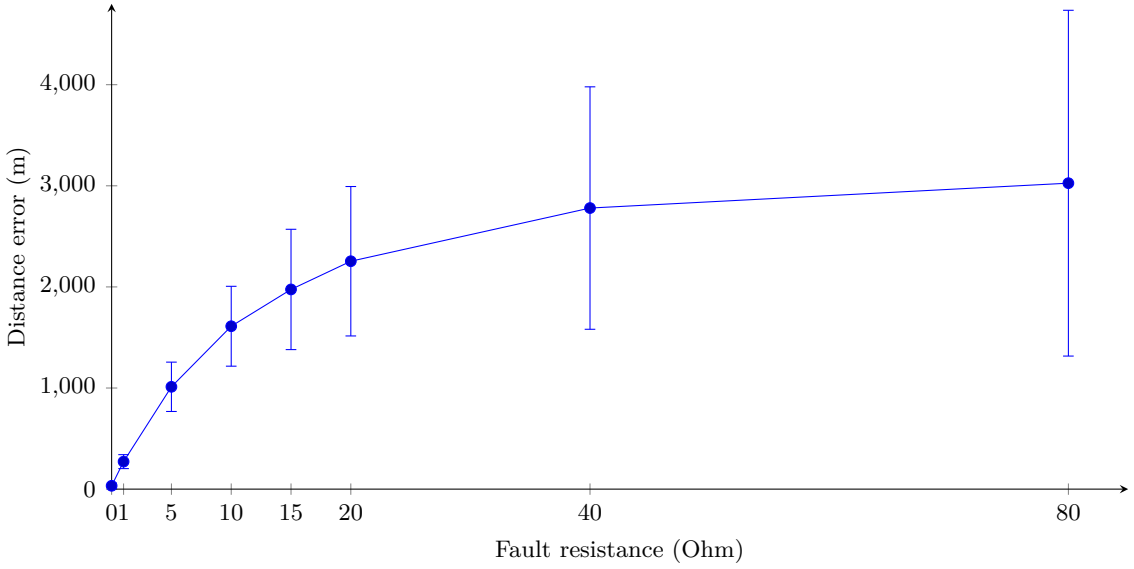

Figure IV.11: Results with I''_a - Mean distance error (m) on all fault locations for each fault resistances and the standard deviations associated

Conclusion: The same conclusion as in the case of the urban network can be made here. The use of the current I''_a is based on a statement which is true for transmission networks but is inexact for distribution networks. The consequences of this approximation is clearly seen in the results presented here: bad performance of the algorithm and strong disparities.

b) **Current used: $\mathbf{I_a}$ - phase current during the fault**

The equation used in this case is the same as equation IV.2 for the urban network in section 3.5.1 b), it uses the current I_a.

	F1 5.07 km	**F2** 10.56 km	**F3** 16.54 km	**F4** 21.14 km	**L1** 17.36 km	**L2** 20.13 km	**L3** 10.82 km	**L4** 14.38km
0 Ω	43	-54	-121	-43	-102	-67	-36	-98
1 Ω	232	94	-63	-37	-89	-58	-23	-83
5 Ω	950	689	-51	-6	-38	-19	21	-31
10 Ω	94	88	417	39	17	33	71	23
15 Ω	352	146	441	87	65	85	118	68
20 Ω	1990	762	270	134	107	136	167	109
40 Ω	431	1868	624	344	258	277	335	280
80 Ω	4005	3076	1215	∨	1230	1012	2851	2061

Table IV.17: Results with I_a - Error in meters for the eight different fault locations and for the eight different fault resistances - "∨" means that the algorithm solution is out of bounds of the network

The results presented in table IV.17 show again, as for the urban network, inconsis-

tencies. Indeed the results do not always show a linear evolution with the increase of the fault resistance or the fault distance. The maximum error occurs for the case F1 - 80 Ω with 4005 m.

These results show one new algorithm behavior in the case F4 - 80 Ω: the algorithm does not find any faulty section nor fault distance because it sees the fault out of bounds of the network. Fault F4 being located a few hundred meters before the end of the feeder, the distance over estimation margin is passed by the algorithm which sees the fault further away than the maximum possible distance.

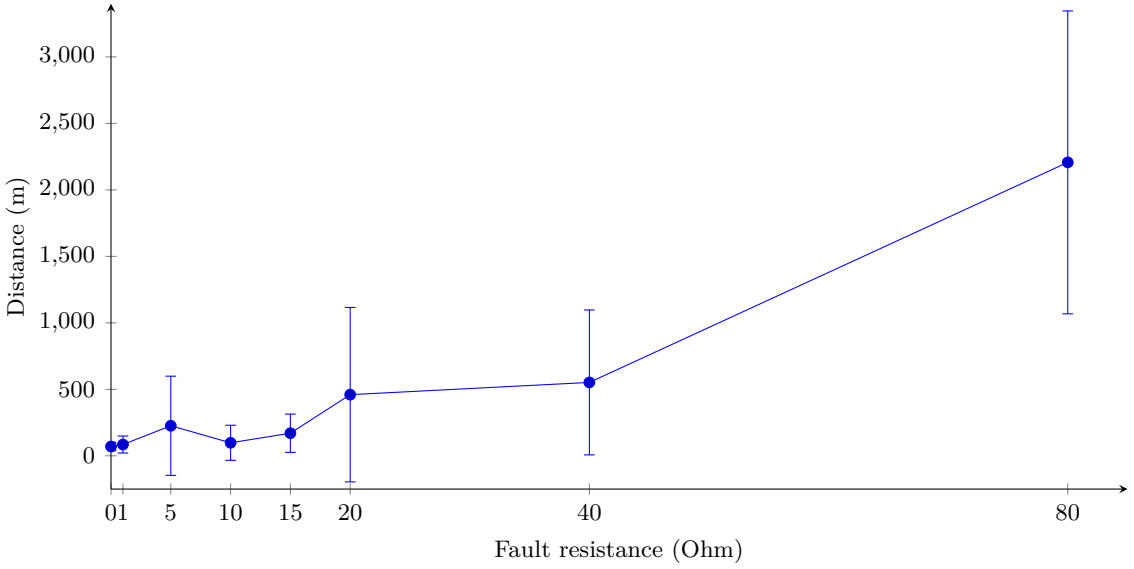

Figure IV.12: Results with I_a - Mean distance error (m) on all fault locations for each fault resistances and the standard deviations associated

Figure IV.12 shows the evolution of the results with the increase of the fault resistance. The evolution of the error is slightly more linear than in the previous case, but the standard deviations are still important and illustrate the strong differences that can occur sometimes from one fault situation to another.

Conclusion: The use of the current I_a in the algorithm gives better results in terms of error amplitude but do not show a strong consistency with the evolution of the different parameters. It is interesting to also note that the case here is the opposite than for the urban network where the results obtained with I_a were worse thant the ones obtained with I''_a.

c) **Current used: $\mathbf{I_{f\ est}}$ - estimated fault current**

The equation used in this case is the same as equation IV.3 for the urban network in section 3.5.1 c), it uses the current I_f.

	F1 5.07 km	**F2** 10.56 km	**F3** 16.54 km	**F4** 21.14 km	**L1** 17.36 km	**L2** 20.13 km	**L3** 10.82 km	**L4** 14.38 km
0 Ω	20	-44	-118	-45	-105	-68	-40	-102
1 Ω	50	5	-85	-17	-73	-39	-8	-71
5 Ω	98	69	36	89	44	71	72	40
10 Ω	179	173	171	212	176	198	178	167
15 Ω	262	274	293	327	297	243	282	283
20 Ω	347	370	405	∨	409	291	382	391
40 Ω	667	719	809	∨	612	400	435	491
80 Ω	1056	341	1496	∨	790	∨	679	695

Table IV.18: Results with $I_{f\ est}$ - Error in meters for the eight different fault locations and for the eight different fault resistances - "∨" means that the algorithm solution is out of bounds of the network

Table IV.18 shows results which seem to be consistent with the increase of the fault resistance, and not so dependent of the fault distance. The maximum error is 1496 m for the case F3 - 80 Ω. Again, as for the results obtained in the previous case, the algorithm finds a fault distance which is out of bounds of the network for a few cases. This occurs when the fault is located near the end of a conductor and that the fault distance is over estimated.

Note: Results without the "treatment" described in section 3.4 can be seen in appendix F.
Figure IV.13 shows the evolution of the results with the increase of the fault resistance. This time the results are much more linear, with an increasing mean error with the increase of the fault resistance.

The distance error made by the algorithm is always "increasing" with the increase of the fault resistance. The results also show a low standard deviation which shows the consistency of the algorithm when computing the results with the estimated fault current $I_{f\ est}$.

Conclusion: The use of the current I_f in the algorithm gives the best results in terms of error amplitude and consistency with the evolution of the different parameters. Even though high fault resistance bring errors of about 1 km, for 10 Ω faults and under, the magnitude order of the errors is of 200 m or less, even for faults located at more than 15 km.

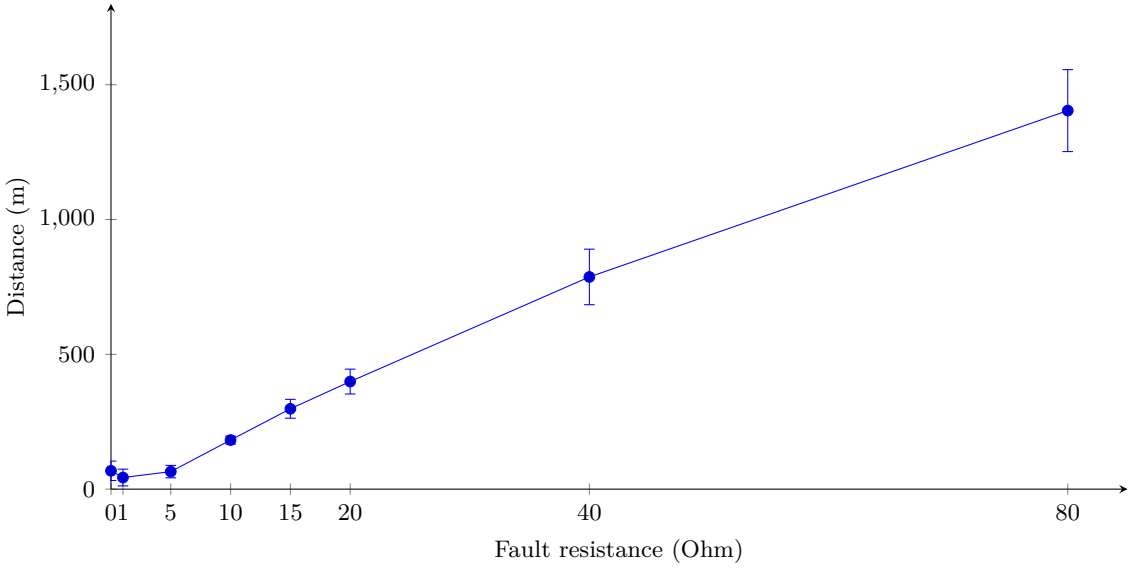

Figure IV.13: Results with $I_{f\ est}$ - Mean distance error (m) on all fault locations for each fault resistances and the standard deviations associated

d) **Summary of the results**

The superposition of the distance results for all three cases in figure IV.14 gives a complete view of the performance of each case.

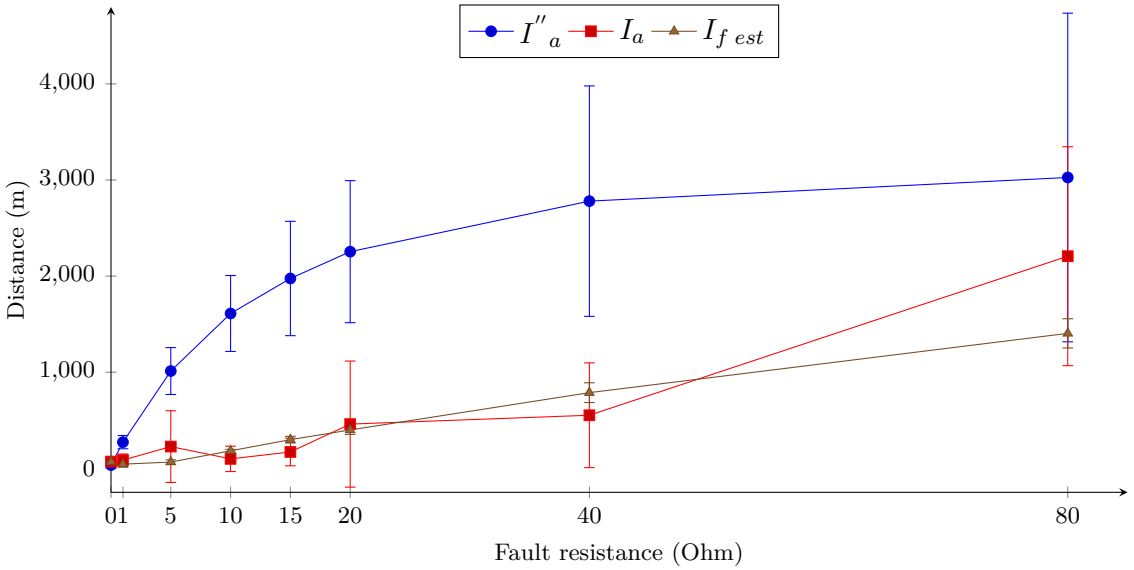

Figure IV.14: Mean distance error (m) on all fault locations for each fault resistances

Again results obtained with the estimated fault current $I_{f\ est}$ come out as the most relevant, as well in terms of amplitude (maximum error of 159 4m) than in terms of

consistency (low standard deviation). The results obtained with I''_a and I_a confirm the strong inconsistency when facing different fault situations (resistance, distance, topology,...).

	F1 5.07 km	**F2** 10.56 km	**F3** 16.54 km	**F4** 21.14 km	**L1** 17.36 km	**L2** 20.13 km	**L3** 10.82 km	**L4** 14.38 km
0 Ω	-8	-5	-67	-26	-66	-46	-2	-46
1 Ω	-123	-224	-306	-270	-330	-296	-292	-332
5 Ω	-502	-805	-1142	-1243	-1088	-1097	-1031	-1188
10 Ω	-773	-1399	-1854	-2007	-1812	-1824	-1459	-1762
15 Ω	-881	-1366	-2331	-2572	-2347	-2433	-1738	-2134
20 Ω	-896	-1662	-2653	-3034	-2722	-2864	-1765	-2435
40 Ω	-591	-1894	-3115	-4154	-3611	-3909	-2071	-2898
80 Ω	212	-892	-3682	-4884	-4269	-4449	-2408	-3414

Table IV.19: Cross results (distance and section) for the rural network using current I''_a

	F1 5.07 km	**F2** 10.56 km	**F3** 16.54 km	**F4** 21.14 km	**L1** 17.36 km	**L2** 20.13 km	**L3** 10.82 km	**L4** 14.38 km
0 Ω	43	-54	-121	-43	-102	-67	-36	-98
1 Ω	232	94	-63	-37	-89	-58	-23	-83
5 Ω	950	689	-51	-6	-38	-19	21	-31
10 Ω	94	88	417	39	17	33	71	23
15 Ω	352	146	441	87	65	85	118	68
20 Ω	1990	762	270	134	107	136	167	109
40 Ω	431	1868	624	344	258	277	335	280
80 Ω	4005	3076	1215	∨	1230	1012	2851	2061

Table IV.20: Cross results (distance and section) for the rural network using current I_a

	F1 5.07 km	**F2** 10.56 km	**F3** 16.54 km	**F4** 21.14 km	**L1** 17.36 km	**L2** 20.13 km	**L3** 10.82 km	**L4** 14.38 km
0 Ω	20	-44	-118	-45	-105	-68	-40	-102
1 Ω	50	5	-85	-17	-73	-39	-8	-71
5 Ω	98	69	36	89	44	71	72	40
10 Ω	179	173	171	212	176	198	178	167
15 Ω	262	274	293	327	297	370	282	283
20 Ω	347	370	405	∨	409	491	382	391
40 Ω	667	719	809	∨	843	971	700	803
80 Ω	1306	1341	1594	∨	1512	∨	1187	1483

Table IV.21: Cross results (distance and section) for the rural network using current $I_{f\,est}$

Once again we can add to the fault distance results the section localization results. Tables IV.19, IV.20 and IV.21 therefore show both fault distance and section localization results in the same table for each cases. The color code used to present the results is the same as the one used for the urban network and is explained in section

3.3.

The results need to be considered again as depending on the topology of the network. Looking at case L4 - 5 Ω for results obtained with I''_a, we can see that the distance error is of 1188 m, and yet the section localization result is "half-success" because the found section is adjacent to the real faulty section. Case F3 - 1 Ω is the opposite with a fault distance of 306 m and yet a "failure" in terms of section localization.

So once again, the results illustrate the possibility for the algorithm to locate correctly or not faulty sections, but for this particular network, and for these particular fault locations. The length of the sections where are located the eight faults are given in table IV.22.

	F1	F2	F3	F4	L1	L2	L3	L4
Faulty section length (m)	549	1965	351	543	711	596	667	917

Table IV.22: Length (m) of the faulty sections for each fault location

The faulty section for fault F2 for example is quite long, 1965 m, which is consistent with the previous statement when looking at the results: fault F2 has the most "success" results in terms of section localization.

The section localization results are clearly better when computed with the current $I_{f\ est}$. It can be noted that for all fault locations and for fault resistances under 10 Ω, the algorithm always succeeds in finding the correct faulty section and gives fault distances inferior to 300 m.

3.6.2 Example of a multiple solutions result

We will show here the complete results obtained with the algorithm (using current $I_{f\ est}$) in the case of a multiple solution situation.

Table IV.23 shows the eight solutions found when processing a fault localization on the fault case F3 - 5 Ω on the rural network. Among the solutions features the real faulty section which is section number 49.

Section number	109	140	187	236	89	65	220	49
Distance (m)	16530,2	16530,2	16529,7	16521,5	16573,1	16574,8	16574,7	16576,8
Estimated R_f (Ω)	4,58	4,58	4,58	4,41	4,77	4,77	4,77	4,76

Table IV.23: Localization results for the fault F3 5 Ω on the rural network: number of the section found faulty, fault distance and estimated fault resistance

Figure IV.15 depicts those results on the feeder representation.

It is interesting to see that despite the strong radial characteristic of the network, and the eight solutions found, they are grouped in only two distinctive zones, reinforcing the

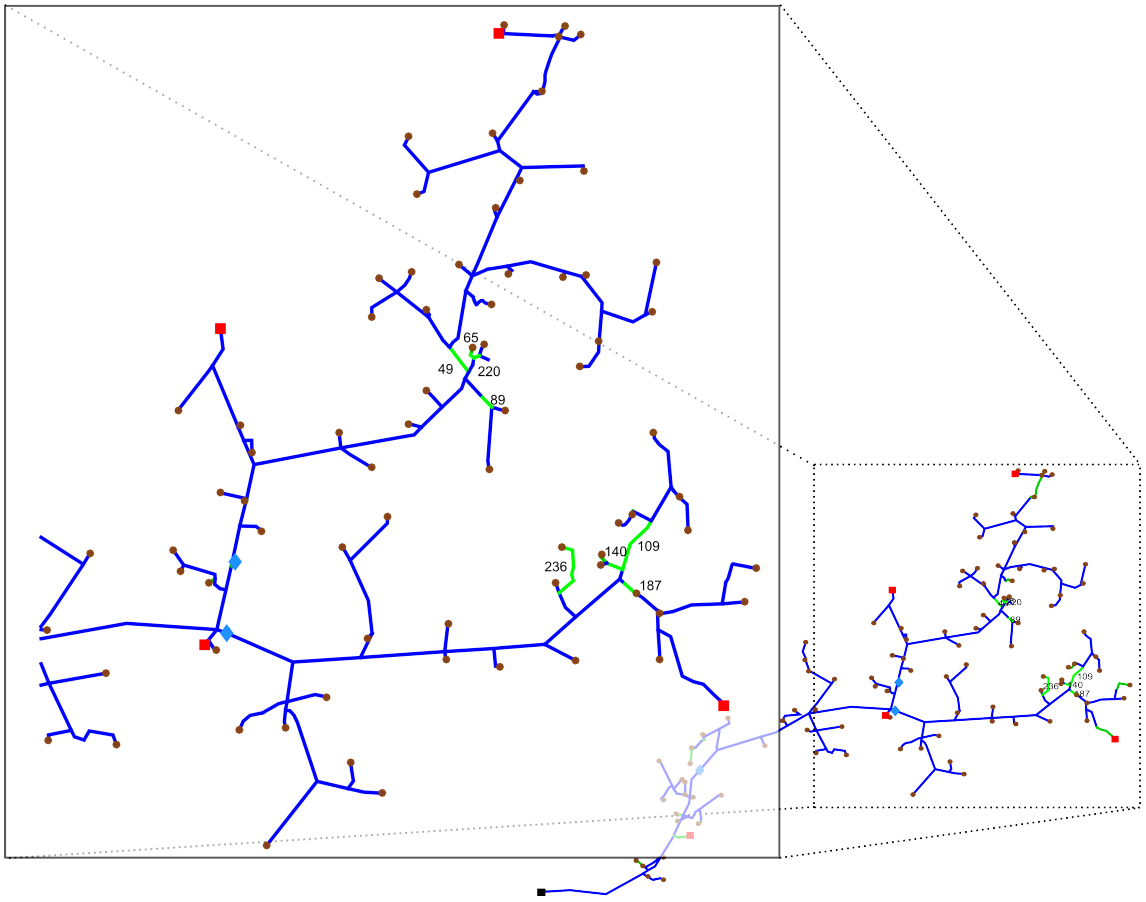

Figure IV.15: Illustration of the eight fault locations found by the algorithm in the case of the fault F3 - 5 Ω (green sections)

idea that completing this localization method by a faulty area discrimination method can help greatly in discriminating the fault localization results.

3.7 Real fault measurements

As described previously, the work in partnership with french DSOs gave us access to interesting and complete date concerning urban and rural feeders. We also obtained real fault measurements of faults which occurred precisely on the feeders which we had information about.

These fault measurements were very interesting for us since they occurred on networks that we could simulate precisely thanks to the completeness of the data.

In the following we will show some of the fault measurements that we obtained (which are sampled at 6400 Hz) and will also point out the differences with the simulated fault signals.

3.7.1 Measured and simulated fault signals

Below are the measurements of the faulted phase voltage and current for different simulated situations and real cases:

- **fault simulation - urban network - fault in F2 with $\mathbf{R_f = 5\,\Omega}$**

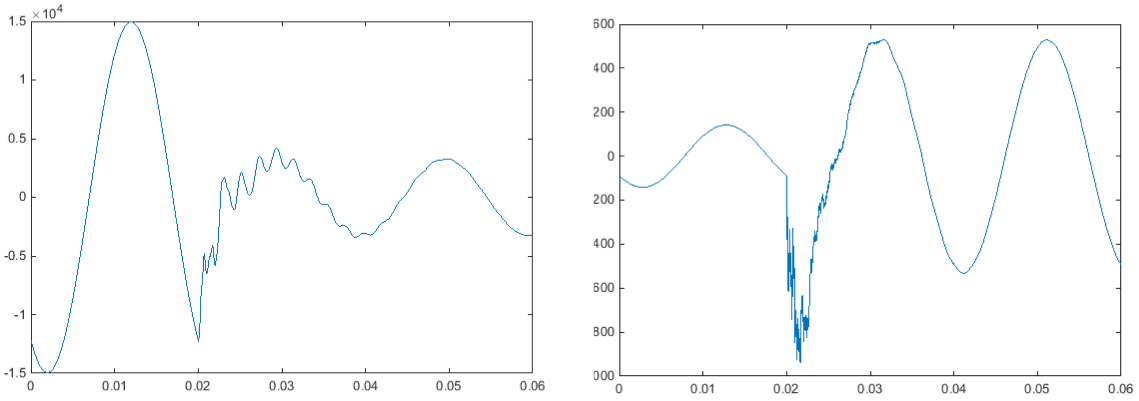

Figure IV.16: Faulted phase voltage (left, in V) and current (right, in A) for the fault simulation case F2 5 Ω on the urban network

On the urban network and for a resistive fault of 5 Ω located at 4178 m, both voltage and current curves (figure IV.16) show a transient which last less than a period. The voltage drop is about 80 % while the current increase is around 370 %.

- **fault simulation - rural network - fault in L2 with $\mathbf{R_f = 0\,\Omega}$**

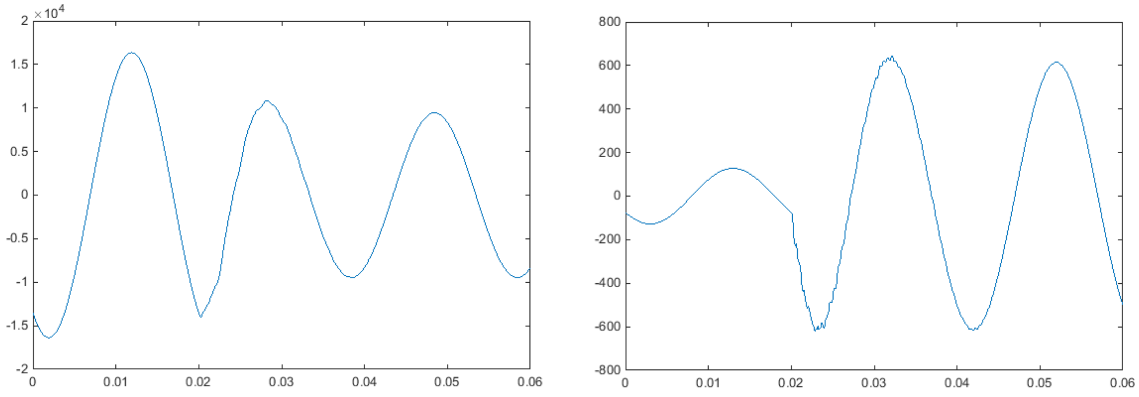

Figure IV.17: Faulted phase voltage (left, in V) and current (right, in A) for the fault simulation case L2 0 Ω on the rural network

On the rural network and for a bolted fault located at 20138 m, for both voltage and current curves (figure IV.17) there is almost no transient. For this case the voltage drop is about 40 % while the current increase is around 480 %.

- **real fault measurement - urban network**

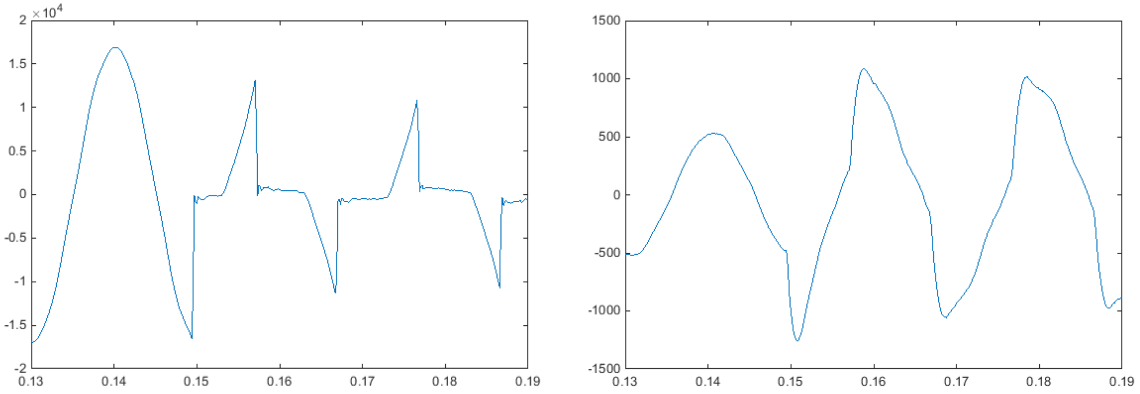

Figure IV.18: Faulted phase voltage (left, in V) and current (right, in A) from a real fault measurements which occurred on the urban network

For this real case (figure IV.18) we can see from the voltage curve that the fault is not a classic resistive fault. Indeed it seems that the fault varies in time periodically. This type of curve corresponds to an arc fault. During one period there are two stages: the first stage corresponds to the increase of the voltage, then once the voltage reaches a rupture point, an arc is created and burns during the second half of the period, then the arc extinguishes itself, the voltage builds up again and the cycle starts over.
The DSO knows approximately the position of this fault and stated that it was located between two consecutive medium voltage/low voltage substation, which in terms of distance is between 678 m and 963 m.

- **real fault measurement - rural network**

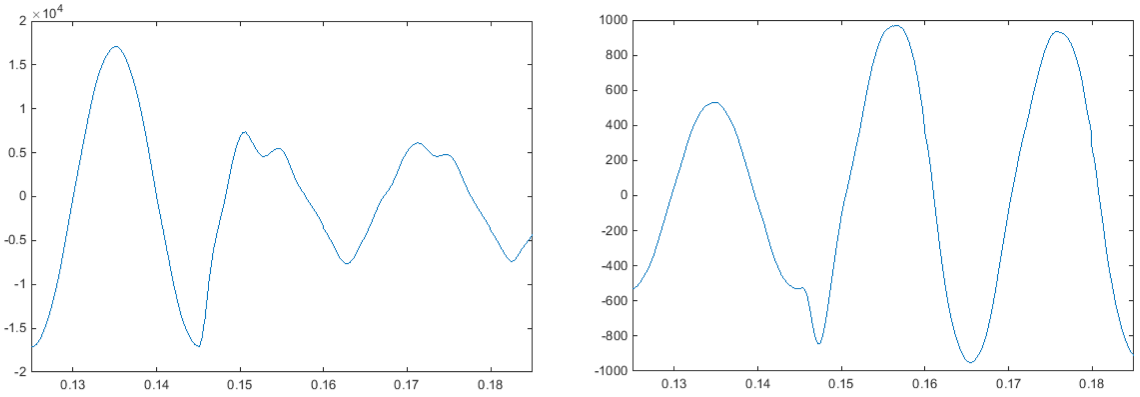

Figure IV.19: Faulted phase voltage (left, in V) and current (right, in A) from a real fault measurements which occurred on the rural network

For this real case (figure IV.19) the curves resemble more to the curves of the fault on the rural network (case L2 0 Ω presented above). However the voltage curve presents

a shape still different and yet not explained. In this case, the DSO states that the fault appeared to be close to the end of the main feeder, at more than 21 km.

3.7.2 Limits with the real fault measurements

As we can see in the presentation of the real fault measurements (see figure IV.18 and IV.19) the electrical signals are not so close to the signals obtained with fault simulations. In one case the type of the fault, a self-reigniting arc, presents particularities which can not be overcome by the developed fault localization method.

For the second case, the fault measurement on the rural network, we face another problem which is the non availability of the needed data. Indeed, the fault localization method proposed does not need many variables but needs, among other, the phase voltages at the measuring point and the phase currents flowing into the faulty feeder. Yet, the data that is available here is effectively the voltage at the measuring point (at the substation and therefore the head of the feeder) and the total phase currents flowing through the substation (therefore the sum of all the currents flowing into the feeders connected to the substation). Without the phase currents per feeder, the method that we propose is inapplicable.

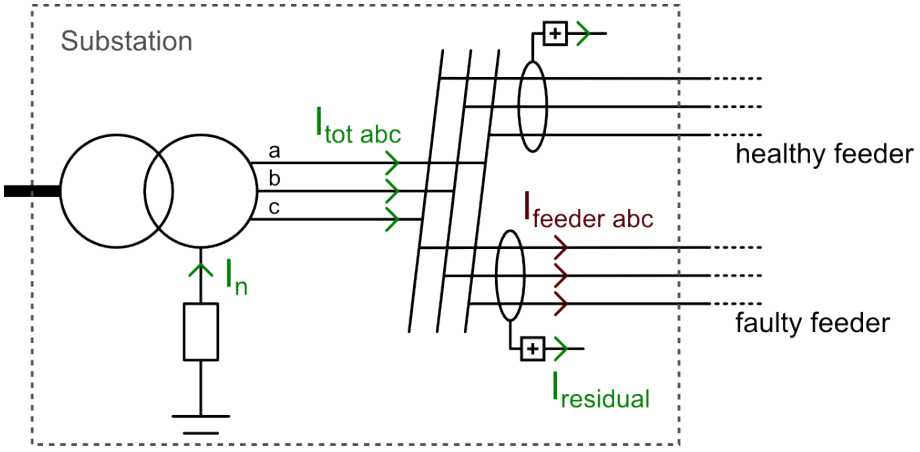

Figure IV.20: Details of the substation measures which are accessible by the DSO (in green) and measures that are needed by the proposed fault localization method (in brown)

Figure IV.20 shows the data that we have access to and the needed data in order to perform the fault localization on the real fault measurements given by the DSO. The DSO could only provide the total phase currents of the substation for the concerned networks that we simulated and from which the real fault measurements come from. As stated previously, the method needs the phase currents of the feeder concerned by the fault in order to perform the fault localization.

Therefore, the fault localization method proposed in this thesis could unfortunately not be tested on theses real fault measurements.

4 Fault resistance estimation

A secondary result of the developed algorithm is the estimation of the fault resistance. Indeed from equation III.6 in section 2.2 of chapter III, and replacing I''_a by $I_{f\,est}$, we can write the following equation:

$$\begin{gathered} \mathrm{Re}(V_a.{I_{f\,est}}^*) = \mathrm{Re}(x.z_1.I_{tot}.{I_{f\,est}}^*) + \mathrm{Re}(R_f.I_{f\,est}.{I_{f\,est}}^*) \\ \text{therefore} \\ R_f = \frac{\mathrm{Re}(V_a.{I_{f\,est}}^*) - \mathrm{Re}(x.z_1.I_{tot}.{I_{f\,est}}^*)}{\mathrm{Re}(I_{f\,est}.{I_{f\,est}}^*)} \end{gathered} \tag{IV.4}$$

At each computation of the fault distance (at each section), the estimated R_f is then computed with the same variables and the fault distance x just computed with the imaginary part of equation III.6.

	F1 2.08 km	**F2** 4.18 km	**F3** 5.75 km	**F4** 7.98 km	**F5** 10.12 km
0 Ω	-0.1	-0.1	0.0	0.1	0.1
1 Ω	1.0	0.9	0.9	1.0	1.0
5 Ω	4.9	4.8	4.8	4.8	4.8
10 Ω	9.8	9.7	9.7	9.7	9.6
15 Ω	14.7	14.6	14.5	14.5	14.5
20 Ω	19.6	19.4	19.4	19.3	19.3
40 Ω	39.3	39.0	38.8	38.6	38.6
80 Ω	NaN	78.1	77.7	77.4	77.1

Table IV.24: Estimated fault resistance R_f (Ω) computed with $I_{f\,est}$ for the five different fault locations on the urban network and for the eight different fault resistances - NaN appears when no fault location is found and therefore no estimation of R_f is made

When a computed fault distance corresponds to a fault on the considered section, the corresponding R_f estimated is stored. We can therefore present the results tables for both urban (table IV.24) and rural networks (table IV.25) filled with the estimated fault resistances for each fault case.

These results show that the algorithm makes a good estimation of the fault resistance in all cases, whatever the position, the network or the fault resistance, even though it constantly underestimates a little the fault resistance. Therefore the estimated fault resistance is a good indicator which can help in interpreting the fault localization results.

	F1 5.07 km	**F2** 10.56 km	**F3** 16.54 km	**F4** 21.14 km	**L1** 17.36 km	**L2** 20.13 km	**L3** 10.82 km	**L4** 14.38 km
0 Ω	0.1	-0.6	-0.3	-0.1	0.0	-0.2	0.1	0.1
1 Ω	1.0	0.4	0.7	0.9	0.9	0.8	1.1	1.1
5 Ω	4.9	4.3	4.7	4.8	4.9	4.7	5.1	5.0
10 Ω	9.8	9.2	9.6	9.6	9.8	9.5	9.9	10.0
15 Ω	14.6	14.1	14.5	14.5	14.7	14.3	14.8	14.9
20 Ω	19.6	19.0	19.3	NaN	19.5	19.2	19.7	19.8
40 Ω	39.1	38.7	38.7	NaN	38.9	38.6	39.4	39.3
80 Ω	78.2	78.1	77.6	NaN	77.6	NaN	78.8	77.9

Table IV.25: Estimated fault resistance R_f (Ω) computed with $I_{f\ est}$ for the eight different fault locations on the rural network and for the eight different fault resistances - NaN appears when no fault location is found and therefore no estimation of R_f is made

5 Sensitivity analysis

5.1 Sensitivity to the estimated fault current

As it has been explained previously, the theory of the developed method is to build a fault localization algorithm robust to fault resistance. The equation used to compute the fault distance are theoretically independent from the fault resistance R_f.

However the results presented in section 3 show that it is not the case. As analyzed previously, the performances of the algorithm are deteriorated with the increase of the fault resistance, thus expressing a dependence to the fault resistance in the equation.

The only way to explain this is to assume that the theoretical process to eliminate the fault resistance of the equation (presented in sections 2.2 and 3.2.1 of chapter III) is not working in practice.

Let us remind that the process consists in multiplying the equation by a current in phase with the fault current I_f, in order to make the term with R_f strictly real and rule it out by taking the imaginary parts of the equation.

We chose to use an estimation of the current I_f: $I_{f\ est}$ (see section 3.2.2 in chapter III). Now let us assume that the estimated current $I_{f\ est}$ is not strictly in phase with I_f and look at the consequences on the fault localization equation.

The error due to the phase difference between $I_{f\ est}$ and I_f will be noted as:

$$err_{ph} = \mathrm{Im}(I_f.{I_{f\ est}}^*) \neq 0 \tag{IV.5}$$

The equation is therefore the following:

$$x = \frac{\mathrm{Im}\,(V_a.{I_f}^*) - R_f.err_{ph}}{\mathrm{Im}\,(z_1.I_{tot}.{I_f}^*)} \tag{IV.6}$$

The total error term is therefore:

$$err_{tot} = \frac{-R_f.err_{ph}}{\mathrm{Im}\,(z_1.I_{tot}.{I_f}^*)} \tag{IV.7}$$

We can see that this error term increases as:

- the fault resistance R_f increases
- the fault current I_f decreases
- the phase difference between $I_{f\ est}$ and I_f increases

5.1.1 Urban network - $I_{f\ est}$ phase error

The results presented in table IV.26 show the angle error made during the fault localization between the real fault current and the estimated fault current for every fault location and fault resistance.

	F1 2.08 km	**F2** 4.18 km	**F3** 5.75 km	**F4** 7.98 km	**F5** 10.12 km
0 Ω	-1.5	-1.4	-1.4	-1.3	-1.3
1 Ω	-1.5	-1.4	-1.4	-1.3	-1.3
5 Ω	-1.6	-1.4	-1.4	-1.3	-1.3
10 Ω	-1.6	-1.4	-1.4	-1.3	-1.3
15 Ω	-1.6	-1.4	-1.4	-1.3	-1.3
20 Ω	-1.6	-1.4	-1.4	-1.3	-1.3
40 Ω	-1.6	-1.4	-1.4	-1.3	-1.3
80 Ω	-1.6	-1.4	-1.4	-1.3	-1.3

Table IV.26: Angle error (in degrees) between I_f and $I_{f\ est}$

As it can be seen, the angle error is roughly always the same, varying between -1.3 ° and -1.6 ° in the case of this network.

This can seem illogical since we previously showed that the localization results were worse with a high R_f, and yet the phase error does not increase with R_f. The explanation is in the error term described by the equation IV.7, where it can be seen that the phase error is multiplied by the fault resistance.

Therefore making a phase error with $R_f = 0\,\Omega$ has no consequences. But making the same error with $R_f = 80\,\Omega$ induces a much higher localization error.

In order to verify the influence of this phase error made in the estimation of I_f, the fault localization algorithm has been computed on this urban network (for the same fault locations and fault resistances) using this time a corrected estimated fault current:

$$I_{f\ est\ corr} = |I_{f\ est}|.\exp(j.\varphi_f) \tag{IV.8}$$

with φ_f the angle of the measured fault current (which of course is not accessible in real life, but is used here for the proof).

When using the corrected estimated fault current, the results are considerably better. They are presented in table IV.27.

The performance of the algorithm is clearly improved:

- for every case the correct faulty section is found by the algorithm
- the maximum error made by the algorithm is of 58.9 m for a fault located at 10127.5 m

	F1 2.08 km	**F2** 4.18 km	**F3** 5.75 km	**F4** 7.98 km	**F5** 10.12 km
0 Ω	-0.8	-10.6	-1.2	38.1	58.9
1 Ω	0.3	-11.5	-2.7	30.5	50.4
5 Ω	4.6	-12.5	-7.3	15.4	30.2
10 Ω	6.0	-12.9	-10.9	7.6	19.5
15 Ω	6.3	-13.1	-13.5	3.9	14.8
20 Ω	6.2	-12.8	-15.4	1.5	12.5
40 Ω	5.1	-9.0	-16.9	-3.8	8.2
80 Ω	3.7	-3.5	-11.9	-7.7	0.8

Table IV.27: Results using current $I_{f\ est\ corr}$, the corrected estimated fault current - Error in meters for the five different fault locations and for the eight different fault resistances

5.1.2 Rural network - $I_{f\ est}$ phase error

The same analysis can be made for the rural network. Results of the phase error are shown in table IV.28.

	F1 5.07 km	**F2** 10.56 km	**F3** 16.54 km	**F4** 21.14 km	**L1** 17.36 km	**L2** 20.13 km	**L3** 10.82 km	**L4** 14.38 km
0 Ω	2.3	2.7	1.1	1.2	1.0	1.1	1.9	1.5
1 Ω	1.5	1.7	0.9	1.1	1.0	1.1	1.0	0.8
5 Ω	0.8	0.7	0.9	1.1	0.9	1.0	0.7	0.8
10 Ω	0.8	0.8	0.9	1.0	0.9	1.0	0.8	0.8
15 Ω	0.8	0.8	0.9	0.9	0.9	0.9	0.8	0.8
20 Ω	0.8	0.8	0.9	0.9	0.9	0.9	0.8	0.8
40 Ω	0.8	0.8	0.9	0.9	0.9	0.9	0.8	0.8
80 Ω	0.8	0.8	0.8	0.8	0.8	0.8	0.8	0.8

Table IV.28: Angle error (in degrees) between I_f and $I_{f\ est}$

As it can be seen, the angle error is maximum 2.7 ° in the case of this network. And the error decreases to 0.8 ° with the increase of the fault resistance.

In order to verify the influence of this phase error, the fault localization algorithm has been computed on this rural network (for the same fault locations and fault resistances) using this time a corrected estimated fault current:

$$I_{f\ est\ corr} = |I_{f\ est}|.\exp(j.\varphi_f) \tag{IV.9}$$

with φ_f the angle of the measured fault current (which of course is not accessible in real life, but is used here for the proof).

Table IV.29 shows the results obtained with this corrected estimated fault current. The results are again considerably better:

- the maximum error is now of 113 m for a fault located at 16.54 km
- for every case the algorithm finds the correct faulty section

	F1 5.07 km	**F2** 10.56 km	**F3** 16.54 km	**F4** 21.14 km	**L1** 17.36 km	**L2** 20.13 km	**L3** 10.82 km	**L4** 14.38 km
0 Ω	12	-36	-113	-43	-102	-66	-35	-97
1 Ω	11	-30	-103	-41	-93	-62	-29	-86
5 Ω	6	-13	-66	-28	-60	-42	-9	-50
10 Ω	1	-1	-32	-9	-28	-18	5	-19
15 Ω	-1	4	-9	9	-6	2	11	0
20 Ω	-1	7	5	23	9	17	15	11
40 Ω	0	11	29	52	35	47	19	29
80 Ω	-6	10	39	72	49	65	22	36

Table IV.29: Results using current $I_{f\ est\ corr}$, the corrected estimated fault current - Error in meters for the eight different fault locations and for the eight different fault resistances

Conclusion: These new results, which are obtained with a corrected estimation of the fault current, confirm that the error made on the estimation of the phase of the fault current is a major cause to the errors made in the fault distance computation. On both networks, the distance error magnitude is less or equal to 100 m which when compared to the total length of the networks (10.662 km for the urban network and 21.507 km for the rural network) reveals a good precision.

5.2 Sensitivity to the precision of the propagated voltages/currents

When using the localization equation with the estimated fault current IV.3, there are other variables that can introduce an error.

V_a, I_a and I_0 are variables which are measured at the head of the feeder, but propagated through the network, using the given network parameters (lines and cables characteristics, lengths, loads). Therefore an error can appear through the propagation process.

Observing in details what variable influences the results and how shows that the second source of error (after the estimation of the phase of $I_{f\ est}$) is the difference between the propagated voltage of the faulty phase and the real voltage. A detailed analysis is presented in appendix E.

The analysis shows that for the urban network, mainly constituted of cables, the error grows at a rate of around 1.24 V/1000 m. Meaning that at 10 km from the head of the feeder, the error on the propagated voltage of the faulty phase will be 12.4 V.

For the rural network, mainly constituted of aerial lines, the error grows at a much higher rate of 7.8 V/1000 m. At 20 km of the head of the feeder, the error will be of 156.1 V.

However, as seen in table IV.30, correcting this error does not lead to significantly better results. This error factor is less important than the error on the phase of the estimated fault current.

	$I_{f\ est}$ No correction	$I_{f\ est}$ V_a corrected
Urban - F3 (5750.5 m) - $R_f = 5\,\Omega$	-123.5	-116.7
Urban - F3 (5750.5 m) - $R_f = 40\,\Omega$	-959	-942.7
Rural - F3 (16540.5 m) - $R_f = 5\,\Omega$	36.3	103.9
Rural - F3 (16540.5 m) - $R_f = 40\,\Omega$	808.8	782

Table IV.30: Distance errors (m) made by the localization algorithm for two cases on each network when correcting or not the propagated voltage

5.3 Results with error corrections

In order to obtain very good results it is necessary to correct both the phase error of the estimated fault current (as described in section 5.1) and the error made on the propagated voltage (as described in section 5.2). Table IV.31 shows the evolution of the results for two cases on each network when correcting or not the various terms of the equation.

	$I_{f\ est}$ No correction	$I_{f\ est}$ V_a corrected	$I_{f\ est}$ phase corrected	$I_{f\ est}$ phase and V_a corrected
Urban F3 (5750.5 m) $R_f = 5\,\Omega$	-123.5	-116.7	-7.3	0.4
Urban F3 (5750.5 m) $R_f = 40\,\Omega$	-959	-942.7	-16.9	-0.1
Rural F3 (16540.5 m) $R_f = 5\,\Omega$	36.3	103.9	-65.5	-0.01
Rural F3 (16540.5 m) $R_f = 40\,\Omega$	808.8	782	28.5	1.3

Table IV.31: Distance errors (m) made by the localization algorithm for two cases on each network when correcting or not the estimated fault current phase and/or the propagated voltage

These results show that the estimation of I_f and the propagation of V_a (for a fault on phase a) introduce errors which can be substantial. However, the correction of the faulty phase voltage does not make a major difference. It is more interesting to concentrate the work on reducing the error due to the estimation of the fault current.

In order to enlighten the confusing results of the case Rural - F3 - 5 Ω, which do not show a “logical” improvement of the results like in the three other cases presented, a detailed analysis of the evolution of the results obtained for the fault F3 on the rural network, and for all fault resistances, is done.

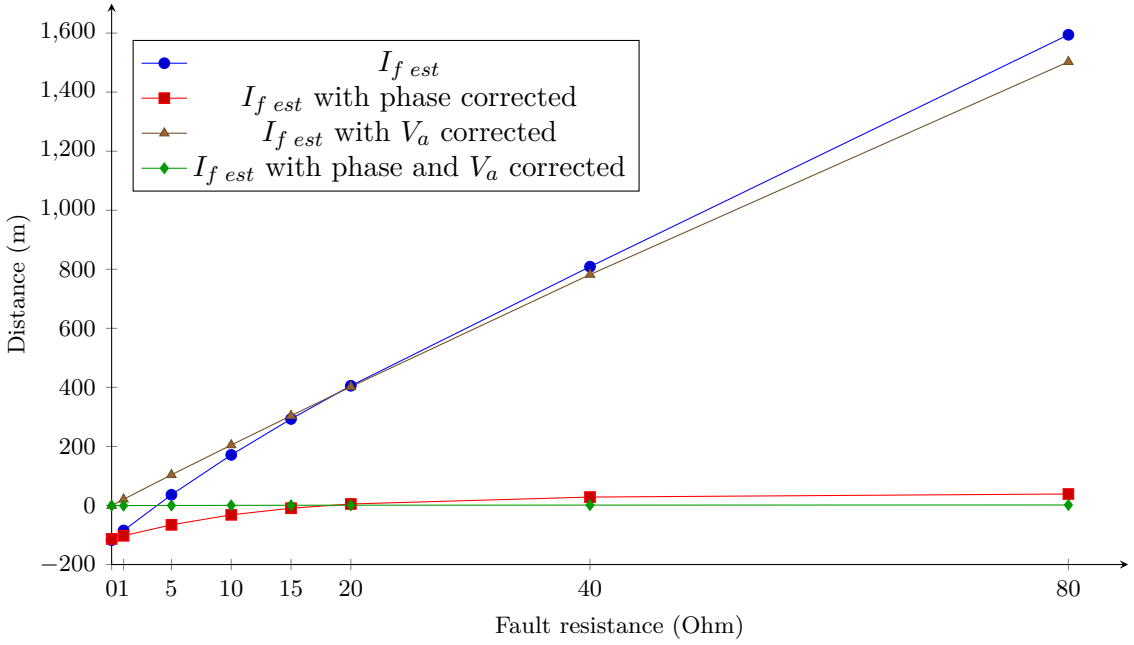

Figure IV.21: Results for fault F3 on the rural network obtained with $I_{f\ est}$ and the correction of the two main error factors (see table IV.32 for detailed numbers)

The detailed results are given in table IV.32 and figure IV.21 illustrates them. It shows the different results that we obtain when correcting one by one the two major factors of error that we identified previously:

- the phase of the estimated fault current $I_{f\ est}$
- and the error made when propagating the faulty phase voltage, V_a, throughout the network

and finally by correcting both error factors at the same time.

	$I_{f\ est}$ No correction	$I_{f\ est}$ phase corrected	$I_{f\ est}$ V_a corrected	$I_{f\ est}$ phase and V_a corrected
0 Ω	-118	-113	-0.6	-0.52
1 Ω	-85	-103	0.9	-0.44
5 Ω	36	-66	104	-0.01
10 Ω	171	-32	205	-0.01
15 Ω	293	-9	304	0.70
20 Ω	405	5	402	0.90
40 Ω	809	29	782	1.30
80 Ω	1594	39	1503	1.67

Table IV.32: Results for fault F3 on the rural network obtained with $I_{f\ est}$ and the correction of the two main error factors

The results show that each factor does not provide the same type of improvements.

Correcting the error made on the phase voltage V_a transforms the initial curve (blue/circle) into a linear curve (brown/triangle).

Correcting the error made on the phase of the estimated fault current $I_{f\ est}$ does not modify the non-linear characteristic of the initial curve but reduces greatly the amplitude of the error.

And finally, correcting both factors transforms the initial curve into a linear curve around 0, which corresponds to the ideal results.

The results evolution seen in figure IV.21 can be explained by the following statements:

- the total phase error term (see equation IV.7) is proportional to the fault resistance. Therefore, if this term is not corrected, the error will logically increase linearly with the fault resistance. It is clearly visible when looking at the curve where V_a is corrected but where the error made on the phase of the estimated fault current remains: the curve starts at 0 and linearly increases as R_f increases.

- the voltage error is proportional to the fault distance, but here we analyze the results for one fault location only, so it is the evolution of the voltage error with the increase of R_f that is non linear. The voltage error made when propagating the measurements is smaller for high resistance fault situations than for low resistance fault situations, and this evolution is not linear with the increase of R_f.
  The error, computed as $V_{a\ measured} - V_{a\ propagated}$ in terms of amplitude, is always positive. Therefore $V_{a\ propagated}$ is always an under estimation of the real V_a value, inducing a smaller numerator term of equation IV.3, and consequently a smaller fault distance than the real one, which corresponds to a negative error, well seen on figure IV.21.

6 Conclusion

In this chapter we presented the results that we obtained using the method we developed throughout chapter III. Thanks to the quite complete and numerous data we obtained from the DSOs partner of the project, the method could be tested on simulation data of real networks, one urban and one rural, the closest as possible from reality.

The results can be seen from two different angles. The first one concerns the precise fault localization in terms of distance from the unique measurement point located at the head of the feeder. We can see that the method provides a fault localization precision range from 0 m to 300 m for resistive faults of 10 Ω or under, and this for both type of networks. The total independence of the method to the fault resistance is clearly not achieved as the error increases with the increase of the fault resistance. However, the lead to explore in order to improve the results is presented in section 5.

The other angle is the section localization, that is the localization of the homogeneous section on which the fault has occurred. The performance of this type of localization greatly depends of the topology of the network. Some networks have long sections, other

short sections, and therefore for the same fault distance error, the section localization can sometimes be correct and sometimes incorrect. We can see that the section localization results on the rural network show a correct faulty section localization for faults of $10\,\Omega$ and under.

We also showed that the algorithm could, for both networks and all fault cases, make a pretty good estimation of the fault resistance, which is a data that can greatly help in interpreting the results.

Finally, the sensitivity analyses show that great improvements of the results can be achieved by making a better estimation of the fault current, and especially of its phase as it is the major error factor. The small error made when propagating the voltage throughout the feeder, and due to model differences between the algorithm pi-model and the simulation model, does not affect much the results.

The fault localization computations made on the simulation of two real networks (urban and rural) tend to show that the proposed method, despite the obvious improvements which can be made, could be used on today's distribution networks as a complete fault localization system, providing an estimation of the fault distance, the associated possibly faulty section and the fault resistance. However, since the method could not be tested on the real fault measurements due to a lack of necessary data, future research need to be lead in order to verify the compatibility of the method with real fault cases.

General Conclusion

Contents

Abstract

This conclusion revisits and summarizes the content of this thesis. We first describe the work done on the improvement of the use of classical fault indicators by developing a probabilistic analysis of their state. Secondly we resume the work concerning the precise fault localization algorithm and the obtained results. Finally the outlooks following this work are discussed.

1 Conclusion

1.1 Section localization by using fault indicators

The first part of our work, presented in chapter II, concerns the development of a fault localization method which concentrates on localizing a faulty section or area in order to isolate it as fast as possible using circuit breakers.

The method is developed as a solution for networks using fault indicators (FIs) with a remote retrieval of their state after a fault occurrence. The principle of the FIs is to measure (either directly or by the mean of electromagnetic field measurements) currents and voltages at different locations on the network. The FIs can inform if they have detected a fault current, and some of them (the directional FIs) can even inform on the fault current direction (downstream or upstream).

However, reliability problems appear when using this type of equipment. Since by definition FIs do not operate often, the failures are discovered when a fault occurs, thus degrading the network operation at a very critical moment and furthermore increasing the fault localization time. In order to counter this effect, we developed a probabilistic method which is robust to the possible FIs failures.

The proposed method processes a probabilistic analysis of the FIs states, therefore sorting the different sections or zones from the most probably faulty to the least probably faulty. The method is therefore robust, to a certain level, to FIs failures which are expressed by wrong FI states during the fault occurrence, consequently reducing the misleading analysis made by the Distribution System Operator (DSO) in order to locate and isolate the fault from the rest of the network.

The presented results show the good performance of this method. The limitations of the method are due to technical constraints that we address in our work (see section 4.2 and 7.2 in chapter II for more details on limits and performance).

This method however is not a precise fault localization method but rather a faulty section localization method which aims in helping and improving the actual faulty section localization method where the main goal is to identify which circuit breaker to operate in order to minimize the number of customers impacted by the fault situation. We will introduce in the perspectives of this work how this method could be coupled with a precise fault localization method in order to obtain a highly efficient fault localization procedure.

1.2 The precise fault localization method

In chapters III and IV we presented the improved method that we propose as well as the obtained results.

The base of the method, as presented in section 2.1 of chapter III, is the use of an equation expressing the distance between the fault and the measuring point in function of electrical measurements and the conductors characteristics. Originally developed for the transmission network which consists of long lines made of a single and consequently homo-

geneous conductor, we worked on the transposition of the Takagi method on distribution networks.

We considered that the method could be applied on each homogeneous section of the distribution networks. Developing previous works we therefore managed to propagate the electrical measurements done at the head of the feeder throughout the feeder, taking into account the loads and the conductors characteristics. The fault distance computation can consequently be done on each homogeneous section of the network, therefore providing a method compatible with one of the major distribution network constraint. The radial aspect of distribution networks is the second important constraint. We therefore developed a logical browsing algorithm which allows to propagate the measurements to every possible node of the network and therefore test every section.

These developments permit to use the Takagi principle, originally developed for transmission networks, on distribution networks. Furthermore the propagation of the measurements allows us to use the Takagi equation without making any strong assumptions such as lumped loads downstream the fault point.

In order to improve the method we developed an estimation of the fault current which is based on the measurements of the neutral grounding current and the estimation of the capacitive currents of the conductors of the network. This new way of producing an estimation of the fault current shows that it gives a very good estimation of the fault current. However, as small as are the errors made when estimating the fault current, their consequences on the final results are quickly important, downgrading the quality of the fault localization.

In chapter III we also present problems which should be further studied in order to increase the working range of the proposed method to compensated neutral groundings as well as highly resistive faults or arc type faults.

Thanks to the Greenlys project and the partnership with one local DSO and one national DSO, we obtained detailed data on different types of feeder. This allowed us to run simulations of realistic networks and thus simulate fault situations the closest as possible to reality. In chapter IV we presented the obtained results and showed the general good working of the method, on a single urban feeder as well as on a very radial rural feeder.

Combining the use of an equation giving the fault distance and a propagation method of the measured variables throughout the network leads to an efficient fault localization method. The results presented in chapter IV show that even at a great distance from the measuring point, with many lateral sub-feeders and many tapped loads, the fault localization algorithm has a good precision. **Note:** A detailed analysis needs to be done in order to improve the results obtained with the underground (rural) network. Indeed the method seems to be more sensitive to the non-exact estimation of the fault current due to higher cable capacitance values.

However, the theoretical independence of the method regarding the fault resistance is not verified. As the sensitivity analysis show, a few parameters introduce errors propor-

tionally to the fault resistance value. The results show that for fault resistances up to 15 Ω the fault localization is precise at about 300 m, which can still be considered as a good result when locating a fault 20 km away.

The method proved also to be quite accurate in computing the fault resistances of the simulated faults. It is important to acknowledge that a precise appreciation of the fault resistance can help in interpreting the algorithm results as well as help in future developments of the method. It is therefore an interesting result.

Finally we will conclude by insisting on the need of the correspondence between all the topology data used by the algorithm and the reality of the network. The results have been obtained by simulating fault situations. Therefore the correspondence between the data used by the algorithm and the simulated network was exact. However it has not been possible to confront the algorithm with real fault measurements which occurred on the same network that we have simulated.

2 Outlooks

Despite our aim in providing a complete and efficient fault localization method for electrical distribution networks, it is obvious that many outlooks ensue from this work. We discuss them in the following paragraphs.

There are first of all many opportunities for improvements of the method itself. Indeed, as depicted in appendix E, the propagation of the voltage and current measured during a fault occurrence needs to be finely studied. The propagation process was validated during our research on the propagation of measurements for a normal situation, but showed small errors when propagating voltage measurements which degrade slightly the results, as showed in section 5.3 of chapter IV. Another necessary improvement concerns the estimation of the fault current. Work presented in sections 5.1 and 5.3 of chapter IV shows that despite the very low error (in terms of amplitude as well as in term of phase), the impact on the results is strong and increasing with the increase of the fault resistance.

Finally, in order to fully validate this method, it is necessary to process the fault localization algorithm on real fault measurements. Doing so on distribution networks which can fully be simulated, like the networks which we worked with, will allow to compare the algorithm performance and efficiently increase its performances for a good working of the method in practical, and not only in theory.

Other desired improvements can be listed concerning the working conditions. Since distribution networks present many disparities, the aim of extending the method needs to be considered. Indeed the method is proved to function only in the case of low resistive faults on aerial or underground distribution networks with an impedant neutral grounding.

Part of our work presents leads which need to be explored. An iterative method, which develops a fine computation of the capacitive currents in the network due to a fault, can help with highly resistive faults. Another lead on the modeling of arc-faults (which do not present the same characteristics than a classic permanent fault) has been presented and should help in future work on the subject.

The case of networks with a compensated neutral grounding needs also to be studied since more and more transformer are grounded this way. And this type of grounding influences the establishment of the fault currents in such a way that the method needs to be adapted. The increase of the presence of distributed generation unit in distribution networks also leads to the need of a fine study of their possible influence on this particular fault localization method.

Finally, the method uses the knowledge of the topology of the network as well as the nominal power of its loads. We think that a detailed study of the influence of the difference between the actual loading of the network during the fault and the nominal load level used by the algorithm should be conducted.

We will conclude this outlook by what we think to be the next major step in developing a complete fault localization method. As we stated previously, the first preoccupation of the DSO is to know which section, between two remotely operated circuit breakers, is faulty in order to isolate it from the rest of the network in order to impact the minimum of users. Secondly the DSO wants to know the exact position of the fault in order to start the maintenance and bring back the faulty zone to normal operation again in order to have a minimum impact on the users.

The two methods that we developed, the faulty section localization done with fault indicators information and the precise fault localization, do not provide the same results. The precise fault localization will, for a radial network, give all the possible fault locations regarding the electrical fault measurements made during the fault occurrence. The multiple solutions that can be found therefore need to be discriminated. The section localization method on the contrary does not give a precise localization of the fault, but will give a unique zone as the faulty zone.

Logically associating both method will allow to discriminate all the fault locations proposed by the precise fault localization algorithm in order to obtain the following complete result a few minutes maximum after the fault occurrence:

- the knowledge of the faulty zone in order to isolate the fault from the rest of the network
- the knowledge of the precise localization of the fault in order to maintain and repair

This knowledge should help greatly the DSOs in order to react quickly and efficiently to a fault occurrence on their distribution network.

Bibliography

[Adu, 2001] Adu, T. (2001). A new transmission line fault locating system. *IEEE Transactions on Power Delivery*, 16:498–503.

[Blanc, 2013] Blanc, M. (2013). Etude de défauts impédant de type arc dans le réseau hta. Technical report, Grenoble INP ENSE3 - G2Elab.

[Bogdashova and Kachesov, 2005] Bogdashova, L. and Kachesov, V. (2005). Parametric on-line fault location methods for distribution mv networks. In *Power Tech, 2005 IEEE Russia*.

[Chamia and Liberman, 1978] Chamia, M. and Liberman, S. (1978). Ultra high speed relay for ehv/uhv transmission lines – development, design and application. *Power Apparatus and Systems, IEEE Transactions on*, PAS-97(6):2104–2116.

[Choi et al., 2004] Choi, M.-S., Lee, S.-J., Lee, D.-S., and Jin, B.-G. (2004). A new fault location algorithm using direct circuit analysis for distribution systems. *Power Delivery, IEEE Transactions on*, 19(1):35 – 41.

[Crossley and McLaren, 1983] Crossley, P. and McLaren, P. (1983). Distance protection based on travelling waves. PAS-102(9):2971–2983.

[Das et al., 2011] Das, S., Kulkarni, S., Karnik, N., and Santoso, S. (2011). Distribution fault location using short-circuit fault current profile approach. In *Power and Energy Society General Meeting, 2011 IEEE*.

[Dasco, 2014] Dasco, A. (2014). Méthode pour la localisation de défauts monophasés dans les réseaux hta. Master's thesis, Grenoble INP/UJF Grenoble - Master 2 Recherche - Spécialité « Génie Eléctrique ».

[Elkalashy et al., 2007] Elkalashy, N., Lehtonen, M., Darwish, H., Izzularab, M., and Taalab, A.-M. (2007). Modeling and experimental verification of high impedance arcing fault in medium voltage networks. *Dielectrics and Electrical Insulation, IEEE Transactions on*, 14(2):375–383.

[Ferracci, 1995] Ferracci, P. (1995). *Etude des regimes transitoires a l'etablissement d'un defaut monophase sur reseau d'energie triphase moyenne tension a neutre compense*. PhD thesis. Thèse de doctorat dirigée par Meunier, M. Sciences appliquées Paris 11 1995.

[Herraiz et al., 2009] Herraiz, S., Melendez, J., Barrera, V., Sanchez, J., and Castro, M. (2009). Estimation of zero-sequence impedance of undergrounds cables for single-phase fault location in distribution systems with electric arc. In *Electrical Power Quality and Utilisation, 2009. EPQU 2009. 10th International Conference on*, pages 1–4.

[Jarventausta et al., 1994] Jarventausta, P., Verho, P., and Partanen, J. (1994). Using fuzzy sets to model the uncertainty in the fault location process of distribution networks. *Power Delivery, IEEE Transactions on*, 9(2):954 –960.

[Jecu, 2011] Jecu, C. (2011). *Système de protections novateur et distribué pour les réseaux Moyenne Tension du futur*. PhD thesis. Thèse de doctorat dirigée par Raison, Bertrand et Caire, Raphaël Sciences et technologie industrielles Grenoble 2011.

[Karnik et al., 2011] Karnik, N., Das, S., Kulkarni, S., and Santoso, S. (2011). Effect of load current on fault location estimates of impedance-based methods. In *Power and Energy Society General Meeting, 2011 IEEE*.

[Kulkarni et al., 2011] Kulkarni, S., Karnik, N., Das, S., and Santoso, S. (2011). Fault location using impedance-based algorithms on non-homogeneous feeders. In *Power and Energy Society General Meeting, 2011 IEEE*.

[Lantz, 1962] Lantz, M. J. (1962). New method for locating transmission line ground faults. *Part III Power Apparatus and Systems Transactions of the American Institute of Electrical Engineers*, 81(3):134–136.

[Magnago and Abur, 1998] Magnago, F. and Abur, A. (1998). Fault location using wavelets. *Power Delivery, IEEE Transactions on*, 13(4):1475 –1480.

[Marguet and Raison, 2013] Marguet, R. and Raison, B. (2013). A probabilistic fault localization method for distribution networks using fault indicators. In *PowerTech (POWERTECH), 2013 IEEE Grenoble*, pages 1–6.

[Marguet and Raison, 2014] Marguet, R. and Raison, B. (2014). Fault distance localization method for heterogeneous distribution networks. In *PES General Meeting | Conference Exposition, 2014 IEEE*, pages 1–5.

[Masa, 2012] Masa, A. V. (2012). *High Impedance Fault Detection Method in Multi-Grounded Distribution Networks*. PhD thesis, Ecole Polytechnique de Bruxelles - Université Libre de Bruxelles.

[Penkov, 2006] Penkov, D. (2006). *Localisation de défauts dans les réseaux HTA en présence de génération d'énergie dispersée*. Theses, Institut National Polytechnique de Grenoble - INPG.

[Pham, 2005] Pham, C. D. (2005). *Détection et localisation de défauts dans les réseaux de distribution HTA*. PhD thesis, Ecole Doctorale Electronique, Electrotechnique, Automatique et Traitement du Signal (EEATS).

[Ramar and Ngu, 2010] Ramar, K. and Ngu, E. (2010). A new impedance-based fault location method for radial distribution systems. In *Power and Energy Society General Meeting, 2010 IEEE*.

[Ramar and Ngu, 2012] Ramar, K. and Ngu, E. E. (2012). Generalized impedance-based fault location for distribution systems. *Power Delivery, IEEE Transactions on*, 27(1):449 –451.

[Sabonnadière and Hadj-Said, 2007] Sabonnadière, J.-C. and Hadj-Said, N. (2007). *Lignes et réseaux électriques. 1, Lignes d'énergie électrique*. Paris : Hermes science publ.

[Saha et al., 2001] Saha, M., Provoost, F., and Rosolowski, E. (2001). Fault location method for mv cable network. In *Developments in Power System Protection, 2001, Seventh International Conference on (IEE)*, pages 323 –326.

[Stevens et al., 1972] Stevens, D., Ott, G., Pomeroy, W., and Tudor, J. (1972). Frequency-modulated fault locator for power lines. PAS-91(5):1760–1768.

[Takagi et al., 1982] Takagi, T., Yamakoshi, Y., Yamaura, M., Kondow, R., and Matsushima, T. (1982). Development of a new type fault locator using the one-terminal voltage and current data. *IEEE Transactions on Power Apparatus and Systems*, PAS-101:2892–2898.

[Tziouvaras, 2006] Tziouvaras, D. (2006). Protection of high-voltage ac cables. In *Power Systems Conference: Advanced Metering, Protection, Control, Communication, and Distributed Resources, 2006. PS '06*, pages 316–328.

[Welfonder, 1998] Welfonder, T. (1998). *Localisation de défauts monophasés dans les réseaux de distribution à neutre compensé*. PhD thesis, Institut National Polytechnique de Grenoble (INPG) - EEATS.

[Wiszniewski, 1983] Wiszniewski, A. (1983). Accurate fault impedance locating algorithm. *Generation, Transmission and Distribution, IEE Proceedings C*, 130(6):311 –314.

[Zhu et al., 1997] Zhu, J., Lubkeman, D., and Girgis, A. (1997). Automated fault location and diagnosis on electric power distribution feeders. *Power Delivery, IEEE Transactions on*, 12(2):801 –809.

Publications

Published international conference articles

2014 IEEE PES General Meeting - National Harbor MD - USA
Fault distance localization method for heterogeneous distribution networks
Marguet R., Raison B.

2013 IEEE PES PowerTech - Grenoble France
A probabilistic fault localization method for distribution networks using fault indicators
Marguet R., Raison B.

2013 IEEE PES PowerTech - Grenoble France
Decentralized self healing solution tested in the framework of GreenLys smart grid project
Chollot Y., Wild J., Berry T., Jourdan A., Raison B., Marguet R., Houssin J., Joubert R.

Appendix A

FI Parameters Evaluation

1 Choice of the values of the parameters α, β, ε, ε' and ε''

1.1 Interactions between the parameters and consequences of the chosen values

When working with non-directional Fault Indicators (FIs), only the parameters α and β are used. α defines the working rate of a FI meanwhile β defines the correct working rate of the FI (see section 3.3.1 in chapter II for more details).

There are no critical values for these parameters. The only behavior to note is that if β is $<$ to 0.5, then $\alpha.(1-\beta) > \alpha.\beta$ which means, considering table II.2, that the probability that the FI's state is 0 during a fault is higher than the probability that the FI state is 1. This behavior can reflect the reality (with equipment which is very deteriorated) but in a "normal" case, the value of β should stay above 0.5. In the following analysis we will therefore consider that the parameters α and β are equal.

When using directional FIs, three other parameters are introduced: ε, ε' and ε''. The use of these parameters is well detailed in section 3.3.2 in chapter II. In the following analysis, we will always consider ε' and ε'' equal since they are "symmetrical" coefficients, and will consider ε equal to 0.5.

It is necessary to understand that the parameters α and β depend on the equipment while the parameters ε, ε' and ε'' are deliberately chosen by the operator. The analysis consists in observing the variation of the different probabilities computation in function of the variation of the α and β values.

Figure A.1 shows the values of the probabilities presented in table A.1, for values of α and β varying between 0 and 1.

Actual state / Ideal state	**Probability**
0 / 0	$1-\alpha+\alpha.\beta$
0 / 1	$1-\alpha+\alpha.(1-\beta).(1-\varepsilon')$
0 / -1	$1-\alpha+\alpha.(1-\beta).(1-\varepsilon'')$

Table A.1: Probabilities of which the variation is studied

What can be deducted from figure A.1 is that above a certain limit value (around 0.4 in this case), the highest probabilities correspond logically to the concerned case:

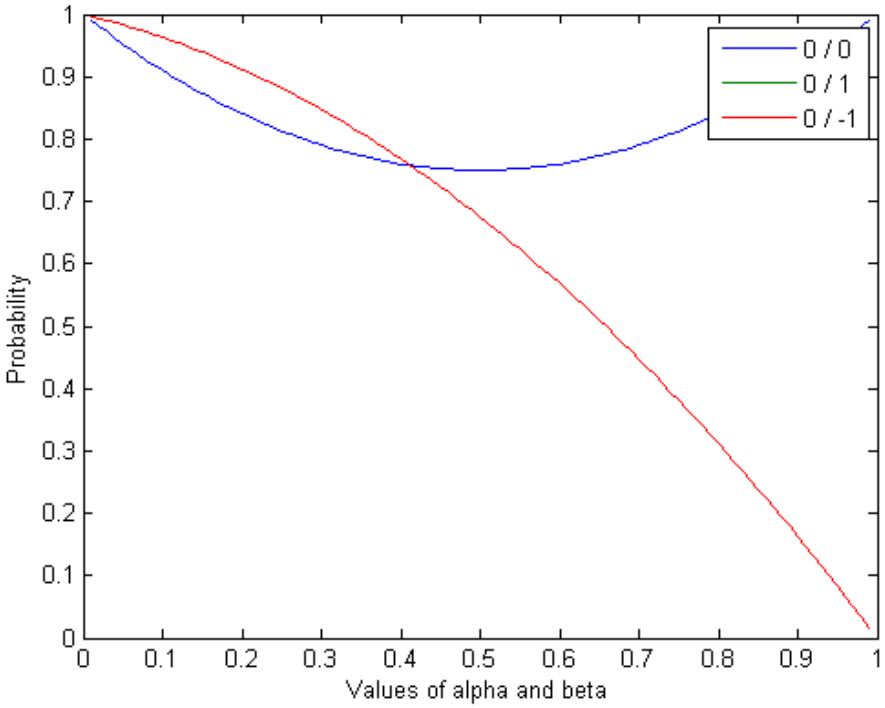

Figure A.1: Computed probabilities for varying values of α and β ($\varepsilon = 0.5$, $\varepsilon' = \varepsilon'' = 0.3$) - the red and green curve are blended

- for 0/0, above 0.4, the probability value of $1 - \alpha + \alpha.\beta$ is higher than the two others
- under 0.4, it is $1 - \alpha + \alpha.(1 - \beta).(1 - \varepsilon')$ for 0/1 (or $1 - \alpha + \alpha.(1 - \beta).(1 - \varepsilon'')$ for $0/-1$) which is higher. In this case the results are inverted and not "logical"

Note: it is important to note that this boundary value of 0.4 depends of the chosen values for ε, ε' and ε''.

The same studies can be conducted for the two others cases (see tables A.2 and A.3), and the results presented in figures A.2 and A.3.

Actual state / Ideal state	**Probability**
1 / 1	$\alpha.\beta$
1 / 0	$\alpha.(1 - \beta).\varepsilon$
1 / −1	$\alpha.(1 - \beta).\varepsilon''$

Table A.2: Probabilities of which the variation is studied

For the two other cases, figures A.2 and A.3 show that above a value of approximately 0.35, the logic of the probabilities values in regard of the fault situations and FI state is respected.

Again, this value of 0.35 depends of the chosen values of parameters ε, ε' and ε''. A quick analysis shows that for extreme values of these parameters, the boundary value can

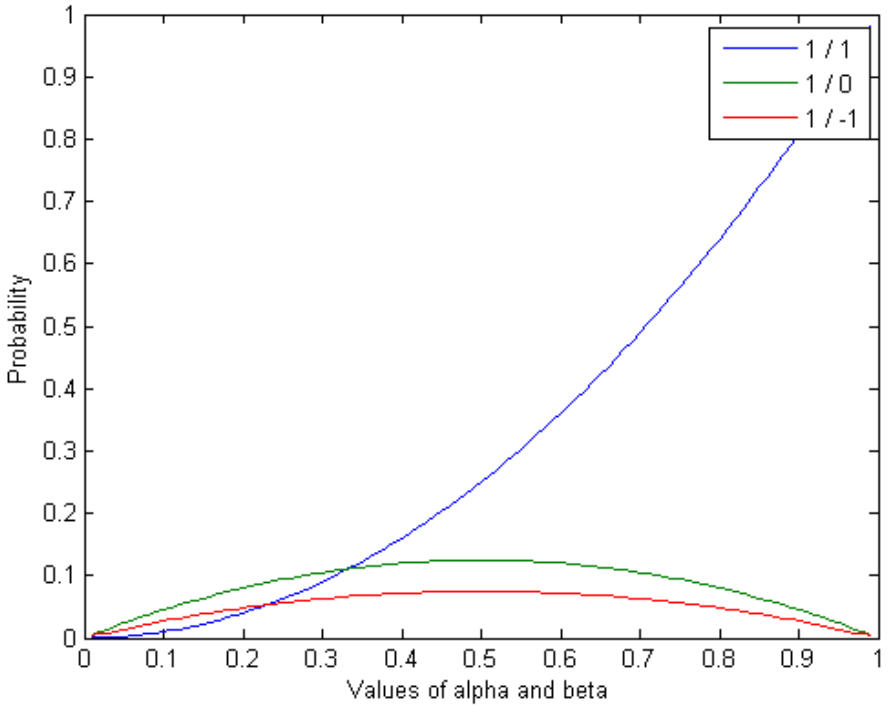

Figure A.2: Computed probabilities for varying values of α and β ($\varepsilon = 0.5$, $\varepsilon' = \varepsilon'' = 0.3$)

Actual state / Ideal state	**Probability**
-1 / -1	$\alpha.\beta$
-1 / 0	$\alpha.(1-\beta).(1-\varepsilon)$
-1 / 1	$\alpha.(1-\beta).\varepsilon'$

Table A.3: Probabilities of which the variation is studied

go up to 0.5.

Conclusion:

It is important that the chosen values of the parameters ε, ε' and ε'' are compatible with the values of α and β (which can not be chosen), so that the "logic" of the algorithm is conserved.

However, we can note that the higher are the values of α and β, the greater will be the differences between the computed probabilities, which can help when evaluating the results.

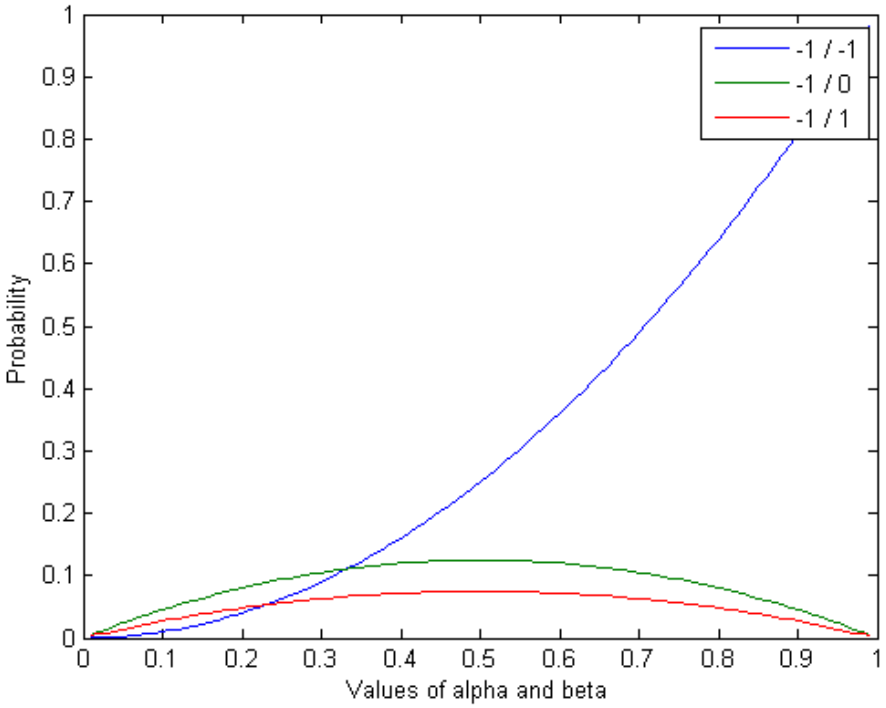

Figure A.3: Computed probabilities for varying values of α and β ($\varepsilon = 0.5$, $\varepsilon' = \varepsilon'' = 0.3$)

1.2 Consequences of the differences between the algorithm and real parameters values

Since the parameters α and β are not chosen but rather determined by the equipment in use, it is important to evaluate how important it is to use the correct values in the algorithm. Indeed, the algorithm works with values entered by the operator. But is it important that these values fit exactly the real values of the equipment.

We first analyze the importance of the parameters α and β. Therefore ε is fixed to 0.5, and ε' and ε'' to 0.3. Figure A.4 shows the percentage of success of the algorithm for values of α and β varying between 0.1 and 0.9 by steps of 0.05 for both the algorithm parameters and the equipment parameters.

This graphic shows first of all an evidence: the percentage of success is higher when the real parameters of the FIs are high (since α and β define the good functioning of the FI). However, concerning the algorithm parameters, it is interesting to note that above a certain value, the percentage of success is almost identical. From 0.45 to 0.95 for the algorithm values of α and β, the percentage of success is the same. Therefore, it is not so important to have a very good correspondence between the real FI parameters and the algorithm parameters. What is important is to have good equipment with high values of α and β.

The same analysis for the parameters ε, ε' and ε'' is not so conclusive. It appears that

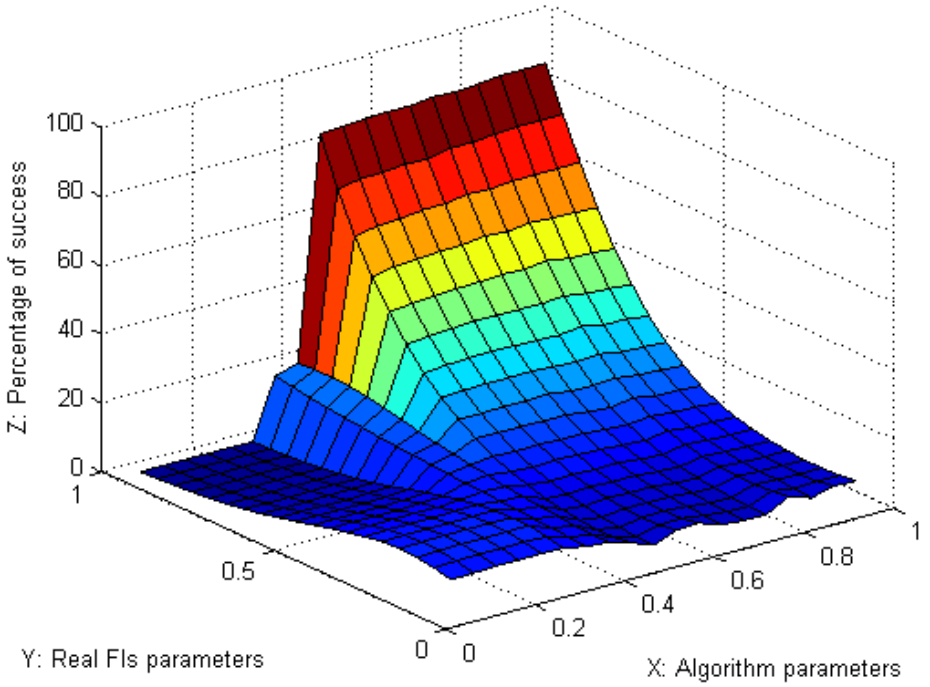

Figure A.4: Percentage of success for different values of the algorithm parameters and the FIs parameters α and β

results are slightly better when these parameters are low independently of its correspondence with the real values. The reason is that with low parameters, incoherent signatures are highlighted therefore helping the algorithm in detecting them.

Appendix B

Takagi Formula - Details

1 Takagi Formula for a single phase to ground fault

In [Takagi et al., 1982], the authors describe the network shown in figure B.1. In their work the authors consider a transmission network which is a meshed network. The associated computation are fully presented in their paper.

Below we will present the same computations, but considering a radial network, therefore with only one upstream source. This configuration simplifies slightly the computations.

Let us first express the fault point voltage as:

$$V_F = R_F.I_F = R_F.I''_a \tag{B.1}$$

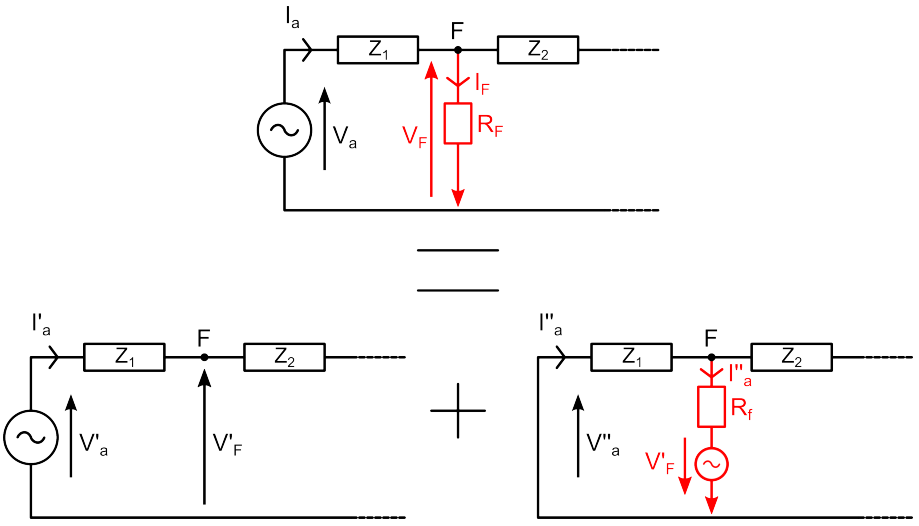

Figure B.1: Superposition principle on a single phase circuit enduring a phase to ground fault

The equations derived from the telegrapher's equations are:

$$\begin{bmatrix} V_F \\ I_F \end{bmatrix} = \begin{bmatrix} cosh(\gamma.x) & Z_{1S}.sinh(\gamma.x) \\ \frac{1}{Z_{1S}}.sinh(\gamma.x) & cosh(\gamma.x) \end{bmatrix} . \begin{bmatrix} V_a \\ -I_a \end{bmatrix} \tag{B.2}$$

$$\begin{bmatrix} V_F \\ I''_a \end{bmatrix} = \begin{bmatrix} cosh(\gamma.x) & Z_{1S}.sinh(\gamma.x) \\ \frac{1}{Z_{1S}}.sinh(\gamma.x) & cosh(\gamma.x) \end{bmatrix} . \begin{bmatrix} V''_a \\ -I''_a \end{bmatrix} \tag{B.3}$$

with:

V_F fault point voltage
V_a terminal voltage
I_a terminal current
V''_a difference between pre-fault and post-fault voltages
I''_a difference between pre-fault and post-fault currents
Z_{1S} surge line impedance between the terminal and the fault point
γ propagation constant of the line between the terminal and fault point
x fault distance

From B.2 and B.3 we can write the two following equations:

$$V_F = V_a.cosh(\gamma.x) - Z_{1S}.I_a.sinh(\gamma.x) \tag{B.4}$$

$$I''_a = \frac{V''_a}{Z_{1S}}.sinh(\gamma.x) - I''_a.cosh(\gamma.x) \tag{B.5}$$

Replacing V_F and I''_a in B.1 by B.4 and B.5 we obtain the following equation:

$$(V_a.cosh(\gamma.x) - Z_{1S}.I_a.sinh(\gamma.x)) - R_F.(\frac{V''_a}{Z_{1S}}.sinh(\gamma.x) - I''_a.cosh(\gamma.x)) = 0 \tag{B.6}$$

Dividing by $cosh(\gamma.x)$ gives:

$$(V_a - Z_{1S}.I_a.tanh(\gamma.x)) - R_F.(\frac{V''_a}{Z_{1S}}.tanh(\gamma.x) - I''_a) = 0 \tag{B.7}$$

Now comes the two mathematical assumptions of the method:

- the author considers $\gamma.x$ small enough to write that $tanh(\gamma.x) = \gamma.x$
- the author considers that $\frac{V''_a}{Z_{1S}}.tanh(\gamma.x)$ physically corresponds to a charging current of the capacitances of the line (Z_{1S} being a surge impedance) and is therefore much lower than the fault current I''_a. Therefore:
  $\frac{V''_a}{Z_{1S}}.tanh(\gamma.x) \ll I''_a$

These two assumptions allow to rewrite equation B.7:

$$(V_a - Z_{1S}.I_a.\gamma.x) + R_F.I''_a = 0 \tag{B.8}$$

Now multiplying B.8 by the conjugate of I''_a, written I''^*_a, and taking the imaginary part gives the equation B.9 since R_F is real, and $I''_a.I''^*_a$ too:

$$\mathrm{Im}\left[(V_a - Z_{1S}.I_a.\gamma.x).I''^*_a + R_F.I''_a.I''^*_a\right] = 0$$

$$\mathrm{Im}\left[V_a.I''^*_a - Z_{1S}.I_a.\gamma.x.I''^*_a\right] = 0 \tag{B.9}$$

Taking the fault distance x out of the imaginary part and considering that $Z_{1S}.\gamma = z_1$ which is the per unit length impedance of the line, the final Takagi equation is:

$$x = \frac{\mathrm{Im}\left(V_a.I''^*_a\right)}{\mathrm{Im}\left(z_1.I_a.I''^*_a\right)} \tag{B.10}$$

2 Takagi Formula for a three phase to ground fault

The Takagi equation is also valid for three phase faults with a few changes. Indeed, it is necessary to replace the phase current and phase voltage by the positive sequence current and voltage of the symmetrical components.

Equation B.11 shows the modified equation:

$$x = \frac{\mathrm{Im}\left(V_d.{I''}_d^*\right)}{\mathrm{Im}\left(z_1.I_d.{I''}_d^*\right)} \tag{B.11}$$

Appendix C

Analysis of the Currents in Phase with the Fault Current

In section 3.2.1 of chapter III, the following fault distance Takagi equation is presented:

$$x = \frac{\mathrm{Im}\left(V.I''_a{}^*\right)}{\mathrm{Im}\left(z_1.I_{tot}.I''_a{}^*\right)} \tag{C.1}$$

Equation C.1 is obtained by multiplying equation C.2 below by $I''_a{}^*$, in order to eliminate the term with R_f

$$\mathrm{Im}\left(V.I''_a{}^*\right) = \mathrm{Im}\left(x.z_1.I_{tot}.I''_a{}^*\right) + \mathrm{Im}\left(R_f.I_f.I''_a{}^*\right) \tag{C.2}$$

The assessment is that in order to really eliminate the term with R_f, then the two currents I_f and I''_a must be exactly in phase, and furthermore their module difference is not important as long as their phase are exactly the same.

This lead to looking for the current which will have the closest phase of I_f, considering that it might not be $I''_a{}^*$ (which as a reminder is the difference between the post-fault current and the pre-fault current of the faulty phase, phase "a" here) as used by the original Takagi method.

The list of the possible currents to use is detailed below:

$I_{a\ \textbf{pre fault}}$	pre fault phase current at the terminal point
$I_{a\ \textbf{post fault}}$	during fault phase current at the terminal point
I''_a	difference between pre and during fault phase current at the terminal point
I_S	$= I_{a\ \text{post fault}} + K.I_0$ (see section 2.2 for description of K)

Computations for various situations were made in order to find the best candidate globally:

- urban network
  - low resistive fault - 1 Ω
    - small fault distance - F1 (2083.5 m)
    - high fault distance - F4 (7981.5 m)
  - highly resistive fault - 40 Ω
    - small fault distance - F1 (2083.5 m)
    - high fault distance - F4 (7981.5 m)
- rural network

- low resistive fault - 1 Ω
  - small fault distance - F1 (5067.5 m)
  - high fault distance - F3 (16540.5 m)
- highly resistive fault - 40 Ω
  - small fault distance - F1 (5067.5 m)
  - high fault distance - F3 (16540.5 m)

Table C.1 shows the phase shift which exist between the real fault current and the different current candidates presented previously.

			$\angle I_{a\ pre}$	$\angle I_{a\ post}$	$\angle I''_a$	$\angle I_S$
Urban	1 Ω	F1 (2083.5 m)	16.69	11.28	-1.12	-17.36
		F4 (7981.5 m)	12.73	6.90	-3.01	-20.66
	40 Ω	F1 (2083.5 m)	16.78	11.96	1.09	-14.84
		F4 (7981.5 m)	12.94	8.13	-0.40	-18.85
Rural	1 Ω	F1 (5067.5 m)	16.53	9.07	-4.94	-6.51
		F3 (16540.5 m)	14.11	2.08	-9.14	-17.31
	40 Ω	F1 (5067.5 m)	17.13	11.10	-0.78	-3.48
		F3 (16540.5 m)	8.85	3.16	-3.34	-15.76

Table C.1: Phase shift (in degrees) between the real fault current and current candidates to use in the Takagi equation

The phase shift differences were computed at the beginning of the faulty section of each fault in order to make a logic comparison. Indeed, if the fault localization algorithm is run normally, in some cases the algorithm does not find the correct faulty section and therefore will compare the real fault current with a current propagated in another location than the real fault location. In this context, the current I''_a appears as the best candidate, but when used with the complete fault localization method, the algorithm finds wrong faulty sections.

What really appears is that between the four different currents, not one presents the needed characteristics. All four currents show strong variations depending of the fault distance and resistance, and a general strong phase shift.

Appendix D
Fault Localization Results for Each Fault Location

This appendix completes the results presented in chapter IV. We illustrate here, for both the urban and rural networks, the detailed results for each fault location. These results are shown in tables IV.12 and IV.18 of sections 3.5.1 and 3.6.1 of chapter IV, the figures presented in this appendix are their graphic representation.

1 Urban network

In figure D.1 we present the fault localization results obtained using the estimated fault current $I_{f\ est}$ for each fault location and for each fault resistance.

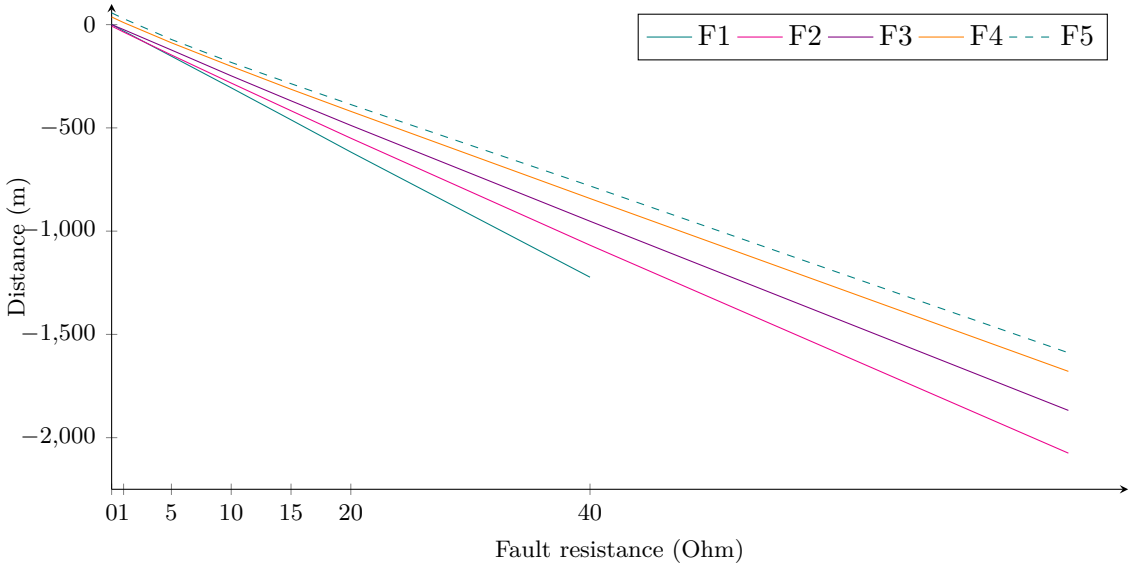

Figure D.1: Results with $I_{f\ est}$ for the urban network - Distance error (m) for all fault locations and for all fault resistances

The results show that the trend is the same for every fault location: the error increases linearly (in absolute value) as the fault resistance increases.

2 Rural network

In figure D.2 we present the fault localization results obtained using the estimated fault current $I_{f\ est}$ for each fault location and for each fault resistance.

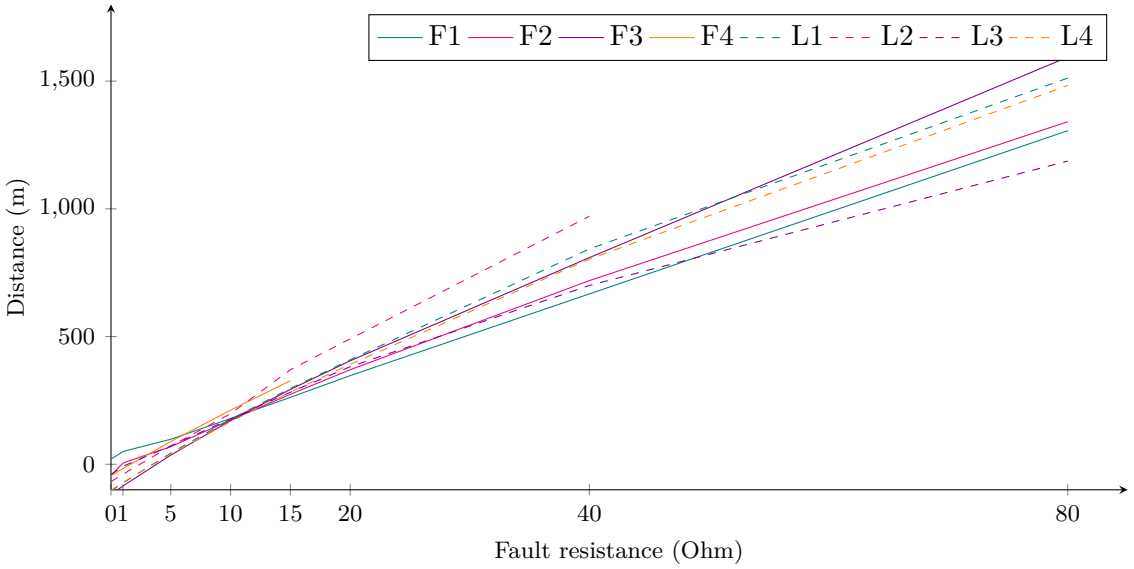

Figure D.2: Results with $I_{f\ est}$ for the rural network - Distance error (m) for all fault locations and for all fault resistances

Again the results show the same trend for each fault location: a quite linear increase of the error with the increase of the fault resistance.

Appendix E

Evolution of the Propagated Voltage Error

As explained in section 3.1 of chapter III, the propagation algorithm used to propagate the measurements from the head of the feeder to the head of each studied sections uses the PI-model description of lines and cables.

This model of course can not correspond exactly to reality. However, considering that distribution networks have line or cable sections that rarely exceed 1 km, using the pi-model, which is generally used for medium length lines ($> 80\,\text{km}$), should bring a good precision.

Concerning the simulations it is the same problem. The program used for the simulations uses a pi-model too, but there are some parameters that are impossible to verify and therefore it is possible that a difference exists between the measurements done on the simulated network, and the propagated values.

1 Urban network

The case observed for the urban network is for a fault located in F3 (see section 2.5.2 in chapter IV), at 5750.5 km. Three different cases of fault resistances have been observed: $1\,\Omega$, $5\,\Omega$ and $40\,\Omega$.

Figure E.1 shows that the error made during the voltage propagation increases quite linearly with the propagated distance. It is in adequacy with the hypothesis that there is a slight "model" difference between the localization algorithm and the simulation program lines/cables model.

Another noticeable point is the increase rate of the error which depends on the fault resistance:

- $R_f = 1\,\Omega$: approximate ratio of $3.31\,\text{V/m}$
- $R_f = 5\,\Omega$: approximate ratio of $3.46\,\text{V/m}$
- $R_f = 40\,\Omega$: approximate ratio of $1.24\,\text{V/m}$

Note: the ratios are computed by taking the slope of the linearization of each curve. Therefore we can notice that the ratio for the $5\,\Omega$ fault is higher than the one for the $1\,\Omega$ fault. However their linearization do not have the same offset which is a sort of bias when trying to estimate the slope.

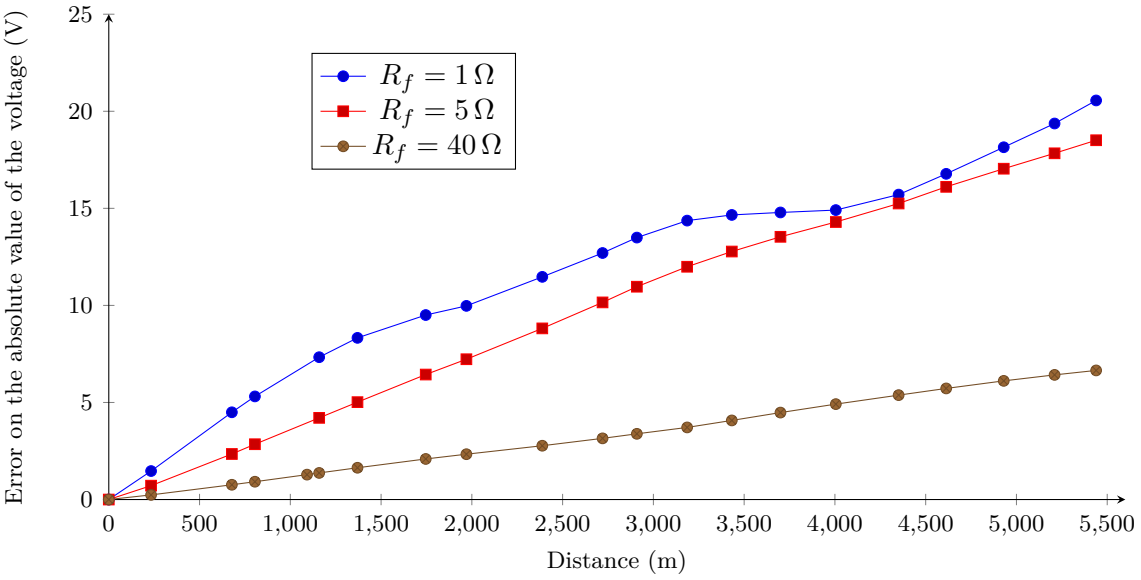

Figure E.1: Evolution with the distance (m) of the error made on the absolute value of the propagated voltage (V) for fault F3 at 5750.5 km

2 Rural network

The case observed for the rural network is for a fault located in F3 (see section 2.5.3 in chapter IV), at 16540.5 km. This time, two analysis were made, one for a fault resistance of 1 Ω and another one for a fault resistance of 5 Ω.

Figure E.2 shows that the error made during the voltage propagation increases also linearly with the propagated distance and that again the increase rate of the error depends of the fault resistance:

- $R_f = 1\,\Omega$: approximate ratio of 7.8 V/m
- $R_f = 5\,\Omega$: approximate ratio of 4.5 V/m
- $R_f = 40\,\Omega$: approximate ratio of 0.0 V/m

Note: the ratios are computed by taking the slope of the linearization of each curve.

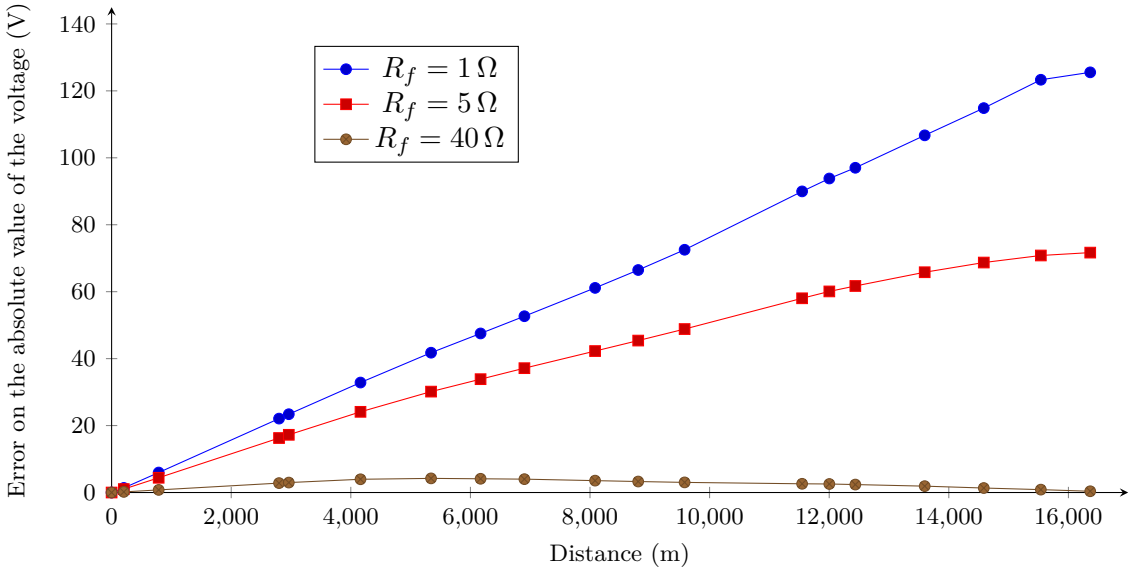

Figure E.2: Evolution with the distance (m) of the error made on the absolute value of the propagated voltage (V) for fault F3 at 16540.5 km

3 General conclusion

This analysis shows that the increase of the error is not the same in the case of the rural network and in the case of the urban network. The error shows a stronger increase rate for the rural network. Since the voltage is always under estimated by the propagation algorithm compared to the measurements, we can suppose that the underestimation is smaller for the urban network because it consists mainly of cables with higher capacitances.

However, what is common to both networks is the decreasing evolution of the error ratio with the increase of the fault resistance. Which is logical since when the fault resistance increases, the voltage drop is smaller, the fault current is smaller, and therefore the error is smaller too. Let us remind here that the propagation algorithm was tested in situation of no fault, and the difference between measurements and propagation were close to zero.

Therefore necessary additional work needs to be done, as stated in the outlooks of this work (section 2 in the general conclusion), on this subject in order to fully understand the phenomenon and improve the final fault localization algorithm.

Appendix F

Untreated Fault Localization Results for the Rural Network

In section 3.4 of chapter IV we described the way that were computed the errors made by the algorithm concerning the fault localization results on a radial distribution network. We also explained why we decided to compute the errors differently depending of the correctness of the results in terms of section localization.

Aware that in reality the DSO does not know which section among the solutions given by the algorithm is really faulty, we decided to show the distance error made by the algorithm without any post treatment.

Therefore in table F.1 we show the distance error computed by computing the average of the found distances corresponding to the proposed faulty section by the algorithm and then computing the error, and so for each fault case. These results are shown, logically, only for the rural network, as for the urban network made of a unique feeder, the algorithm can always find only one fault distance and faulty section.

Note: as a reminder see section 3.4 to see how were computed the errors and results presented in chapter IV.

	F1 5.07 km	**F2** 10.56 km	**F3** 16.54 km	**F4** 21.14 km	**L1** 17.36 km	**L2** 20.13 km	**L3** 10.82 km	**L4** 14.38 km
0 Ω	14	-71	-141	-45	-85	-58	-32	-75
1 Ω	45	-12	-107	-17	-54	-28	-4	-47
5 Ω	96	70	11	89	64	88	71	61
10 Ω	180	183	148	212	206	221	174	194
15 Ω	266	293	279	327	323	370	272	312
20 Ω	354	396	393	∨	424	491	367	417
40 Ω	707	776	807	∨	843	971	700	803
80 Ω	1306	1346	1594	∨	1512	∨	1187	1483

Table F.1: Results with $I_{f\ est}$ - Average error in meters for the eight different fault locations and for the eight different fault resistances - "∨" means that the algorithm solution is out of bounds of the network

These results are not very different from the ones presented in table IV.18. Sometimes the results are slightly worse and sometimes slightly better. For an easier comparison, table IV.18 is reproduces in this appendix as table F.2.

	F1 5.07 km	**F2** 10.56 km	**F3** 16.54 km	**F4** 21.14 km	**L1** 17.36 km	**L2** 20.13 km	**L3** 10.82 km	**L4** 14.38 km
0 Ω	20	-44	-118	-45	-105	-68	-40	-102
1 Ω	50	5	-85	-17	-73	-39	-8	-71
5 Ω	98	69	36	89	44	71	72	40
10 Ω	179	173	171	212	176	198	178	167
15 Ω	262	274	293	327	297	243	282	283
20 Ω	347	370	405	∨	409	291	382	391
40 Ω	667	719	809	∨	612	400	435	491
80 Ω	1056	341	1496	∨	790	∨	679	695

Table F.2: Results with $I_{f\ est}$ - Error in meters for the eight different fault locations and for the eight different fault resistances - "∨" means that the algorithm solution is out of bounds of the network

Below we show an example of the differences between the two ways of reporting the results and the associated fault distance error. In figure F.1 we show the eight fault locations found by the algorithm (using the current $I_{f\ est}$ in the case of the fault F3 - 5 ω.

- in table F.1, the error reported for this case is 11 m, it is obtained by computing the difference between the real fault distance and the average of the eight possible fault locations found by the algorithm (sections in green on figure F.1).

- in table F.2, the error reported for this case is 36 m, it is obtained by computing the difference between the real fault distance and the fault distance associated to the solution corresponding to the correct faulty section (section 49, circled in red on figure F.1).

On a radial network, two different branches will probably have different cables/lines lengths and characteristics, and also different loads. Therefore, for one voltage and current measurement at the head of the feeder, it can correspond to multiple locations into the network. But not necessarily at the same exact distance. It is why when finding multiple solutions there are fault distances variations between the different solutions. Depending of the topology, the variation can be one way or the other. And therefore making the average of all these found fault distances randomly (depending of the topology) worsen or improve slightly the results. But since the network topology variations are not extreme and neither are the fault distances variations, the order of magnitude of the results is the same in table F.1 and table F.2.

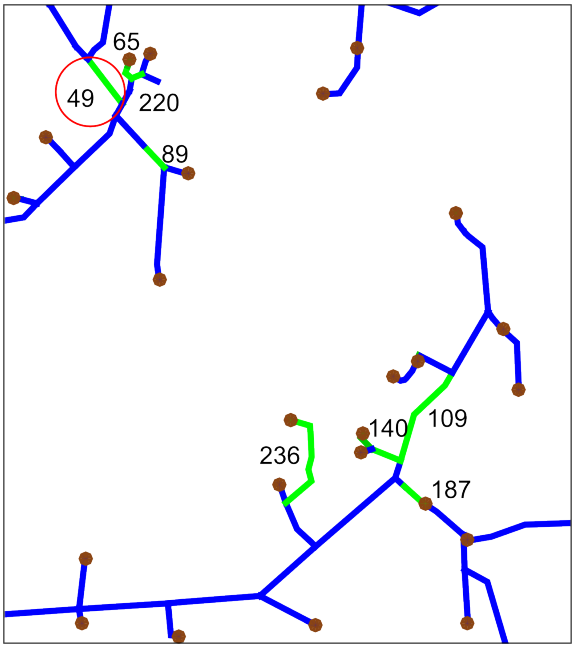

Figure F.1: Illustration of the eight fault locations found by the algorithm in the case of the fault F3 - 5 Ω (green sections)

Résumé français

1 Introduction Générale

1.1 Etat du développement des réseaux de distribution

Les réseaux de distribution ont été historiquement exploités de manière simple et pratique. En effet, face à la diversité de ces réseaux (rural, urbain, lignes aériennes, câbles souterrains), des territoires sur lesquels ils sont installés et des conditions climatiques auxquelles ils sont soumis, les Gestionnaires de Réseaux de Distribution (GRD) s'adaptent localement. Les équipements présents sur ces réseaux sont principalement analogiques et permettent d'assurer en priorité la sécurité du réseau et de ses utilisateurs.

Les réseaux de distribution sont contrôlés et gérés en direct, mais à la différence des réseaux de transport, où les méthodes de localisation des défauts et de protection du réseau sont beaucoup plus développées, peu de relevés de données ou mesures sont disponibles en temps réel.

L'un des nouveaux défis des GRD aujourd'hui est le développement d'une gestion durable et intelligente de l'énergie. Cela amène les différents acteurs à travailler ensemble et à repenser l'ensemble du réseau électrique de distribution, en accord avec les nouveaux enjeux et nouveaux usages d'aujourd'hui.

Aujourd'hui les équipements présents sur le réseau électrique de distribution sont peu à peu mis à jour en termes de technologies, les appareils numériques remplacent les appareils analogiques. Toutefois l'équipement actuel ne permet pas de répondre au défi présenté précédemment. C'est dans ce contexte de développement de nouvelles technologies et de l'apparition de nouveaux défis que les notions de "réseaux intelligents" et "d'automatisme de distribution avancé" ont émergé. Ces notions décrivent un réseau connecté, en termes de flux d'information mais aussi en termes de commandes de contrôle et d'exploitation qui doivent donc posséder les outils nécessaires pour permettre de nouvelles méthodes d'exploitation afin de répondre aux défis énergétiques qui se posent.

1.2 Le projet Greenlys

Le travail présenté dans cette thèse fait partie du projet GreenLys, “1er démonstrateur à échelle réelle de réseaux et système électriques intelligents”.

Ce projet est financé par le programme d'investissements d'avenir qui alloue des financements à travers des appels à manifestation d'intérêts. L'Agence De l'Environnement et de la Maitrise de l'Energie (ADEME) propose de nombreux appels à manifestation d'intérêts (AMI) concernant les quatre programmes de ses compétences: les plates-formes de démonstration technologiques dans les énergies renouvelables et la chimie verte, les réseaux intelligents, l'économie circulaire et les véhicules de l'avenir. GreenLys est le fruit de l'un de ces AMI.

GreenLys, qui a commencé en 2012 et prendra fin en 2016, a été mis en place par un consortium de partenaires, les principaux acteurs du marché français de l'électricité ayant des compétences complémentaires: Électricité Réseau Distribution France (ERDF), le chef de projet, GDF Suez, Gaz Électricité de Grenoble (GEG), Schneider Electric, Grenoble INP, Atos Worldgrid, RTE, Alstom, l'institut national de l'énergie solaire CEA (CEA INES), Rhône-Alpes Energie Environnement (RAEE), Hespul et le laboratoire CNRS LEPII-Edden (économie du développement durable et de l'énergie).

Le G2Elab (Laboratoire de Génie Electrique de Grenoble), qui fait partie de Grenoble INP, participe à de nombreux lots du projet.

Le lot dans lequel ce travail s'inscrit s'intitule “Agilité et Performance du Réseau du Distribution, le Réseau Auto Cicatrisant”.

1.3 Données de réseaux de distribution

Les deux gestionnaire de réseaux de distribution participant au projet (ERDF et GEG) nous ont fourni des données concernant leurs réseaux. Ces données ont permis d'effectuer des simulations de réseaux complètes avec le minimum d'inconnues, permettant ainsi des simulations le plus proche possible de la réalité.

Nous avons aussi pu obtenir des relevés réels de défauts qui se sont produits sur ces mêmes départs. Malgré les nombreuses données fournies par le GRD, les informations nécessaires n'étaient pas toutes disponibles pour permettre de faire fonctionner correctement l'algorithme de localisation développé dans nos travaux. Cependant notre méthode se place dans un contexte de développement des réseaux intelligents et des nouvelles technologies associées où l'accès à ces informations devraient être facilité.

Les données fournies ont toutefois été utilisées pour effectuer des simulations en utilisant des modèles le plus proches possible de la réalité. En conséquence les résultats obtenus tout au long de notre travail l'ont été avec des défauts simulés assez proches de la réalité.

1.4 Plan de thèse

Dans le premier chapitre de cette thèse est présenté l'état de l'art des différentes méthodes de localisation de défaut existantes en général et, plus spécifiquement, pour les réseaux de distribution. Nous présentons également les grandes lignes de la méthode améliorée que nous développons dans le reste du document.

Le deuxième chapitre présente une méthode de localisation de défaut, utilisant les équipements présents sur la plupart des réseaux de distribution, qui localise une section ou une zone du réseau sur laquelle survient le défaut mais n'effectue pas de calcul de distance de défaut. Grâce à une approche probabiliste, la méthode montre qu'il est possible d'utiliser efficacement les données déjà disponibles afin de localiser la section en défaut avec un taux de réussite élevé, et cela malgré les pannes d'équipement possibles.

Le chapitre trois décrit en détails la théorie de la méthode de localisation précise de défaut qui est proposée. Il détaille les différentes étapes de la méthode, les conditions de fonctionnement ainsi que ses limites.

Le dernier chapitre présente les résultats que nous obtenons en appliquant notre méthode sur les réseaux réels simulés. Nous analysons les différentes performances, en fonction des paramètres de la méthode, les situations de défaut ou le type de réseau, ainsi que les perspectives d'amélioration de la méthode.

Le document se termine par une conclusion générale.

2 Chapitre 1: Etat de l'art sur la localisation de défaut et objectifs des travaux

2.1 Introduction

En s'intéressant de près au domaine de la localisation des défauts sur les réseaux électriques, on trouvera premièrement des méthodes et techniques permettant d'isoler les défauts et d'identifier la zone en défaut. C'est en effet la première préoccupation des gestionnaires de réseau. En situation de défaut, ils doivent connaître la zone afin d'effectuer les manœuvres nécessaires pour isoler la zone en défaut du reste du réseau.

Les différents acteurs ont donc développé des solutions simples, robustes et faciles à mettre en œuvre, tels que les relais d'impédance pour les réseaux de transport, ou des indicateurs de passage de courant de défaut pour les réseaux de distribution. Ces solutions permettent donc de localiser une zone en défaut, mais la localisation précise qui se fait hors ligne (une fois le défaut isolé du réseau) prend souvent beaucoup de temps et nécessite des d'autres outils et méthodes dédiées.

D'autres méthodes se concentrant sur la localisation précise des défauts ont donc été développées. Tout en étant plus complexes, ces méthodes permettent de localiser la zone

en défaut, et donc d'effectuer les manœuvres d'isolement du défaut, et de donner une localisation précise du défaut, en termes de distance par rapport au point de mesure. C'est ce type de méthode qui est amélioré et développé dans ces travaux de thèse et qui est développé dans l'état de l'art suivant.

2.2 Conclusion

Cet état de l'art montre qu'un certain nombre de méthodes ou de variantes de méthodes ont été développées dans le domaine de la localisation des défauts sur les réseaux de distribution. La plupart de ces méthodes se concentrent sur un aspect particulier mais aucune méthode générale ou universelle n'a été développée. Compte tenu de la grande diversité des réseaux de distribution à travers le monde, c'est un défi de taille.

3 Chapitre 2: Méthode de localisation de défaut probabiliste utilisant les indicateurs de passage de défaut

3.1 Introduction

Les indicateurs de passage de défaut (IPD) font partie du plan de protection d'un réseau de distribution et sont utilisés lors du processus de localisation de défaut. Les IPD sont des appareils conçus pour détecter la circulation d'un courant de défaut sur la ligne ou le câble où ils sont installés. Ils fonctionnent avec une logique de seuil de courant maximal qui permet de détecter une situation anormale, donc de défaut, lorsque ce seuil est dépassé.

Si la logique d'un IPD est toujours basée sur un seuil de courant, certains modèles appelés "IPD directionnel" peuvent également détecter la sens de circulation du courant de défaut. Ils nécessitent pour cela d'aussi connaître la tension. Cette grandeur est souvent obtenue par des mesures de champs magnétiques et électriques produits par les conducteurs. En revanche, lorsqu'un IPD est non directionnel, il faut observer consécutivement les IPD afin de déduire le sens du courant de défaut.

Si l'on considère que les IPD non-directionnels ont deux états lors d'une situation de défaut: pas de courant de défaut détecté / courant de défaut détecté. Les IPD directionnels auront donc eux trois états: pas de courant de défaut détecté / courant de défaut amont détecté / courant de défaut aval détecté. Lors du processus de localisation de défaut, les états des IPD sont donc récupérés en vue d'analyser la circulation du courant de défaut dans le départ.

Il existe deux types d'IPD: les IPD "communicants" et les IPD "non-communicants", qui peuvent tout deux être présents sur un même départ. L'état des IPD communicants est donc relevé à distance et peut immédiatement être utilisé par les système automatique d'exploitation du réseau afin d'isoler rapidement la section en défaut en manœvrant les organes de coupure télécommandés. Les IPD non-communicants possèdent eux un signal lumineux local qu'un technicien doit relever sur place. En France, les IPD communicants sont souvent associés à un organe de coupure télécommandé, alors que les IPD

non-communicants peuvent être associés à un organe de coupure manuel. Les états des IPD sont donc utilisés en deux temps: les IPD communicants sont d'abord utilisés pour une isolation automatique et rapide d'une large zone en défaut, alors que les IPD non-communicants sont utilisés dans un deuxième temps pour effectuer une isolation plus fine de la zone en défaut.

3.2 Conclusion

La nouvelle méthode de localisation de zone en défaut présentée dans ce chapitre se place dans un contexte de développement des réseaux de distribution vers les réseaux intelligents (smartgrids).

Comme rappelé dans la section 2, les méthodes de localisation actuelles font face à certaines limitations. La méthode qui a été développée ici se base sur l'existant, les indicateurs de passage de défaut, et leur évolution en terme de communication grâce aux réseaux intelligents.

La méthode est qualifiée d'approche probabiliste. En effet, elle utilise des calculs simples de probabilités et des définitions de probabilités d'état des IPD, de leurs états attendus selon les différents lieux de défaut (voir section 3.1) et des états réels des IPD relevés lors de l'apparition d'un défaut (voir section 3.6).

Les résultats présentés montrent un pourcentage moyen de succès d'identification de la section en défaut de plus de 85 % sur le réseau étudié. Cela montre une bonne performance et robustesse à la défaillance des IPD. Les cas de "mauvaise" localisation n'identifient effectivement pas la bonne section en défaut mais donnent toujours une section dans la même "zone", donnant une information importante au GRD sur la localisation grossière de la zone en défaut.

Lorsque l'algorithme identifie correctement la section en défaut et que la signature des IPD contient des erreurs par rapport à la signature idéale de le section en défaut, alors les différences entre ces deux signatures indiquent de possibles dysfonctionnements d'IPD. C'est une information importante pour le GRD puisque la méthode permet de trouver la bonne section en défaut dans la grande majorité des cas et en même temps de détecter de possibles défaillances d'équipements, ce qui n'est pas possible actuellement.

Cette méthode apporte de nombreuses améliorations aux techniques de localisation de section en défaut, sans pour autant nécessiter de grands investissements. De plus, elle peut être associée à un algorithme de calcul de distance de défaut afin d'avoir un algorithme complet et précis de localisation de défaut.

4 Chapitre 3: Méthode de localisation précise de défaut

4.1 Introduction

La méthode de localisation de défaut développée et présentée dans ce chapitre est basée sur le calcul direct de la distance du défaut, et non sur le calcul d'une impédance ramenée à une distance selon les impédances linéiques des conducteurs. Ce type de calcul est compliqué car il dépend de nombreux facteurs: précision des mesures, connaissances et précision des caractéristiques du réseau, qui peuvent être connus plus ou moins précisément. Mais il dépend aussi de facteur inconnus: caractéristiques du défaut, résistance du défaut, etc.

Les techniques de localisation de défaut qui ont atteint un développement avancé ont été conçues pour les réseaux de transport qui sont des réseaux plus simples en raison de leurs longues lignes homogènes, avec peu ou pas de charges. Toutefois, la nature maillée des réseaux de transport apporte des problèmes spécifiques lors de la localisation de défaut puisque les courants de défaut peuvent circuler vers l'aval ainsi que vers l'amont.

Les réseaux de distribution ont entre autres les particularités suivantes: topologie radiale, charges en piquage, non connaissance de leur consommation en temps réel, forte hétérogénéité des conducteurs. Tous ces paramètres entraînent la nécessité d'adapter les méthodes de localisation de défaut déjà existantes pour les réseaux de transport.

4.2 Conclusion

La méthode présentée dans ce chapitre est une méthode de localisation précise de défaut, dont le résultat est une distance du défaut par rapport au point de mesure. Elle utilise les mesures de tensions et courants en tête de départ et effectue la localisation sur chaque section homogène du départ, propageant les mesures de nœud en nœud, et tenant compte des charges et des caractéristiques des conducteurs.

L'algorithme fournit en sortie une distance de défaut ainsi que la section associée à cette distance de défaut. Si le réseau est radial, l'algorithme peut trouver plusieurs distances et sections associées.

La méthode de calcul de la distance de défaut a été développée pour le réseau de transport. Cette méthode nécessite d'approximer le courant de défaut afin d'obtenir une expression de la distance de défaut indépendante de la résistance de défaut qui est inconnue. Dans notre procédé, nous proposons une amélioration de l'estimation du courant de défaut afin d'améliorer la précision de la localisation.

Afin d'effectuer la localisation sur chaque section homogène du départ, la méthode modélise les différents éléments du réseau (conducteurs et charges) par des quadripoles. Ainsi la propagation des mesures de tensions et courants de nœud en nœud est facilitée et prend en compte les différentes chutes de tension et consommations par les charges ou branches latérales. Il est donc nécessaire de connaître la topologie précise du départ et les

caractéristiques électriques des différents éléments qui le compose.

Dans la dernière partie de ce chapitre, nous introduisons aussi quelques pistes de réflexions pour des cas particuliers qui ne peuvent être traités par la méthode proposée telle quelle.

5 Chapitre 4: Résultats de localisation de défaut sur des réseaux réels simulés

5.1 Introduction

Pour obtenir la méthode finale de localisation de défaut présentée dans le chapitre III, de nombreux réseaux ont été utilisés en fonction de l'avancement du développement de la méthode. Les premiers réseaux, simplistes et irréalistes, ont permis de développer une version simple de la méthode. Au fur et à mesure de son développement, les réseaux ont été complété. Finalement, les réseaux utilisés en simulation pour tester la version finale de la méthode sont des réseaux réels urbains et ruraux dont les données nous ont été fournies par un GRD.

Les simulations de ces réseaux ont été réalisées avec le logiciel "ATPDraw" qui est un préprocesseur graphique du programme "Alternative Transient Program" (ATP), une version de "Electromagnetic Transients Program" (EMTP).

Les mesures obtenues grâce aux simulations ont ensuite été converties en ".mat", le format de Matlab, pour être traitées par l'algorithme développé sous Matlab.

Dans la suite de ce chapitre, nous détaillons ces réseaux utilisés ainsi que les paramètres de simulation afin de détailler le contexte dans lequel ont été obtenus les résultats qui sont présentés.

5.2 Conclusion

Dans ce chapitre, nous avons présenté les résultats que nous avons obtenus en utilisant la méthode développée dans le chapitre III. Grâce aux nombreuses données obtenues par un GRD partenaire du projet, la méthode a pu être testée sur des données de simulations de réseaux réels, un départ urbain et un départ rural.

Les résultats peuvent être analysés sous plusieurs angles. Le premier est la localisation précise de défaut, en termes de distance par rapport au point de mesure situé en tête de départ. La méthode fournit une précision de localisation de l'ordre de 0 m à 300 m pour les défauts résistifs de 10 Ω ou moins, et ce pour les deux départs. Cependant la méthode ne parvient pas à obtenir des résultats non influencés par la résistance de défaut. En effet, l'erreur générée par la méthode augmente avec l'augmentation de la résistance de défaut. Une piste à explorer pour améliorer les résultats est présentée dans la section 5 du chaptire

IV.

Le deuxième angle est la localisation en termes de section. C'est la localisation de la section homogène sur lequel le défaut s'est produit. Les performances de ce type de localisation dépendent fortement de la topologie du réseau. Pour une même erreur de distance de défaut, la méthode peut donner un résultat correct ou incorrect selon la topologie du départ. En effet, certains départs possèdent de longues sections alors que d'autres possèdent de nombreuses petites sections. A titre d'exemple, les résultats obtenus sur le réseau rural montrent une localisation de section en défaut correcte pour tous les défauts de $10\,\Omega$ et moins.

Nous avons également montré que l'algorithme permet, pour les deux départs et pour tous les cas de défaut, de faire une assez bonne estimation de la résistance de défaut. C'est une donnée qui en soit peut aider à l'interprétation des résultats, notamment à l'évaluation de la probabilité d'exactitude des résultats (pour les faibles résistances de défaut).

Les analyses de sensibilité effectuées montrent que des améliorations des résultats peuvent être attendues. Notamment par une meilleure estimation du courant de défaut et en particulier de sa phase puisque c'est le principal facteur d'erreur. L'erreur faite lors de la propagation de la tension le long du départ, et due aux différences entre le modèle en Pi de l'algorithme et le modèle de simulation, n'affecte pas significativement les résultats.

Les calculs de localisation de défaut effectués sur les simulations des deux réseaux réels (urbain et rural) tendent à montrer que la méthode proposée pourrait à terme être utilisée sur les réseaux de distribution. Cette méthode correspondrait à un système de localisation de défaut complet, fournissant une estimation de la distance du défaut, de la section sur lequel il est survenu et de la résistance de défaut. Cependant, des améliorations évidentes sont à envisager. Les recherches futures doivent tester cette méthode sur des mesures réelles de défaut, ce qui n'a pu être fait correctement dans le cadre de ce projet, afin de vérifier la compatibilité de la méthode avec des cas réels de défaut.

6 Conclusion Générale

6.1 Conclusion

6.1.1 Localisation de section à l'aide d'indicateurs de passage de défaut

Dans la première partie de ce travail (chapitre II) nous avons développé une méthode de localisation de défaut qui se concentre sur la localisation d'une zone en défaut afin de l'isoler le plus rapidement possible du reste du réseau.

Cette méthode peut être une solution pour les réseaux utilisant des indicateurs de passage de défaut (IPD) avec un relevé à distance de leur état lors d'un défaut. Le principe de l'IPD est d'effectuer une mesure de courant (et parfois aussi de tension) là où il est installé, afin d'informer le GRD si un courant de défaut a été détecté. Les IPD directionnels, en mesurant aussi la tension, peuvent aussi indiquer le sens de circulation du courant

de défaut.

Cependant l'utilisation des IPD n'est pas toujours fiable. Par définition ces appareils ne fonctionnent pas de manière régulière, et leur défaillance est souvent découverte lors de l'apparition d'un défaut. Cela entraîne des temps de localisation des défauts plus longs et dégrade ainsi la capacité à bien exploiter le réseau à un moment critique. Pour contrer cet effet, nous avons développé une méthode probabiliste qui apporte une robustesse aux possibles défaillances des IPD.

La méthode proposée effectue une analyse probabiliste des états des IPD, triant les différentes sections ou zones de la plus probablement en défaut à la moins probablement en défaut. De cette manière le procédé est robuste à certaines erreurs d'état des IPD et identifie tout de même la bonne section en défaut. Cela permet au GRD d'effectuer une bonne analyse de la situation et une bonne localisation et isolement du défaut, malgré des appareils défectueux.

les résultats présentés montrent que cette méthode possède une bonne performance globale. Les limites de la méthode sont dues à des contraintes techniques que nous abordons dans les sections 4.2 et 7.2 du chapitre II.

Cette méthode n'est cependant pas un procédé de localisation précise de défaut mais bien un procédé de localisation de section en défaut. L'objectif du GRD étant de localiser correctement la section à isoler, et donc les interrupteurs à actionner, de manière à minimiser le nombre de clients affectés par le défaut. Nous introduisons en perspectives le couplage de cette méthode avec une méthode de localisation précise de défaut afin d'obtenir une procédure de localisation de défaut complète et efficace.

6.1.2 Méthode de localisation précise de défaut

Dans les chapitres III et IV, nous avons présenté la méthode de localisation précise de défaut améliorée que nous proposons ainsi que les résultats obtenus.

Le principe de base de la méthode, tel que présenté dans la section 2.1 du chapitre III, est l'utilisation d'une équation exprimant la distance entre le lieu de défaut et le point des mesures en fonction des grandeurs électriques et des caractéristiques des conducteurs. Développée à l'origine pour le réseau de transport, composé de longues lignes homogènes, nous avons transposé la méthode de Takagi aux réseaux de distribution.

Nous avons considéré que le réseau de distribution est une suite de sections homogènes et que la méthode peut être appliquée indépendamment sur chacune d'entre elle. En développant des travaux précédents, nous propageons les mesures électriques effectuées au poste source tout au long du départ, en tenant compte des charges présentes et des caractéristiques des conducteurs. Le calcul de la distance du défaut peut donc être fait sur chaque section homogène du réseau, offrant ainsi une méthode compatible avec la forte hétérogénéité des réseaux de distribution. Ces réseaux ayant une structure radiale, nous

avons aussi développé un algorithme logique de parcours de réseau parcourant toutes ses branches.

Ces développements permettent d'utiliser le principe de Takagi sur les réseaux de distribution. De plus, la propagation des mesures nous permet d'utiliser cette méthode sans faire d'hypothèses fortes telles que l'agrégation des charges en aval du point de défaut.

Afin d'améliorer la méthode, nous avons développé une estimation du courant de défaut utilisant les mesures du courant circulant dans le neutre, et l'estimation des courants capacitifs des conducteurs du réseau. Cette nouvelle manière d'estimer le courant de défaut nous permet d'avoir une estimation plus précise que celle utilisée dans la méthode de Takagi. Cependant si les erreurs commises lors de l'estimation du courant de défaut sont petites, leurs conséquences sur les résultats finaux sont rapidement importantes et dégradent la qualité de la localisation de défaut.

Afin d'augmenter la plage de fonctionnement de la méthode proposée (réseaux à neutre compensé, défauts très résistifs ou encore défauts de type arc), nous présentons dans le chapitre III les questions qui doivent être étudiées plus précisément.

Grâce au projet GreenLys et au partenariat avec un GRD local et un GRD national, nous avons obtenu des données détaillées sur différents types de départ. Cela nous a permis d'effectuer des simulations réalistes de réseaux et donc de simuler des situations de défaut le plus proche possible de la réalité. Dans le chapitre IV nous avons présenté les résultats obtenus et montré le bon fonctionnement général de la méthode, sur un départ urbain ainsi que sur un départ rural très radial.

En combinant l'utilisation d'une équation donnant la distance de défaut et une méthode de propagation à travers le réseau des variables mesurées, nous avons obtenu un procédé de localisation de défaut efficace. Les résultats présentés dans le chapitre IV montrent que l'algorithme de localisation possède une bonne précision pour tout type de situation dès lors que la résistance du défaut est faible. **Note:** les résultats obtenus avec le réseau souterrain (urbain) méritent une analyse plus détaillée afin de les améliorer. En effet, le procédé semble être plus sensible aux valeurs élevées des capacités des câbles et entraine une mauvaise estimation de défaut.

L'indépendance théorique de la méthode vis à vis de la résistance de défaut n'est pas vérifiée. L'analyse de sensibilité montre que certains paramètres introduisent des erreurs proportionnelles à la valeur de la résistance de défaut. Pour des résistances de défaut allant jusqu'à $15\,\Omega$ la localisation de défaut est précise à 300 m, près, ce qui peut encore être considéré comme un bon résultat sachant que certains défauts sont situés à 20 km.

En revanche, la méthode apporte de très bon résultats en termes de calculs des résistances de défaut. Ce point est important puisqu'une estimation précise de la résistance de défaut peut aider à interpréter la fiabilité des résultats de l'algorithme, c'est donc un résultat important.

Enfin, nous insistons sur la nécessité d'une bonne correspondance entre toutes les données de topologie utilisées par l'algorithme et la réalité du réseau. Les résultats ayant

été obtenus sur des simulations de défaut, la correspondance entre les données utilisées par l'algorithme et le réseau simulé était donc exacte, et il n'a pas été possible de confronter l'algorithme avec des mesures réelles de défaut.

6.2 Perspectives

Malgré notre objectif de fournir une méthode de localisation de défaut complète et efficace pour les réseaux de distribution électrique, il est évident que de nombreuses perspectives découlent de ces travaux. Nous en discutons dans les paragraphes suivants.

Il y a tout d'abord de nombreuses pistes d'améliorations de la méthode en elle-même. En effet, comme présenté dans l'annexe E, la propagation de la tension et du courant mesurés au cours d'un défaut doit être finement étudiée. Le processus de propagation a été validé lors de nos recherches sur la propagation de mesures pour une situation sans défaut, mais a montré de petites erreurs lors de la propagation des mesures de tension qui dégradent légèrement les résultats, comme montré dans la section 5.3 du chapitre IV. Une autre amélioration nécessaire concerne l'estimation du courant de défaut. Les travaux présentés dans les sections 5.1 et 5.3 du chapitre IV montrent que malgré la très faible erreur (en termes d'amplitude ainsi qu'en termes de phase), l'impact sur les résultats est fort et augmente avec l'augmentation de la résistance de défaut.

Enfin, afin de valider pleinement cette méthode, il est nécessaire d'utiliser l'algorithme de localisation de défauts sur des mesures de défauts réels. Idéalement ces mesures doivent provenir de réseaux de distribution qui peuvent être entièrement simulés, comme les réseaux sur lesquels nous avons travaillé, ce qui permettra de comparer et d'augmenter efficacement les performances de l'algorithme pour un bon fonctionnement de la méthode en pratique, et pas seulement en théorie.

D'autres améliorations sont à envisager afin de minimiser les conditions de fonctionnement de l'algorithme. Les réseaux de distribution présentent de nombreuses différences les uns des autres, il est donc nécessaire d'essayer d'étendre le plus possible la portée de la méthode. Pour l'instant la méthode s'avère ne fonctionner que dans le cas de défauts de faible résistance sur les réseaux de distribution aériens et souterrains avec un neutre impédant.

Une partie de notre travail présente les pistes qui doivent être explorées. Une méthode itérative, qui développe un calcul fin des courants capacitifs dus au défaut dans le réseau, peut aider pour le cas des défauts très résistifs. Une autre piste sur la modélisation des défauts d'arc (qui ne présentent pas les mêmes caractéristiques que les défauts permanents impédants) a été présentée.

Le cas des réseaux avec un neutre compensé doit également être étudié car de plus en plus de transformateur sont mis à la terre de cette manière. Ce type de mise à la terre influence les courants de défaut de telle sorte que le procédé doit être adapté. L'augmentation de la présence de générateurs d'énergie distribués dans les réseaux de distribution nécessite aussi une étude fine de leur influence possible sur cette méthode de localisation.

Pour finir, la méthode actuelle utilise la connaissance de la topologie du réseau, ainsi

que la puissance nominale de ses charges. Nous pensons qu'une étude approfondie de l'influence de la différence entre la charge réelle du réseau pendant le défaut et le niveau de charge nominale utilisé par l'algorithme doit absolument être menée.

Nous concluons ces perspectives par ce que nous pensons être la prochaine étape majeure du développement d'une méthode de localisation de défaut complète. Comme nous l'avons dit précédemment, la préoccupation première du GRD est de savoir quelle section (entre deux interrupteurs commandés à distance) est en défaut afin de l'isoler du reste du réseau et d'impacter le minimum d'utilisateurs. Par la suite le GRD veut connaître la position exacte du défaut afin d'effectuer les opérations de maintenance et de ramener le réseau à un fonctionnement normal le plus rapidement possible.

Les deux méthodes que nous avons développées, la localisation de section en défaut à l'aide d'indicateurs de passage de défaut et la localisation précise de défaut, répondent à ces deux questions. La localisation précise de défaut pourra, pour un réseau radial, donner tous les emplacements de défauts possibles à partir des mesures effectuées lors du défaut. Les multiples solutions qui peuvent être trouvées doivent donc être discriminées. La méthode de localisation de section au contraire ne donne pas une localisation précise du défaut, mais indiquera la zone en défaut la plus probable.

En associant logiquement ces deux méthodes, cela permet de discriminer les multiples solutions données par la localisation précise de défaut et d'obtenir un résultat complet quelques minutes seulement après l'apparition du défaut:

- la connaissance de la zone en défaut afin d'isoler le défaut du reste du réseau
- la connaissance de la localisation précise du défaut afin d'effectuer la maintenance et de minimiser la zone isolée en défaut

La connaissance rapide de ces résultats devrait aider les GRD afin de réagir rapidement et efficacement à un défaut sur leur réseau de distribution.

Improved Fault Localization Methods for Electrical Power Distribution Networks

Abstract This thesis proposes to improve fault localization methods for electrical power distribution networks. Transmission networks were quickly equipped with protection and fault localization equipments. Indeed, faults on the transmission network need to be dealt with quickly in order to avoid serious consequences. Unlike transmission networks, distribution networks have a minimal protection scheme. The smart grid developments bring new possibilities with the installation of new equipments giving access to many new variables. The work presented in this thesis develop two fault localization method. The first aims in using the equipment already installed (fault indicators) in order to isolate quickly and efficiently the zone concerned by the fault. The second method performs a precise localization (in distance) of the different possible fault locations from the electrical measurements made on the network.

Améliorations de Méthodes de Localisation de Défauts pour les Réseaux de Distribution Electrique

Résumé Ces travaux proposent des améliorations de méthodes de localisation des défauts électriques sur les réseaux électriques de distribution. Les réseaux de transport ont rapidement été instrumenté en élément de protection. En effet, un incident survenant sur le réseau de transport peut entrainer de graves conséquences s'il n'est pas traité rapidement. Les réseaux de distribution quand à eux possèdent un schéma de protection minimal. Cependant le développement des smart grids (ou réseaux intelligents) amène de nouvelles possibilités avec l'ajout d'équipements de mesures sur le réseau de distribution. Les travaux présentés dans cette thèse développent deux méthodes de localisation de défaut. La première permet de mieux utiliser l'équipement déjà en place (indicateurs de passage de défaut) afin d'isoler de manière rapide et fiable la zone concernée par le défaut. La deuxième permet une localisation précise (en distance) des différents lieux de défauts possibles à partir de mesures électriques.